ADVANCED ENERGY MATERIALS
www.advenergymat.de

Merging Biology and Photovoltaics: How Nature Helps Sun-Catching

*Luca M. Cavinato, Elisa Fresta, Sara Ferrara, and Rubén D. Costa**

Accomplishing sustainability in optoelectronics, in general, and photovoltaics (PV), in particular, represents a crucial milestone in green photonics. Third generation PV technologies, such as organic solar cells (OSCs), perovskite solar cells (PSCs), and dye-sensitized solar cells (DSSCs) have reached a mature age and are slowly making their way in the market as complementary devices to the first generation solar cells. For example, they are well suited for high-end smart applications, like flexible and wearable devices, fully transparent solar cells and windows, and biocompatible devices for medical applications. In this context, major efforts have been conducted to realize easy-to-do and low-cost recycling devices without losing performance level. This has fueled a strong cooperation between engineering, biology, chemistry, and physics fields to discover new strategies for cost-effectiveness preparation and implementation of bio-derived materials in highly performing PVs. The recent efforts of these groups are honored here, providing a general overview on bio-derived materials suitable for PV applications as well as an in-depth revision of the most relevant and recent advances obtained by merging biology and third generation PV technologies.

1. Introduction

In 2017, the international renewable energy agency (IRENA) reported that the world can meet around 90% of the decarburization goals set by the Paris Agreement through accelerated deployment of renewable energy and their conversion efficiency.[1] Among the plethora of green sources able to produce electricity, solar energy is the largest global renewable one[2] and, in turn, it is one of the most promising options.[3–5] Up to date, the market is still dominated by the first generation solar cells (SC) based on silicon wafers, which accounts for 95% of the total production.[6] They are expensive to manufacture, but feature high power conversion efficiencies (PCEs), close to their theoretical maximum, and excellent stabilities under outdoor operation conditions. This makes difficult to further reduce the cost of electricity production.[7,8] Furthermore, although solar energy is a renewable source, it does not mean that any kind of photovoltaics (PV) is sustainable. For instance, silicon is an essential material in electronics and solar industries and, up to date, is irreplaceable. Despite its abundancy in Earth's crust, it is for the vast majority (80%) present as ferrosilicon, whose purification is expensive and highly pollutant. The production of 1 ton of silicon requires 6 tons of raw materials, almost 3 tons of Quartz, 1.5 tons of reducing agents, 1.5 tons of wood and 13 000 kWh of energy.[9,10] Therefore, in 2014 the EU commission included silicon metal in the critical raw material (CRM) list.[11]

In this context, the third generation PV has reborn, offering cost-effective and efficient CRM-free devices with a lower reliance on the incident angle of light and integration in smart-end applications, like flexible and wearable devices,[12–14] fully transparent solar cells and windows,[15,16] and biocompatible devices.[17–19] The leading third generation SCs are organic solar cells (OSCs),[20–22] perovskite solar cells (PSCs),[23–27] and dye-sensitized solar cells (DSSCs).[28–30] Despite their versatile applications and high performances, sustainability still represents a major issue toward becoming an ideal energy technology in the mid-long term future. Among others, fullerene-based materials are toxic,[31] indium tin oxide (ITO) is brittle, chemically unstable, and expensive due to limited indium sources on Earth's crust.[32,33] Cobalt is also listed as CRM,[11] while cadmium, selenium, lead and ruthenium are toxic materials.[34,35] With regard to flexible devices, polyethylene terephthalate (PET) is the standard substrate; though its environmental footprint is critical and its nonbiodegradable properties lead to harmful effects in living organisms.[36] This has fueled a strong cooperation among the fields of engineering, biology, chemistry, and physics to discover new strategies for cost-effectiveness preparation and implementation of bio-derived materials in highly performing PVs.

In general, this cooperation constitutes a part of the emerging and multidisciplinary field of biophotonics,[37] which involves biomedical optics,[38] living light,[39–41] biomimetic, biomaterials and bioengineered compounds, as well as fabrication/implementation methods applied to optoelectronics[42] and photonics,[43] among others. For instance, artificial lightning and biology have been recently merged with the implementation of cellulose, chitosan, silk, and fluorescent proteins as

L. M. Cavinato, Dr. E. Fresta, S. Ferrara, Prof. R. D. Costa
Chair of Biogenic Functional Materials
Technical University of Munich
Schulgasse 22, D-94315 Straubing, Germany
E-mail: ruben.costa@tum.de

The ORCID identification number(s) for the author(s) of this article can be found under https://doi.org/10.1002/aenm.202100520.

© 2021 The Authors. Advanced Energy Materials published by Wiley-VCH GmbH. This is an open access article under the terms of the Creative Commons Attribution License, which permits use, distribution and reproduction in any medium, provided the original work is properly cited.

DOI: 10.1002/aenm.202100520

active device components, i.e., substrates, electrodes, emitters, etc. toward highly performing bio-based lighting devices.[44–46] It is worth to mention that the term "biomaterial" refers to any substance of synthetic, biological, and hybrid nature that interfaces with living tissues.[47] Thus, biomaterials are not necessarily biological or based on bio-related matter. However, biogenic materials are per se eco-friendly. Again, this does not directly imply that they are sustainable, especially when they are derived from superior organisms. The sustainability goal could be reached either if a bacteria-based production is implemented in the fabrication process or if the source materials are recovered from large quantity wastes of other sectors.[48] Similar to the artificial lighting, many research groups working on PV are endeavored to introduce bio-derived materials, managing to keep the performances of standard components and eventually even outperforming them.[49–54]

This review aims at providing an extensive description of the most relevant and recent advances in bio-based PV devices, considering the last five years as period of interest (2015–2020 and over 150 works) and the third generation PV technologies. The reader will be redirected to previous reviews focused on the sustainability and biodegradability of SCs and more specific contributions when necessary.[55–62] This allows us to provide a comprehensive and accurate review to reflect the actual evolution of PVs that blurs the lines between physics, chemistry, biology, and engineering, building up the knowledge bridges between these worlds. As such, this review is divided in five follow-up sections: i) a brief historical view of SCs and their integration with biology (Section 2), ii) an overview about the different types of third generation PVs (Section 3), iii) an introduction on the most used biological materials in SCs and their actual bacterial-based production (Section 4), iv) an in-depth discussion about the current scenario in merging biology and PV (Section 5), and v) a final conclusion section that aims to summarize the most relevant strengths, drawbacks, and perspectives of the field (Section 6). The authors hope that this manuscript will inspire scientists and engineers to realize the importance of interdisciplinary co-operation in order to open new horizons toward sustainable and high performing bio-based PV devices.

2. Brief Historical View

The PV effect is the essential basis of the conversion of light into electricity. Even though an extensive description of the history of PVs is not the aim of this review, the authors care about reminding the discovery of Edmond Bequerel. In 1839, while doing experiments involving electrolytic cells, he noticed that the voltage of the cell increased when its silver plates were exposed to the sunlight.[63] In 1905, Albert Einstein theorized the photoelectric effect, whose direct consequence is the PV one. Thanks to the latter, he was awarded with the Nobel Prize in 1921, further promoting the knowledge about photons, namely quantized packets of energy that are the building blocks of light. In short, when light impacts a semiconductor bearing photons with energies higher than the energy bandgap of the material (i.e., 1.1 eV for silicon) they can be absorbed. Therefore, electrons are promoted from the valence band to the conduction band, leaving a corresponding number of holes in the former. A built-in potential barrier in a PV cell acts on these electrons to produce voltage.[64]

In 1954, the era of PV power generation began with the first crystalline silicon solar cell by Chapin's group, featuring a 6% PCE.[65] To overcome the issues related to the silicon supply chain and the high production cost, two strategies were proposed: i) the use of amorphous silicon wafer or optimal light-harvesting materials, and ii) the reduction of the thickness of the silicon wafer from 100 to 5–50 μm (crystalline silicon thin film solar cells).[66,67] Thin-film technology (namely second generation PVs) developed fast, since the mid-1980s with the introduction of ternary compound semiconductors, like $CuGaSe_2$ and $CuInS_2$, and multinary alloy $Cu(In,Ga)(S,Se)_2$.[68]

Inspired by natural photosynthesis in 1991, O'Regan and Grätzel made significant progresses within the DSSC concept, reaching promising efficiencies of almost 8%.[30] In this device, the presence of impurities in either the starting materials and in the final device became of less relevance. Hence, the fabrication cost of DSSCs is lower compared to that of monocrystalline silicon SCs. A few years later, fully OSCs were developed with a modest efficiency around 1%, but they outperformed DSSCs in the early-2010s, reaching today remarkable efficiencies of 18%.[69,70] Perovskites were first discovered by Weber in 1978, then further explored by Kagan et al. for light-emitting applications.[71–73] Evolving from the DSSCs concept, the first perovskite-sensitized SCs were fabricated by Miyaska and co-workers,[74] reaching today high efficiencies over 25%.[75]

Along these timelines, all the aforementioned PVs met Biology in the form of innovative materials, components, architectures, etc.[55–62] Among them, DSSCs was the first and the most prolific area in terms of using bio-inspired and bio-derived materials and/or components up to date. In fact, around ten years after the first DSSC example, the scientific community started to look for solutions related to the toxicity involved in device fabrication, e.g., highly volatile solvents, dyes, etc. For instance, high efficiencies have been reached thanks to toxic ruthenium based photosensitizers, mostly N719 and N3. In this case, natural dyes extracted from vegetable species have been widely tested in DSSCs. The first attempt was carried out in 2002 by Minoura's group.[76] They applied more than 20 dyes extracted from their natural source as photosensitizers for DSSCs, reaching efficiencies of 1.5% with red cabbage derived photosensitizers. This approach has been particularly active since 2014.[77–79] More recently, the use of bio-inspired and water compatible compounds in DSSCs has opened a new horizon toward eco-friendly aqueous cells featuring record efficiencies of 7%.[80] Although promising results have been obtained turning DSSCs in a greener and more sustainable technology compared to its origins, major efforts are required to achieve milestones related to stability and up-scaled production (Section 5.3).

In OSCs and PSCs, the appearance of Biology into the field happened only much later. In 2005, the concept of paper electronics was introduced by Lamprecht et al.,[81] while the first use of photo-/electro-active compounds, such as carotenoids in combination with an electron-acceptor fullerene derivative

© 2021 The Authors. Advanced Energy Materials published by Wiley-VCH GmbH

16146840, 2021, 43, Downloaded from https://onlinelibrary.wiley.com/doi/10.1002/aenm.202100520 by Universita Di Torino, Wiley Online Library on [21/02/2025]. See the Terms and Conditions (https://onlinelibrary.wiley.com/terms-and-conditions) on Wiley Online Library for rules of use; OA articles are governed by the applicable Creative Commons License

in OSCs, dates back to 2013.[82] Since these pioneering works, research efforts have been conducted toward introducing bio-derived materials as electron/hole transport layers (deoxyribonucleic acid (DNA), L-arginine), donor/acceptor (photosystems, natural dyes), and electrodes (cellulose, catecholamine).[52,83–86] Recently, Uchiyama et al. studied the encapsulation of electron donor beta carotene semiconducting layers to provide highly durable solar cells.[87] In fact, similar to DSSCs, the major limitation of Bio-OSCs is the device stability and an efficient processability (Section 5.1).[84]

As the most recent PV technology, PSCs were merged with Biology in the very last years, achieving a remarkable success. First examples refer to the use of dopamine as dopant in poly(3,4-ethylenedioxythiophene) polystyrene sulfonate (PEDOT:PSS) hole transport layers (HTLs),[88,89] while recent work reports on its use in electron transport layers (ETLs) crosslinked with titania oxide electrodes.[90] Researchers are also increasingly focused on using i) biogenic compounds to stabilize perovskite layers (surface passivation)[91–93] reaching over 250 h stability under operation condition and ii) biomimetic strategies to enhance sun-bath enhancing the overall optical efficiencies of 25% regardless of the illumination angle and others.[94] This recent success is based on the previous knowledge acquired in bio-based OSCs and DSSCs. Up to date, there is no review focused on bio-PSCs.

In order to provide a state-of-the-art synopsis to the reader, **Figure 1** displays a timeline of the most efficient PVs,[75] focusing on DSSCs, OSCs, and PSCs and their respective bio-based versions. This is complemented with the below summary that takes into account the Watt cost production for reference purposes:

- monocrystalline Si: 26.1% (≈3$ W^{-1}), very close to the theoretical maximum around 29%;[7,8]
- DSSCs: 12.6% (<0.4$ W^{-1});[64]
- OSCs: 18.2% (<0.2$ W^{-1});[70]
- PSCs: 25.5% (0.2$ W^{-1});[95]

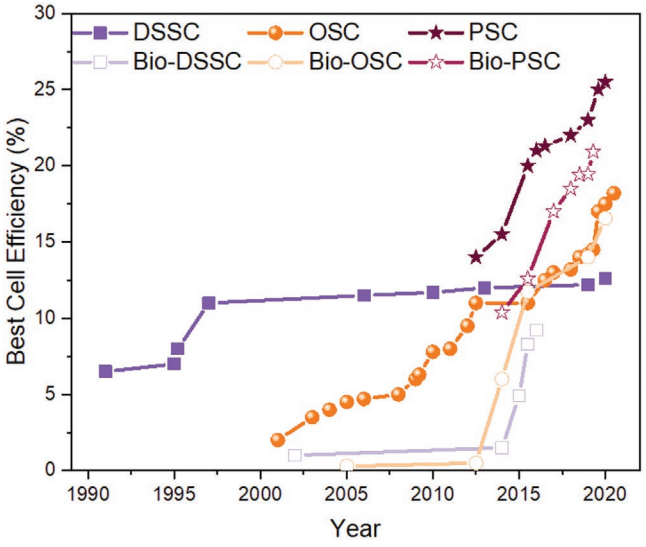

Figure 1. Chart of the best performing DSSCs, OSCs, and PSCs[75] as well as their bio-based version since 1991.

3. Device Architecture, Materials, Operation, and Characterization

3.1. Organic Solar Cells

The standard OSC features an ITO anode coated onto glass or plastic substrates, a multilayered architecture of hole/electron transport layers and light absorbing active layer (bilayer donor/acceptor or donor/acceptor single layer bulk heterojunction (BHJ) devices), high work-function metallic electrodes, and encapsulation layers (**Figure 2**). Upon sun illumination, the donor material is photoexcited and the acceptor material can extract the electron from the former, without long-range diffusion of the charge carrier thanks to the close contact. Both holes and electrons diffuse toward the electrodes and finally transferred to the external electric circuit.[96] Despite high efficiencies of 18.2%,[70] their commercialization is blocked, among others, by issues related to the thickness of the active layer, the stability in air, the transparency of the final device and the lack of efficient alternatives to fullerene-based acceptor materials.[97,98] In addition, the complicate architecture limits large-scale production.[99,100] This review will revise the recent advances and major limitations.

To efficiently harvest sun light, the achievement of a panchromatic absorption is required. Tandem OSCs, in which photoactive layers with complementary absorption spectra are interconnected, were consequently designed to accomplish the requirement. To date, the most promising approach is the ternary active layer strategy, which comprises either two acceptors and one donor or one acceptor and two donors in a BHJ configuration to maximize the interfacial area (Figure 2). Both small molecules and polymers have been used in OSCs reaching panchromatic absorption and remarkable hole/electron mobilities,[101–104] and bio-based donor/acceptor compounds have been proposed with a moderate success. In particular, the implementation of photosynthetic systems has been very attractive due to their availability, extremely high internal quantum efficiency (IQE), and rapid charge separation.[105–107]

ITO is the most widely used transparent conducting electrode for OSCs owing to its high electrical conductivity and good optical transparency. However, it is brittle, chemically unstable, and expensive due to limited indium sources on Earth's crust and difficult preparation processes. This results in limitations toward the widespread use of ITO in the next-generation devices.[32,33] It is urgently desirable to find new materials to replace ITO for organic electronics. The widely used PEDOT:PSS is a promising candidate due to its mechanical flexibility, high transparency, and compatibility with solution-based deposition techniques.[108] Other main alternatives to ITO include metal meshes, metal nanowires, graphene, and carbon nanotubes.[109,110] Nevertheless, in the prospective of further commercial applications, there are still shortcomings that must be overcome. Herein, we discuss how biological derived materials can also help to unlock greener and more sustainable electrode materials. For instance, cellulose is an abundant and low-cost material that is emerging as matrix for innovative flexible electrodes thanks to its suitable compatibility with conductive materials, like graphene and PEDOT:PSS.[111] In addition, the strong adhesive properties of catecholamine derivatives have an

© 2021 The Authors. Advanced Energy Materials published by Wiley-VCH GmbH

16146840, 2021, 43, Downloaded from https://onlinelibrary.wiley.com/doi/10.1002/aenm.202100520 by Universita Di Torino, Wiley Online Library on [21/02/2025]. See the Terms and Conditions (https://onlinelibrary.wiley.com/terms-and-conditions) on Wiley Online Library for rules of use; OA articles are governed by the applicable Creative Commons License

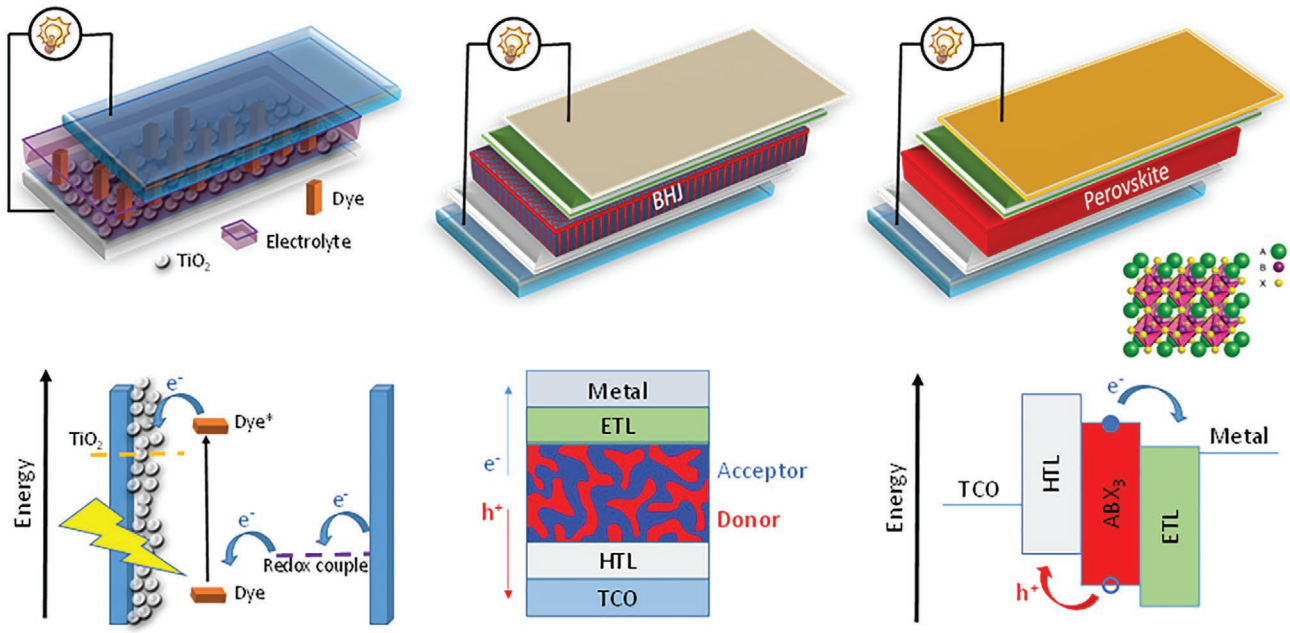

Figure 2. Schematic views of the standard architectures (top) and working mechanisms (bottom) in: DSSCs (left), OSCs (center), and PSCs (right). Inset: generic ABX_3 perovskite structure.

enormous impact in enhancing the performances of innovative electrode materials like metal grids and nanotubes.

The moderate stability of OSCs is mostly caused by the interfacial instability and diffusion of water and oxygen into the device. The introduction of an interlayer between the electrode and the photoactive material prevents these side reactions and improves charge-collection efficiency, carrier selectivity in the device due to a better energy levels alignment, balancing propagation and distribution of light and optimizing the morphology of the active layer.[112–114] In the past decades, significant progress has been achieved as far as the cathode interface modification in OSCs is concerned. For instance, transition metal oxides,[115] self-assembled layers,[116] polyelectrolytes,[117] nonconjugated and conjugate organic materials,[118] and hybrid materials have already been employed;[118] among them, the nonconjugated polyethylenimine (PEI)-based analogs are the most used.[119,120] All of them feature several drawbacks, namely poor electron/hole transport, stability, and complicated synthetic routes. Therefore, the design and synthesis of novel interface materials is still considered a challenging task. The application of bio-derived materials as interlayers in OSCs has recently received great research interest.[121–124] Small molecules with functional polar groups, such as amino acids, are contemplated to be the most effective ETL owing to the formation of dipoles at the interface that improve the work function of ITO and the consequent reduction of the interface energy barrier.[125,126] These advances are summarized in depth in Section 5.1.

3.2. Perovskite Solar Cells

A typical PSC comprises a five-layered-structure (Figure 2),[127,128] involving i) a transparent fluorine-doped tin oxide (FTO) coated glass/plastic as anode, ii) a compact metal oxide layer (MO_x) that helps electron transport, iii) a multi crystalline metal halide perovskite (P) layer as absorbing layer, iv) an organic HTL, and v) a metallic counter electrode.

The device mechanism is similar to that described in OSCs. The main processes are described as: i) photoexcitation of the perovskite layer: $P + h\nu \rightarrow (e^-\cdots h^+)P$; ii) carrier injection: $(e^-\cdots h^+)P \rightarrow e^-(MO_x)//(e^-\cdots h^+)P \rightarrow h^+(HTL)$; iii) radiative and nonradiative loss at P: $(e^-\cdots h^+)P \rightarrow h\nu//(e^-\cdots h^+)P \rightarrow \nabla$; and iv) back electron/hole transfer: $e^-(MO_x) + h^+(P) \rightarrow \nabla//h^+(HTL) + e^-(P) \rightarrow \nabla$.

In contrast to BHJ-OSCs, the exciton formation at the perovskite layer and its dissociation at the donor–acceptor interface are excellent, reaching PCEs of ≈25% for a single, non-tandem PSCs.[129,130] Their high efficiency is mainly attributed to the suitable band gap, ambipolar transport property, and broad range and long charge-carrier diffusion length of perovskites layers. They have a general chemical formula of ABX_3, where A, B, and X are an amine cation, metal cation, and halogen anion, respectively (Figure 2).[131,132] Not only the high performance, but also the low-cost solution-based processes used for device fabrication attest to a huge potential of PSCs.[133–136] Nevertheless, there are still limited choices of perovskite materials and their toxicity and instability remain extremely challenging issues to be solved.[137–139] In detail, the main factors affecting the instability of perovskite materials include:

i) Humidity: as an example, $CH_3NH_3PbI_3$ is hygroscopic and eventually decomposes into CH_3NH_3I and PbI_2 when exposed to water.[140]
ii) Thermal stress: overcoming the limits of the tetragonal $CH_3NH_3PbI_3$ phase (slightly below ≈50 °C) shortens the durability of the device.[141,142]
iii) Photoinduced oxidation:[143] O_2 and UV light may accelerate perovskite degradation.[141,143] Additionally, degradation was

© 2021 The Authors. Advanced Energy Materials published by Wiley-VCH GmbH

16146840, 2021, 43, Downloaded from https://onlinelibrary.wiley.com/doi/10.1002/aenm.202100520 by Universita Di Torino, Wiley Online Library on [21/02/2025]. See the Terms and Conditions (https://onlinelibrary.wiley.com/terms-and-conditions) on Wiley Online Library for rules of use; OA articles are governed by the applicable Creative Commons License

also reported under normal light conditions by Ito et al., in the absence of a surface blocking layer between TiO_2 and the perovskite.[144]

iv) Device operation: accelerated degradation takes place under open-circuit conditions. This is ascribed to trap charging combined with radical formation and assisted by undesirable extrinsic ion diffusion that is not prevented by internal fields.[143] Slow degradation under short-circuit and maximum power-point conditions is attributed to internal and external ion migration due to internal interfacial fields.

v) Other factors: vacancies in the perovskite structure upon film forming are quite common.[145,146] These defects can encourage ion migration through the perovskite film, the surface morphology, crystal phase transition, photo trap states, and grain boundary behavior of the material, which can also affect the stability of the perovskite material itself.

A cospicuous number of research efforts are still in progress to address the issue of stability by way of interface engineering and new device architectures.

In this context, bio-derived materials with polar groups, such as amino acids and catecholamine, have been mostly implemented in order to i) mitigate intrinsic elements of stability: they improve the morphology of the deposited perovskite, increasing the grain size and reducing the number of defects, voids, and grain boundaries, and ii) modify the TiO_2/perovskite heterojunction interface toward enhanced charge extraction.

These phenomena are favored by the dipolar nature of the bio-derived materials, whose carboxylic group is prone to anchor on the TiO_2 surface through COO^- bidentate coordination, while the amino group stretches outward from the surface.[147] Such conformation would facilitate the interaction between amino acids and the perovskite crystals formed at the interface.

3.3. DSSCs

As in natural photosynthesis, DSSCs utilize pigments to transfer electrons to inorganic electrodes converting sun irradiation into electrical energy instead of chemical energy (adenosine triphosphate (ATP) or NADPH). The sandwich architecture of a typical DSSC consists of i) two electrodes, i.e., nanocrystalline mesoporous metal oxide photoanode/cathode and platinum counter electrode deposited onto FTO glass or plastic substrates, ii) donor or acceptor dyes attached onto the metal oxide photoelectrode, and iii) a liquid, solid state or quasi-solid state electrolyte bearing a redox couple that connects both electrodes (Figure 2).[148]

The working mechanism involves four steps: i) the dye is excited by sun irradiation; ii) charge injection, e.g., the electron in the excited state is injected into the conduction band of the mesoporous material; iii) the oxidized/reduced dye is regenerated by the electrolyte; iv) the electrolyte is regenerated at the counter electrode interface.[28] Unfortunately, several undesired processes can also take place: i) decay of the excited dye to the ground state, ii) back electron transfer from the metal oxide to the dye, and iii) dark current generates by electron transfer from the metal oxide to the electrolyte. The latter is considered the main loss mechanism in DSSCs.[56,149,150]

Although they present lower efficiencies and stabilities compared to other PV devices,[151,152] they shine in term of cost-effectiveness, sustainable production, and little maintenance requirements. Furthermore, DSSCs remain functional even under diffuse light, reaching astonishing efficiencies of 32%[153] and they can be realized as fully transparent device.[154–156] In this context, they are ideal SCs for in-door purposes.[157–159]

Since each part of the DSSCs can independently be optimized, several approaches have been demonstrated toward sustainable electrodes/substrates, dyes, and electrolytes. Concerning electrodes/substrates the materials and approaches developed in OSCs have been also applied to DSSCs.[160–162] More innovative ideas toward bio-based dyes and electrolytes are present in the prior art. In short, the design of dyes for highly performing DSSCs should fulfill several requirements: i) high molar extinction coefficient, ii) broadband absorption spectra covering visible and Near-IR range, iii) strong binding or electron coupling with the mesoporous semiconductor, iv) alignment of energy levels, with regard to the conduction band of the semiconductor and the redox couple potential, and v) stability upon continuous sunlight exposition.[163,164] Along these lines, sustainable and/or bio-based dyes include proteins and natural dyes.[165–167] Their device performance, implementation and limitations will be summarized in Section 5.3. As far as the electrolyte is concerned, liquid, quasi-solid, and solid electrolytes based on several redox species have been investigated.[168] Some of the most known redox couples, especially among liquid electrolytes, are iodide/triiodide (I^-/I_3^-) systems, as well as bromide/tribromide (Br^-/Br_3^-). Interhalogen redox systems such as I^-/IBr_2^- and I^-/I_2Br^- have been tested, although the search was limited to ruthenium-based sensitizers. Moreover, the most known pseudohalogen redox couples are $SCN^-/(SCN)_3^-$ and $SeCN^-/(SeCN)_3^-$, besides electrolytes exploiting Co-complex-based redox systems. At the laboratory scale, a solution of iodide/triiodide in an organic solvent, like acetonitrile, is the most used due to several advantages of the solvent, namely poor absorption in UV–vis region, strong polarity, chemical stability, and low-cost. Nevertheless, it is well known that organic solvents are associated to high toxicity and low boiling point, while iodide/triiodide is highly corrosive in the long-term, hampering the scaling-up of the panels and the production of large-area devices. To circumvent this issue, two main strategies have been followed: i) the use of a sealant film to encapsulate the cell, and ii) the use of the aforementioned solid or quasi-solid electrolytes.[169] In the latter case, solid electrolytes are related to the use of either polymer thin films with salts, e.g., polyethylene oxide containing iodide/triiodide, or hole transport materials such as 2,2′,7,7′-tetrakis[N,N-di(4-methoxyphenyl)amino]-9,9′-spirobifluorene (spiro-OMeTAD). The quasi-solid ones usually bear the same salts and additives as the liquid electrolytes along with polymers to promote a jellification process. Both, photosensitizer and electrolyte, have been extensively reviewed in literature.[56,59,60,170] Herein, we focus on the implementation of bio-inspired photosensitizers, electrolytes, electrodes, light trapping layers, and sealant films in DSSCs. We highlight how versatile can be the integration of these materials in such

© 2021 The Authors. Advanced Energy Materials published by Wiley-VCH GmbH

16146840, 2021, 43, Downloaded from https://onlinelibrary.wiley.com/doi/10.1002/aenm.202100520 by Universita Di Torino, Wiley Online Library on [21/02/2025]. See the Terms and Conditions (https://onlinelibrary.wiley.com/terms-and-conditions) on Wiley Online Library for rules of use; OA articles are governed by the applicable Creative Commons License

a device, potentially paving the way to a fully bio-derived solar cell.

3.4. Figures of Merit

As anticipated in Section 2, SCs generate electricity upon photoexcitation. The resulting excitons dissociate into separated charge carriers, namely holes and electrons. The dissociation efficiency relies onto the excitons binding energy, E_b, defined as

$$E_b = \mathrm{IE} - \mathrm{EA} - E_{op} \quad (1)$$

where IE is the ionization energy, EA the electronic affinity, and E_{op} is the energy of the relaxed exciton relative to the ground state. Usually, in inorganic materials E_b is small, while organic compounds show greater exciton binding energies, which implies very inefficient charge separation if only one organic material is used. The donor–acceptor approach efficiently solved the issue.[171]

The main figures of merit of PVs are displayed in **Figure 3** and summarized as follows:

i) Short-circuit photocurrent density (J_{SC}) represents the photocurrent per unit area (mA cm^{-2}) of the cell under short circuit conditions (when the resistance is zero, $V = 0$ V).
ii) Open circuit voltage (V_{OC}) is the electrical potential difference under open circuit conditions (when the resistance is infinite, $I = 0$ A) between the photoanode and the counter electrode.
iii) Fill factor (FF) is defined as

$$\mathrm{FF} = \frac{P_{max}}{J_{SC} \times V_{OC}} \quad (2)$$

Where P_{max} is the maximum power output of the cell per unit area. In a current–voltage (J–V) plot, the FF describes how the area embedded by the curve of the measured device fills-in the maximum rectangle described by the product $J_{SC} \times V_{OC}$.

iv) PCE (η) of a SC can be expressed as

$$\eta = \frac{V_{OC} \times J_{SC} \times \mathrm{FF}}{P} \quad (3)$$

where P is the power of radiation incident P [W m^{-2}].

Usually the tested solar cells are illuminated with a simulated air mass (AM) spectrum of AM1.5G, which means a power of radiation incident P of 963 W m^{-2}.[172]

For a better insight into the device mechanism, another useful parameter is the incident photon conversion efficiency (IPCE) or external quantum efficiency (EQE) that corresponds to the photocurrent generated in the external circuit per monochromatic photons flux that irradiates the cell. The IPCE is directly correlated with the absorption features of the sensitizer, the amount of photoactive species, and the yield of carrier extraction. The value is calculated under short circuit conditions

$$\mathrm{IPCE} = 1240 \frac{J_{SC}}{\lambda \times \phi_{in}(\lambda)} \quad (4)$$

where λ is the given excitation wavelength and ϕ_{in} (λ) is the photon flux of the incident monochromatic light.

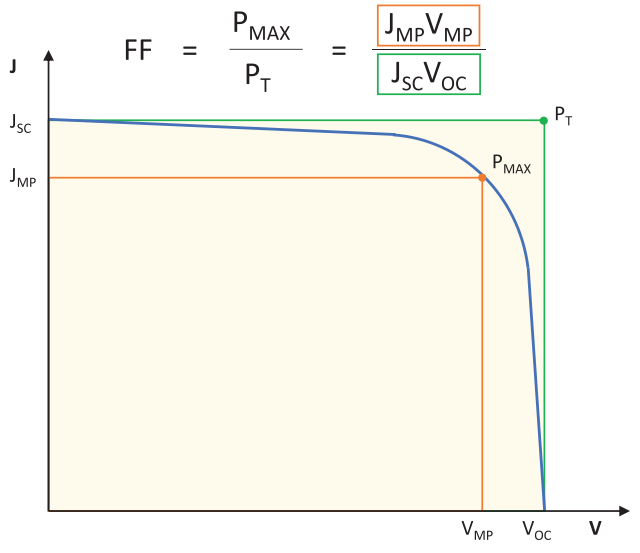

Figure 3. Schematic description of the figures of merit. Left: general IPCE curve. Right: general J–V curve and the correlated parameters.

4. Bio-Related Materials: Description, Characteristics, and Eco-Friendly Production

As above mentioned, a large number of works on bio-based PVs have been published over the last 15 years. However, this has experienced a significant thrust over the last 5 years since the use of innovative and eco-friendly materials have been explored to address the sustainability challenge.[43,59–62,173–175] This section briefly introduces the most common used bio-related materials in the PV field, focusing on their spectroscopic, optical, and mechanical features as well as its ecofriendly production.

4.1. Mono- and Poly-Saccharides

4.1.1. Monosaccharides

Monosaccharides are polyhydroxy aldehydes or ketones with more than one hydroxyl (−OH) and carbonyl (−C=O) groups placed at either the terminal carbon atom (aldose) or at the second carbon atom (ketose) (**Figure 4**). According to their chain length, monosaccharides fall into several categories, of which the most nutritionally important are the pentoses (5-carbon atom skeleton, ribose) and the hexoses (6-carbon atom skeleton, glucose).[176] However, the presence of asymmetrical carbons in monosaccharides with different functional groups attached gives rise to optical activity and enhanced ionic conductivity. For instance, the Bio-DSSCs have been highlighted by the use of sugars as sensitizers and electrolytes (Section 5.3).[169] Here, the selection of an ion conductive additives as electrolyte must meet the ability to solvate ions and an optimum glass transition

© 2021 The Authors. Advanced Energy Materials published by Wiley-VCH GmbH

16146840, 2021, 43, Downloaded from https://onlinelibrary.wiley.com/doi/10.1002/aenm.202100520 by Universita Di Torino, Wiley Online Library on [21/02/2025]. See the Terms and Conditions (https://onlinelibrary.wiley.com/terms-and-conditions) on Wiley Online Library for rules of use; OA articles are governed by the applicable Creative Commons License

16146840, 2021, 43, Downloaded from https://onlinelibrary.wiley.com/doi/10.1002/aenm.202100520 by Universita Di Torino, Wiley Online Library on [21/02/2025]. See the Terms and Conditions (https://onlinelibrary.wiley.com/terms-and-conditions) on Wiley Online Library for rules of use; OA articles are governed by the applicable Creative Commons License

temperature (T_g).[102,177] Monosaccharides feature a high density of polar residues that can form electrostatic bonds with the ions, facilitating their solvation, while low T_g promotes the segmental motion. Indeed, they have been successfully applied to batteries and supercapacitors as electrolytes.[178–181] Finally, they are commonly produced through hydrolysis by hydrolytic agents (enzymes, acids, or bases) or with immobilized enzymatic method. In both cases, the raw materials are first hydrolyzed or isomerized in a reactor and then dissolved in water at low-temperature. Subsequently, several purification steps follow via filtration, desalination, concentration, and crystallization. In addition, if a mixture of isomers is obtained, a further purification through chromatography is required before crystallization.[182] The major sources of raw materials are wastes from corn industry, in particular starch - vide infra, hence their production cost is extremely low and they do not display interference with food supply chain.

4.1.2. Cellulose and Derivatives

Cellulose is the most abundant biopolymer on earth. Besides its traditional uses in paper manufactory, paper optoelectronics is recently arising. Cellulose is biocompatible, biodegradable, recyclable, lightweight, flexible, foldable, and low cost. These features are especially remarkable when compared to petroleum-based plastics.[183,184] It can be extracted from cotton, wood, hemp, algae, bacteria, agro-industrial wastes, among others. The cellulose production cost is very low (<0.5 cent m^{-2}), while it can reach a cost between 0.3 and 3 \$ m^{-2} in the form of printing paper.[185] In addition, it can also be produced using bacteria, leading to the so-called nanocellulose.[169] The BC (bacterial cellulose) market was valued at US\$ 207.36 million in 2016, and is expected to reach US\$ 497.76 million by the end of 2022 and to surpass US\$ 700 million in 2026. The total capital investment for an industrial facility capable of producing 504 tons of BC per year was about US\$ 13 million. The manufacturing cost of BC is estimated to be US\$ 7.4 million per year, and the net profit to be US\$ 3.3 million per year.[186] Commonly, BC is produced through a fermentation process involving *Acetobacter xylinum*, a nonpathogenic mesophilie and an aerobic Gram-negative bacterium. The fermentation process requires pH values between 3 and 7 and a mild temperature (25–30 °C). The use of glucose as carbon source during BC production leads to the formation of gluconic acid that complicates the pH stabilization in the medium, requiring the presence of various additives. Almost 30% of the overall production cost depends on the fermentation medium; hence this is a huge limiting factor to the industrial production of BC. Thus, innovative and cost-effective carbon sources as well as culture mediums are necessary toward a sustainable and competitive BC production on an industrial scale.[187]

In general, cellulose consists of fibers of a polydisperse linear homopolysaccharide (poly-β(1,4)-D-glucose) with a syndiotactic configuration, i.e., an ordered arrangement of the pendants groups along the chain. The peripheral chains exhibit both interchain and intrachain hydrogen bonds, which enhance the structural and thermal stabilities, leading to a tensile strength of up to 140 GPa and withstanding temperature up to 250 °C.[37,188] The most relevant mesostructures derived from cellulose are rod-like cellulose nanocrystals (CNCs) and cellulose nanofibrils (CNFs). CNCs are highly crystalline needle-like cellulose crystals of 10–20 nm in width and several hundred nanometers in length. CNFs, whose morphology and dimensions can vary significantly according to the degree of fibrillation, contain amorphous cellulose and are not as highly crystalline as CNCs. The former is generated from the amorphous regions between crystallites, upon acid hydrolysis of wood cellulose fibers. The latter are isolated by breaking the interfibril hydrogen bondings, leading to long and flexible nanofibrils that resemble the individual elementary fibrils in cell walls (Figure 4).[61]

Regarding its suitability for thin-film device applications, standard uncoated paper presents some disadvantages, such as microscale surface roughness, opaqueness, high porosity with large pores, hygroscopicity, and poor dimensional stability upon changing the moisture level.[189] However, the physical properties of cellulose-based materials can be easily engineered to a high degree, allowing the construction of ideal substrates with i) flat surface, ii) excellent optical features, e.g., transmittance of up to 90% in the visible region and refractive index of 1.48, iii) good mechanical features, e.g., Young modulus varying up to 80 GPa,[189,190] iv) thermal properties, stability over 300 °C for dehydrated cellulose,[191] v) chemical stabilities , e.g., excellent inertness toward solvents, as well as numerous oxidation and reduction agents, and vi) enable an inexpensive and scalable production. In addition, it has recently been shown how to straightforward optimize the transparency and haze, i.e., ratio between diffuse and total light intensity of paper-like material with beneficial optical properties.[192] This chemical structure results in a linear polymer with a high polar surface because of the multiple hydroxyl groups, and biodegradable properties, which makes it an excellent candidate for the manufacturing of cheap and ecofriendly electronic devices.[193] The field has, therefore, quickly advanced, as presented in these excellent reviews dealing with paper optoelectronics.[57,62,194,195]

4.1.3. Chitin and Chitosan

An enormous number of living organisms use chitin,[196] while it is the single largest waste resource for the fish processing industry (10^6 tons annually), the global market of chitin and derivatives should reach \$4.2 billion by 2021.[197] Chitin consists of units of *N*-acetyl-D-glucosamine covalently bonded via β(1,4) glycosidic bonds (Figure 4). It occurs naturally as ordered crystalline microfibrils mainly forming structural components in the exoskeleton of arthropods or in the cell walls of fungi and yeasts. Up to date, the principal chitin sources have been crab and shrimp shells. The variability in the raw materials, the harshness conditions of the deacetylation process (strong alkali treatment), and the inconsistency of the grade of deacetylation and protein contamination are the most relevant issues limiting the industrial scale production of chitin and chitosan.[198] However, a "green conversion" of agro-industrial wastes by the biological activity of *Rhizopus arrhizus* and *Cunninghamella elegans* bacteria strains can also be used to produce chitin and chitosan. Such industrial sources have significant advantages including independence from seasonal factors, avoiding allergic

© 2021 The Authors. Advanced Energy Materials published by Wiley-VCH GmbH

reactions in individuals susceptible to shellfish antigens, ease of large-scale production and reduction in time and cost of production. In addition, the standard extraction process from the fermentation medium is simple and cheap. This consists mainly in deprotonation in weak basis condition and separation of insoluble component via centrifugation. Upon adjusting the pH of the acidic extract, chitin and chitosan are then separated between each other and the crude products are washed and finally air-dried.[199,200]

Like other natural glucose-based polymers, chitin is generally insoluble or partially soluble in water or common organic solvents owing to its intrinsic structural stability. When chitin is deacetylated with a degree above 50%, it becomes soluble in aqueous acidic media and it is called chitosan. Furthermore, the presence of numerous functional groups, like hydroxyl, carboxyl and amino, allows the main chain of the polymer to be functionalized in different ways, allowing the control of its optical, e.g., transmittance of 91% in the entire visible range as well as refractive index of 1.54 at 633 nm, which minimizes light scattering, mechanical, e.g., elastic modulus of 4–5 GPa and low coefficient, and thermal features, e.g., low coefficient thermal expansion (CTE) of 18 ppm K^{-1}. Chitosan is largely used in different applications in the form of solutions, gels, fibers, or stable thin-films.[51,196,201,202] Noteworthy, chitin and derivatives have been already employed successfully in optoelectronic devices in the form of thin film (Section 5).[202,203]

4.1.4. Lignin and lignosulfonates (LS)

Lignin and lignosulfonates are water-soluble anionic polyelectrolyte polymers obtained as by-products from the production of wood pulp using sulfite pulping, currently almost 70 milion tons of lignin are produced annually worldwide. Despite huge efforts to find higher end-life applications for these by-products, most of the lignin and lignosulfonates produced from paper industry are burned as low-value fuel to generate electricity. Better valorization of these by-products is highly desired by either paper industry (more profit) and environment (less greenhouse gases emission).[204,205] Thanks to its stiffening properties, e.g., crosslinking is obtained in mild conditions through condensation and repolymerization, the different forms of isolated lignins have been harnessed in manmade polymeric materials for many decades. Owing to lignin's character as small, mostly spherically shaped, multifunctional molecule, the longest and the most intensively investigated application has been the use in thermosetting materials, in general, and in phenolic resins for wood bonding, in particular.[206] The well-recognized variabilities of isolated lignins can be solved by targeted chemical modification, opening pathways to the use of pulp lignins in biodegradable (or compostable) polymeric materials. The aromatic structure and electron transfer property of lignin has recently attracted some attention for its use in optoelectronics, especially as superior hole transporter in OSCs and PSCs.[207,208] Indeed, lignin and its derivatives contain several aromatic rings that strongly absorb in the ultraviolet range of the electromagnetic spectrum. In organic electronic devices, hole transport process is associated with the oxidation of electron-rich compounds, such as thiophene in PEDOT:PSS and carbazole in poly(vinylcarbazole). Lignosulfonate poses exceptional hole-transfer characteristics owing to oxidation of phenols and J aggregation phenomenon. The latter is responsible for the semiconductive nature of lignosulfonates, showing promising hole mobility in thin films of 3.75×10^{-6} cm^2 V^{-1} s^{-1}.[206,209]

4.1.5. Starch

Starch is an abundant polysaccharide found in plants,[210] and it is composed of two kinds of polysaccharides, amylose and amylopectin. Amylose bears D-glucose residues with linear α-(1→4) linkages, while amilopectine in a linear amylose-like α-(1→4) linkages and α-(1→6) branch linkages. The most relevant types of starch sources are potatoes, maize, wheat, and rice. The wide range of properties of the starches from these species lies not only in the different ratio of amylose and amylopectin, ranging from 17% to 70% and 83% to 30%, respectively, but also on the differences in the nonstarch components (lipids, proteins, and inorganic salts). Commonly, upon extraction from the raw material, chemical and physical modification steps are required to improve the properties of the starch-derivative. However, enhancement of the physico-chemical properties may also be achieved by the handling of starch biosynthesis in the plant itself by breeding or through genetic manipulation.[211]

Starch is commonly functionalized through crosslinking, to increase the resistance against high temperatures, low pH, and high shear stress. As well, the functionalization rules viscosity and textural properties.[212] In PVs, it has been used to fabricate bio-based electrolyte gels for DSSCs (Section 5.3).[213] As its stability and ion conductivity depend on the amylose content, only starch with high amylose content has been applied.[169] In addition, disposable organic electronics have also been demonstrated with starch paper, featuring, for example, a transparency of 93% in the visible and IR range, tensile strength of 20.0 MPa, and an elongation of 0.48 mm for a 20 mm^2 sample containing 0.5% in weight of poly vinyl alcohol.[214]

4.2. Amino Acids and Proteins

4.2.1. Amino Acids

They are organic compounds containing carboxylic and amino groups along with a specific side group that defines each amino acid (Figure 4). Although hundreds of amino acids are known, only 20 are genetically encoded. They are building blocks for proteins and are used in many industrial applications as bulk biochemicals to produce a wide range of products, such as animal feed additives and flavor enhancers in human nutrition, or as ingredient in cosmetic and medical products.

The amino acid market demand is increasing since the production of monosodium glutamate started, in far 1907.[215] Therefore, the interest in investigating and developing new routes to produce them in a more cost-effective and sustainable way has significantly increased in the last years. Amino acids can be produced by different processes, such as extraction from protein hydrolysates, chemical synthesis or via enzymatic fer-

© 2021 The Authors. Advanced Energy Materials published by Wiley-VCH GmbH

16146840, 2021, 43, Downloaded from https://onlinelibrary.wiley.com/doi/10.1002/aenm.202100520 by Universita Di Torino, Wiley Online Library on [21/02/2025]. See the Terms and Conditions (https://onlinelibrary.wiley.com/terms-and-conditions) on Wiley Online Library for rules of use; OA articles are governed by the applicable Creative Commons License

16146840, 2021, 43, Downloaded from https://onlinelibrary.wiley.com/doi/10.1002/aenm.202100520 by Universita Di Torino, Wiley Online Library on [21/02/2025]. See the Terms and Conditions (https://onlinelibrary.wiley.com/terms-and-conditions) on Wiley Online Library for rules of use; OA articles are governed by the applicable Creative Commons License

mentation through microorganisms, in particular *Corynebacterium glutamicum* and *Escherichia coli*.[216] The main advantages of the former method concern the use of industrial by-products as raw materials, its simplicity and the well-established chemical plants. Nevertheless, the amino acids yields are usually low, since the production of toxic by-products may take place. In this case, the amount of wastewater is huge. In addition, it is suitable only for a few amino acids, such as L-cysteine, L-leucine, and L-tyrosine. The chemical synthesis consists in the reaction of hydrogen cyanide, D-methylbenzylamine, and an aldehyde in methanol. Then, the hydrolysis of the amino nitrile leads to an *N*-methylbenzyl amino acid and, finally, a hydrogenolysis step removes the methylbenzyl group leading to the desired amino acid. The major limitations are the hazardousness of the cyanide sources and the separation steps required to obtain an enantiomeric pure product. Up to date, the fermentation process is the most used one at the industrial scale, due to economic and environmental advantages, as well as to the development of new genetic engineering techniques. Furthermore, it can be operated at mild conditions. In addition, nowadays it is possible to produce amino acids using also residues and waste streams as feedstock that do not competes with human food. By contrast, fermentation based on aerobic bacteria requires sterility, high-energy consumption for oxygenic transfer, and water addition that affect capital and operation costs. In addition, innovative and expensive separation techniques, such as the nanofiltration membranes, are required for an effective isolation of the products.[217] In PVs, they have been applied to process films, as electrochemical redox species, additives for surface passivation or dipole surface enhancement (Section 5.1). For instance, the presence of a polar amino group can be exploited to form interfacial dipole moment at the electrode interface, while the carboxylic group allows for a successful adhesion to titania nanoparticles (NPs) used in both DSSCs and PSCs. In the latter, it has been demonstrated that amino acids reduce the defect density upon perovskite crystallization, leading to a remarkably enhanced charge extraction and transfer. The excellent results and easy production are, indeed, fueling an increasing interest in PSCs and DSSCs.

4.2.2. Polypeptides

Two consecutive α-amino acids can form a peptide bond, leading to a linear chain of amino acid residues called polypeptide. The latter can be arranged in a biologically functional protein (Section 4.2.3). Generally, proteins own a unique sequence of different amino acids that is encoded in the genome, but it is also possible to find polypeptides made of only one type of amino acid. Polylysine is the most common homopolypeptide that can be found in nature, and contains two different amino groups, i.e., those bonded with either α-carbon or ε-carbon, leading to α-polylysine (α-PL) or ε-polylysine (ε-PL). The latter is mainly used as food additive,[218] while the former is commonly used to coat tissue culture as an attachment factor.[219] This unique features is based on the positively charged hydrophilic amino group at pH 7 that polylysine owns and makes this biopolymer appealing for various application, such us delivery of DNA,[220] proteins[221] or therapeutic agent[222] and surface modifier-vide infra. Despite ε-polylysine is produced commonly by natural fermentation in strains of bacteria in the genus *Streptomyces*, α-polylysine is still synthetically produced by polycondensation reaction. The cost of ε-PL production using traditional raw materials is estimated to be 4.94 \$ kg^{-1}.[223] Although a proper cost analysis has not been found for the α counterpart, the different productions result in a selling price around 2.25 \$ g^{-1} for ε-PL and 6000 \$ g^{-1} α-PL. Their use in optoelectronics is similar to that of amino acids, owing to their dipolar nature and the surface modification properties (Section 5.1).

4.2.3. Proteins

Proteins are macromolecules consisting of one or more polypeptides that rearrange to perform a vast array of functions within organisms like catalysis (enzymes), cell signaling, and structural support (fibrous proteins like collagen, elastine, and keratin). Proteins can also interact with other small molecules, such as co-factor, and with other proteins to perform complex tasks like photosynthesis. Photosynthesis is the largest-scale sustainable effective solar-to-energy conversion system in nature,[224,225] which already inspired artificial PV systems.[226] Using natural protein complexes from biosources present some advantages, such as abundance, cost-effectiveness, easy scale-up, nontoxicity, sustainability, and very high absorption efficiency. However, their stability out of cells and the lack of optimized charge transfer events represent critical bottlenecks.

There are four major protein complexes involved in light-dependent reaction, namely photosystem II (PSII), cytochrome b6f complex, photosystem I (PSI) and ATP synthase that work together to produce ATP and NADPH. PSII absorbs photons at 680 nm, and splits water in electrons, protons, and oxygen, cytochrome b6f complex helps the transfer of electrons, while PSI absorbs photons at 700 nm and helps in pumping protons and transfer electrons. The competition for mostly the same wavelength range for the two photosystems required in photosynthesis reduces the overall photochemical efficiency of the process. In this regard, efforts have been done to control the energetic gap between the photosystems by, for example, engineering variants present in cyanobacteria that absorbs further into the near-IR.[227,228] Moreover, all photosynthetic organisms also contain light-gathering antenna systems, such as light-harvesting complex II (LHCII), with pigments able to collect energy and transfer it to the reaction centers (Figure 4). The integration of this very efficient antenna, or directly of the pigment, in hybrid devices with an optimal energy level alignment could lead to relatively high performing devices. Efforts have been already done in this direction, especially thanks to the DSSC concept, and the reader is invited to have a look at Section 5 and these dedicated reviews.[56,59,60,229]

With regard to photosystem protein complexes, the standard extraction process is applied directly to the leaves. A homogenization step in a buffer solution leads to a slurry that is purified through centrifugation and filtration. A final purification step by column chromatography leads to a concentrated solution of the desired proteins.[230]

© 2021 The Authors. Advanced Energy Materials published by Wiley-VCH GmbH

16146840, 2021, 43, Downloaded from https://onlinelibrary.wiley.com/doi/10.1002/aenm.202100520 by Universita Di Torino, Wiley Online Library on [21/02/2025]. See the Terms and Conditions (https://onlinelibrary.wiley.com/terms-and-conditions) on Wiley Online Library for rules of use; OA articles are governed by the applicable Creative Commons License

4.3. Others

4.3.1. Catecholamine and Derivatives

Catecholamine is a class of neurotransmitters and hormones that display a catechol (*o*-dihydroxylbenzene) and an amino group as side chain (Figure 4). Leading examples are dopamine and norepinephrine. All the catecholamine's derivatives are synthesized from the amino acid L-tyrosine in the brain, in the adrenal medulla, and by some nerve fibers. The development of catecholamine-based coatings in 2007 by Lee et al.[231] was a major advance in surface science. Thanks to the rich density of functional groups, this class of compounds is able to functionalize numerous types of surface in an effective way.[232] They are very susceptible to oxidation and polymerization in eumelanin-like structure, displaying a strong adhesion capability with a controllable film thickness and a long stability under ambient conditions. In addition, polydopamine (PDA) displays appealing properties similar to melanin with respect to optics, i.e., intense and broadband absorption ranging from UV to visible region and electronics, e.g., hydration-dependent electrical and photoconductivity ranging from 10^{-8} to 10^{-4} S cm^{-1}, depending on the hydrated state.[233,234] Moreover, the presence of peripheral groups serve as anchors for the loading of transition metal ions, realizing hybrid materials.[235] In general, hybrid catecholamine-based materials have been already successfully employed in different fields, such as batteries,[236] supercapacitors,[237] drug delivery,[238] water treatment,[239] optoelectronics,[240–242] and of course, PVs.[243–245]

Since the supply of catecholamine derivatives is vital in case of neural diseases, such as Parkinson's one, their production has been widely investigated. For instance, the total global market of only L-3,4-dihydroxyphenylalanine (L-DOPA), a precursor of dopamine, is about $101 billion per year and its production still relies on asymmetric chemical synthesis proposed by Monsanto in the 1960s.[246] However, this method presents low conversion rate and enantioselectivity and depends on expensive metal catalysts. Several biotechnological productions of catecholamine derivatives have been proposed since the early 2000s, but, in order to be effectively competitive, they still need to face the long operation times and complex purification steps issues. For instance, compared to fast chemical synthesis, microbial fermentation takes over 10 days and the culture media usually includes hundreds of other molecules and proteins.[247] The most promising biotechnological production process involve biocatalytic conversion with immobilized enzymes. It is a single step process, which occurs under mild conditions, and it is based on a reusable immobilized biocatalyst. It shows outstanding enantioselectivity, but the low yield and stability of the enzymes hamper its use on an industrial scale. Efforts have been done to fabricate more suitable supports for the immobilization of the enzymes, reaching promising stability of over 120 days.[248] Nevertheless, the conversion rate were not really enhanced and intense research is still needed in this direction.

4.3.2. DNA

DNA is a biopolymer that contains crucial genetic information for the synthesis of RNA and proteins. It consists of two strands coiled around each other in a double-helix structure of monomeric units called nucleotides (Figure 4). Each nucleotide owns a phosphate group, a pentose sugar, and a nitrogenous base and, noteworthy, the phosphate backbone is negatively charged, with Na^+ or H^+ as counter ions, which make DNA soluble in polar solvents and easily processable by spin coating. In most cases, DNA for bio-based optoelectronic devices is extracted from natural resources like salmon fish. Usually, the samples are seeded with bacterial culture and homogenized with a solution buffer. The homogenate is centrifuged, while the pellets are resuspended in a solution buffer and finally incubated. Then, a solution of hexadecyl trimethylammonium bromide (CTAB) and sodium chloride is added before the next incubation step. Proteins are, then, removed by a single liquid extraction, while DNA is precipitated. Further purification steps involve centrifugation, ether separation, and/or column purification. Through this standard protocol, the yield of DNA is often low due to the multiple steps.[249]

DNA was shown to exhibit, i) excellent thermal stabilities up to 140 °C in its solid form,[250] and ii) easy tunability via chemical and physical treatments.[251] Indeed, DNA has successfully been used in optoelectronics,[46,252–257] especially as anionic template of gold nanowires,[258] gate dielectric,[259] hole-transport layer and electron blocking layers due to the favorable energy levels (HOMO: −5.2 eV; LUMO: −1.1 eV) to inject charges.[254] Despite its successful application in optoelectronics, it has received by far less attention in the PV field. We will review the handful number of paper on DNA-based PVs, highlighting the most relevant benefits and limitations.[83,121,162,260–263]

4.3.3. Natural Pigments

Flavonoids consist of two benzene rings connected via γ ring (Figure 4), leading to two types of Flavonoid structures. They can be easily extracted from vegetables species from different parts of the plants, like roots, stems, leaves, flowers, and fruits. Several compounds of this family have been applied to PVs due to their interesting absorption features, e.g., wide range of colors, extended π conjugation and absorption in the visible range, tunability of the color stability features depending on pH. For instance, anthocyanins are the most abundant and widespread pigment, they exhibit a broad band absorption spectra in the visible region and their derivatives can be easily anchored onto mesoporous metal oxide electrode via carboxylic and hydroxyl groups.[264] Likewise, betalains are a small group of water-soluble indole derivatives featuring a broad absorption in the visible region and a short excited state lifetime that has been successfully exploited in DSSCs.[265]

Carotenoids are organic natural pigments present in plants, algae, fungi and in several bacteria. Most of them are composed of a C_{40} hydrocarbon backbone including structural and oxygenic transformations. They present absorption spectra ranging from 380 to 550 nm and an extinction absorption coefficient that far exceed those of standard electron donors, like P3HT, i.e., 1.4×10^5 versus 2×10^4 cm^{-1} mol^{-1} L.[266] Thanks to their extended π-conjugation, carotenoids are good candidates to substitute p-type semiconductors, but they lack effective functional groups to attach to semiconducting electrodes, leading to low photocurrents.[267] Up to date, crocetin is the most performing

© 2021 The Authors. Advanced Energy Materials published by Wiley-VCH GmbH

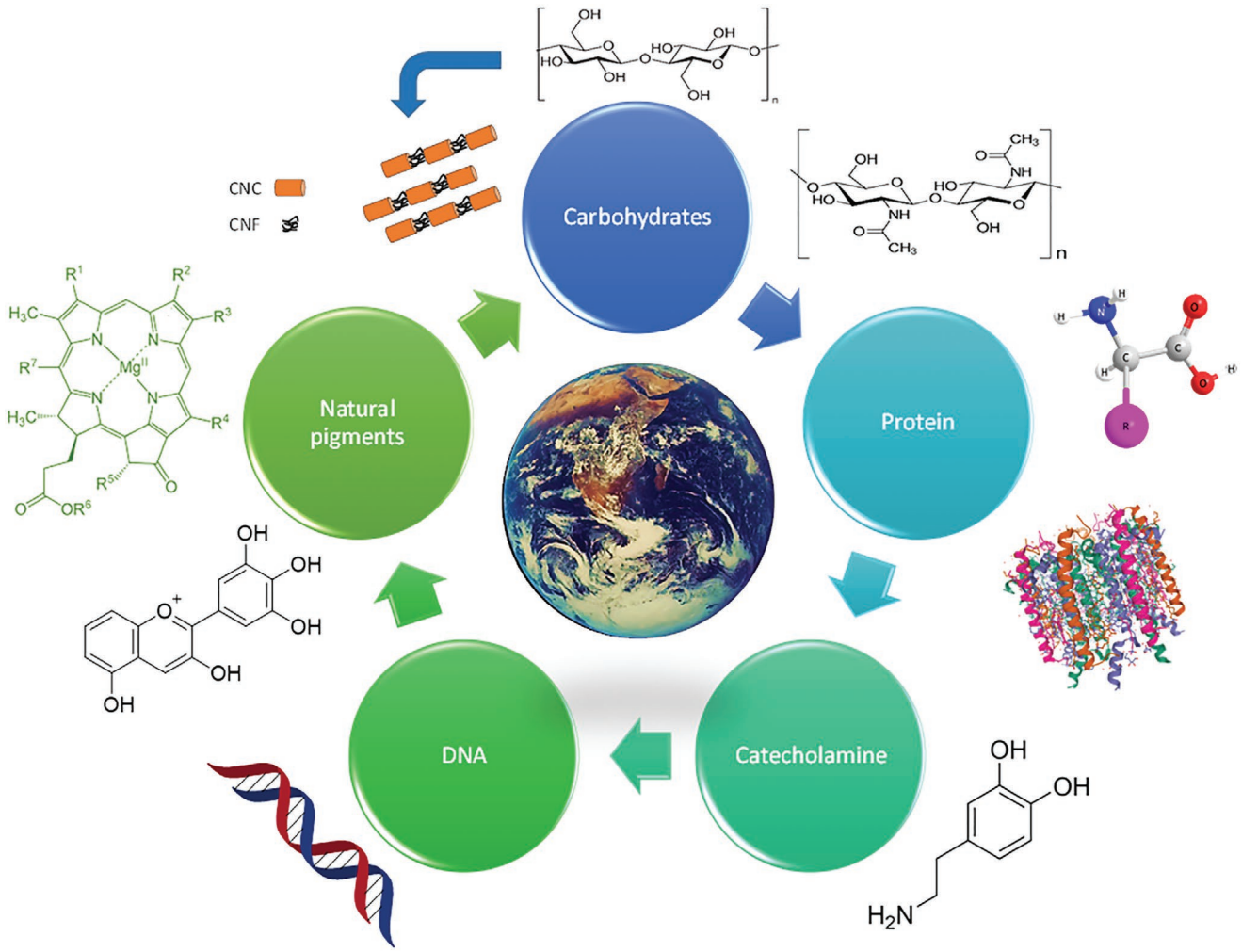

Figure 4. Principal categories of bio-derived materials that have led to an improvement in device performances, stability, and sustainability.

carotenoid that has been employed in DSSCs.[268] Chlorophylls are the natural photosynthetic pigment found in plants and bacteria. The basic structure includes a porphyrin ring coordinated with a central metal ion bearing different side chains (Figure 4). There are six different types of chlorophyll and the most common one is chlorophyll-α. Despite their efficient light-harvesting mechanism and electron-transfer reactions, they suffer lack of stability and they are extremely dependent on the conditions of the extraction process.[269] This has limited their use in solar cells, as they reached poor efficiencies (<1%).[270] Usually, lipids and cellular components are removed through consequential steps of washing and centrifuging. Then, a final step of purification involving filtration or column chromatography is required to achieve pure product.

5. Bio-Derived Materials in Devices

This section describes the most relevant concepts and achievements realized implementing bio-derived materials in the active layer/photosensitizers, charge transporting layers, electrolytes, substrates, electrodes, light-trapping layers, and sealant films. These constitute the core of the following section that is divided into OSC, PSC, and DSSCs. **Tables 1–3** summarize the figures of merit of all the discussed devices in this section.

5.1. Bio-OSCs

5.1.1. Active Layer

Proteins: Among the plethora of photosynthetic membrane proteins, LHCII is the most abundant on Earth and it has already shown high efficiencies in absorbing and transferring solar energy.[271–273] Unfortunately, LHCII complexes are bulky poor conductors and this might be attributed to the non-ohmic contact with the electrode for a thicker LHCII modification layer, while a single protein monolayer absorbs a relatively small portion (<1%) of the sunlight. This represents the major challenge in the field. In 2016, Yao et al. reported a ground-breaking work coupling metallic nanoparticles that exhibited strong localized surface plasmon resonance to the LHCII.[105] The implementation of metallic nanoparticles is a promising strategy due to

© 2021 The Authors. Advanced Energy Materials published by Wiley-VCH GmbH

16146840, 2021, 43, Downloaded from https://onlinelibrary.wiley.com/doi/10.1002/aenm.202100520 by Universita Di Torino, Wiley Online Library on [21/02/2025]. See the Terms and Conditions (https://onlinelibrary.wiley.com/terms-and-conditions) on Wiley Online Library for rules of use; OA articles are governed by the applicable Creative Commons License

their tunable optical properties and the ability to enhance the total number of excitons created in adjacent photoactive. This is caused by the intense local electric field upon resonant excitation.[274–276] In detail, the group built a plasmonic metal/photosensitizer nano–bio hybrid for broadband light harvesting by mixing silver nanoprisms (Ag-530) with the natural sensitizer LHCII. This innovative layer displayed multiple advances: i) broad-band optical absorption enhancement and a consequent photocurrent increase from the complementary contribution of Ag-530 and LHCII, ii) enhanced light harvesting from the protein complex induced by the plasmonic field of Ag-530, and iii) excellent compatibility with the well-established fullerene-based acceptor. The devices featured the architecture ITO/ZnO/Ag-530:LHCII/polymer:$PC_{71}BM$/MoO_3/Ag, in which they used PIDTT–DFBT, PBDT–DTNT, and PTB7-Th as polymers. Among them, the latter showed the best performance, namely PCE of 10.57%, J_{SC} of 17.99 mA cm^{-2}, V_{OC} of 0.80 V and FF of 73% (Table 1). This represents a ≈20% enhancement in device efficiency compared to reference devices.

In 2017 Ajeian's group,[106] inspired by the works of Cliffel's group,[277,278] and Gordiichuck,[279] who demonstrated that biological components can be integrated in OSC without diminishing the optoelectronic properties, built a bio-organic solid state SC based on PSI extracted from young spinach leaves. PSI is involved in both direct and indirect electron transfer reactions, and exhibit a perfect conversion of absorbed photons to electrons, reaching EQE of almost 100% (Section 4.2).[230] Here, the major challenge is the control of the PSI morphology to achieve high efficiencies. In this case, they disclosed that the presence of a Tyrosine layer deposited onto ITO prior to the deposition of PSI film has an enormous impact onto the performances of the solar cell. Tyrosine improves the alignment of the PSI layers increasing carrier mobilities. The solar cells with architecture ITO/Tyrosine/PSI/C_{60}/Au exhibited PCE of 0.52%, J_{SC} of 3.47 mA cm^{-2}, V_{OC} of 0.36 V, and FF of 33% (Table 1). Although the PCE is low compared to those of the state-of-the-art of OSCs, the regulation of the PSI layer morphology through the presence of Tyrosine to control carrier mobility is demonstrated by the high value of current density. In detail, the introduction of a Tyrosine buffer layer led to a fivefold enhancement of J_{SC} compared with the prior art of PSI-based PV.[279] The fine control of the PSI active layer might be key for future achievements-vide infra. In parallel, the same group also proposed a new strategy to achieve a favorable energetic band alignment for an efficient charge transfer from the PSI to electrodes.[85] Remarkably, upon photoexcitation of PSI, almost 66% of the formed charge carrier are concentrated in the top of the system, where the iron–sulfur clusters are located (F_b^-). Consequently, a permanent dipole is formed with the positive terminal side (P_{700}^+) and it is possible to exploit the charge separation to build a single-component bio-SC, without the requirement of an acceptor compound. The device with structure FTO/PEDOT:PSS/PSI(800 nm)/LiF(2 nm)/Al exhibited the following figures of merit: PCE = 0.07%, J_{SC} = 0.96 mA cm^{-2}, V_{OC} = 0.25 V, and FF = 31% (Table 1). Despite the promising results for a single-component OSC, the random distribution of PSI systems is still a challenge. Ideally, PSI should be deposited layer-by-layer, generating a vertically assembled network, allowing the direct flow of dissociated charge carriers through the PSI layers toward the electrodes.

In this context, it is important to give visibility to the pioneering work of Kumar and collaborators.[280] They used the so-called artificial membrane approach introducing a PSI-based poly(butadiene)$_{12}$–poly(ethylene oxide)$_8$ (PB_{12}–PEO_8) block copolymer membrane, miming the lipid double layer and stabilizing PSI. To efficiently couple the structure with an electrode, they introduced a second layer based on the same copolymer and a conjugated polymer with a phenylene vinylene core and two alkyl chains with terminal quaternary ammonium groups that allows electron transfer across the artificial membranes (**Figure 5**). The proof-of-concept devices achieved photocurrents of 35 μA cm^{-2} that represented a twofold enhancement comparing with the state-of-the-art of PSI-based system achieved in 2014.[281] The development of new systems able to stabilize membrane proteins will play a crucial role in the development of new bio-electrochemical devices as well as bio-derived PV devices.

DNA: Supramolecular polymerization represents a powerful bottom-up concept to achieve 2D and 3D chromophore arrangements for functional π-systems. In this sense, DNA has been successfully used to control shape, size, and arrangement of chromophore assemblies.

In 2013, Sezi and Wagenknecht's groups showed that oligo-2′-deoxyadenosines $(dA)_x$ provides an excellent template for the self-assembly of an ethynylpyrene-2-deoxyuridine conjugated (Py-dU), circumventing the limitations concerning the covalently linked oligochromophores.[282] Indeed, further progress was, for example, demonstrated in mixed assemblies of Py-dU and ethynyl-Nile-red-modified nucleoside (Nr-dU) along $(dA)_{20}$, realizing dual emission as a result of energy transfer between the two different chromophores.[283] In 2016, the same group did a pioneering work by covalently attaching a fullerene to the $(dA)_{20}$ template to obtain charge separation after energy transfer and light-harvesting in the oligonucleotide–chromophore stacks.[107] The fullerene–DNA conjugate was incorporated into OSCs with inverted structures, i.e., ITO/ZnO cathode and a MoO_3/Ag anode. The photoactive layer comprised representative assemblies with a chromophore ratio Py–dU:Nr–dU of 8:12. Upon illumination of AM1.5, these devices showed a V_{OC} of 0.67 V and an EQE of 0.2%. The low EQE was attributed to the low fullerene concentration (3.5 wt%) that hampers the transport of electrons to the cathode. Nevertheless, this work clearly demonstrated that DNA has a significant potential as key structural element for chromophore assemblies in functional π-systems, which may be further exploited in PVs.

Natural Dyes: Recently, Vohra et al.[270] successfully used β-carotene as electron donor in OSCs, achieving a fourfold enhanced performance compared to the state-of-the-art of carotenoid-based solar cells, i.e., PCE = 0.15%; J_{SC} = 0.86 mA cm^{-2}; V_{OC} = 0.63 V; and FF = 28%.[82] This result was thoroughly investigated via microscopy and spectroscopic assays. The authors pointed out an unexpected thickness dependence behavior that correlate the best performing output with an ultrathin active layer (≈30 nm). Using thin active layers improved the J_{SC} without showing a trade-off a lack of light absorption through the entire active layer caused by the high extinction absorption coefficient of β-carotene. The device with structure ITO/ZnO/β-carotene:$PC_{71}BM$ (1:4)/MoO_3/Ag showed a PCE of 0.53%, J_{SC} of 3.51 mA cm^{-2}, V_{OC} of 0.46 V, and FF of 33% (Table 1). Higher

© 2021 The Authors. Advanced Energy Materials published by Wiley-VCH GmbH

16146840, 2021, 43, Downloaded from https://onlinelibrary.wiley.com/doi/10.1002/aenm.202100520 by Universita Di Torino, Wiley Online Library on [21/02/2025]. See the Terms and Conditions (https://onlinelibrary.wiley.com/terms-and-conditions) on Wiley Online Library for rules of use; OA articles are governed by the applicable Creative Commons License

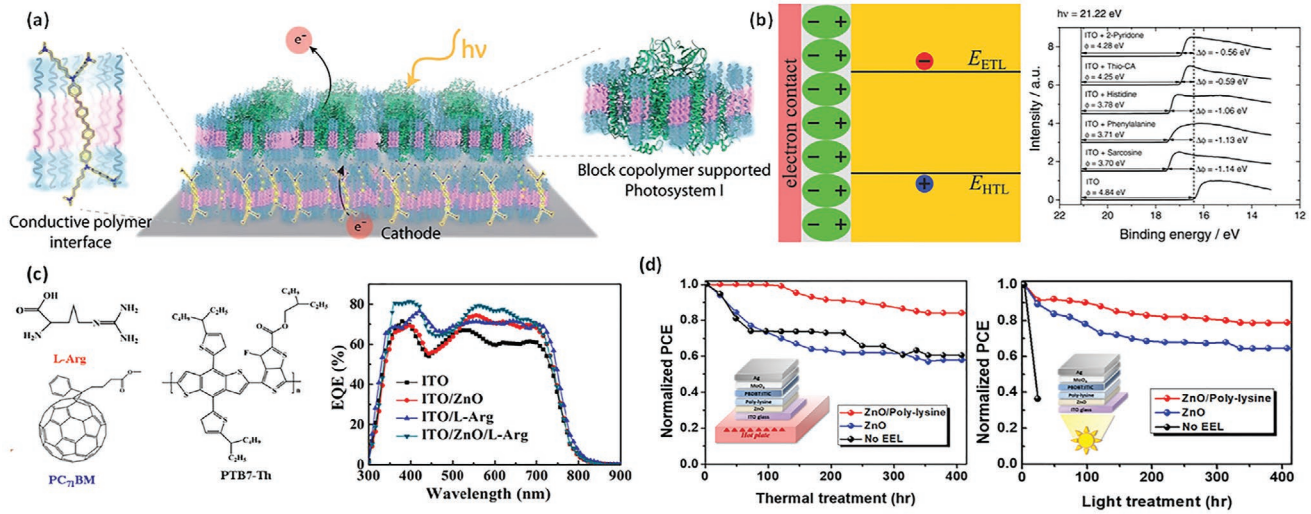

Figure 5. a) Design of photosystem I (PSI) block copolymer integrated membrane.[280] Copyright 2016, The Royal Society of Chemistry. b) Scheme of the device geometry used for numerical simulations; work function values determined by UPS measurements of five different dipole layers adsorbed on ITO coated glass substrates.[49] Copyright 2016, Wiley-VCH GmbH & Co. KGaA, Weinheim. c) Chemical structure of L-Arg, PTB7-Th and PC71BM and EQE curves of different ETLs devices.[84] d) Thermal- and photostability of different PV devices with and without PLL interface layer. The active layer of the stability study was PBDB-T:ITIC BHJ. Reproduced with permission.[50] Copyright 2020, The Royal Society of Chemistry. Copyright 2020, Elsevier B.V.

thicknesses led to a detrimental impact of the device efficiency, reaching, for instance, PCE 0.28% with 90 nm active layer.

Chlorophyll show an ambipolar behavior, being suitable as both electron donor and electron acceptor, when coupled with, for instance, P_3HT and $PC_{61}BM$, respectively.[284,285] A recent progress by Wang's group[286] showed that it is possible to build OSCs with entire active layers consisting of linear carotenoids (i.e., lycopene) and chlorophyll derivatives. The device with architecture ITO/MoO_3/lycopene:chlorophyll (1:4)/Ca/Al exhibited a PCE of 0.045%, J_{SC} of 0.23 mA cm^{-2}, V_{OC} of 0.85 V, and FF of 23% (Table 1). The poor performances of the so-fabricated devices were mainly attributed to the low electron mobility of disordered spin-coated chlorophyll-based thin film. Likewise proteins - vide supra, natural components have evolved in a well-organized system, and such order has to be maintained to ensure efficient charge/energy transfer processes.

To summarize, the introduction of bio-derived hybrid materials in the active layer allows i) broad-band optical absorption enhancement and a consequent photocurrent increase, ii) enhanced light harvesting due to the high extinction absorption coefficient that unlock the fabrication of extremely thin devices, and iii) outstanding compatibility with established photoactive materials. Nevertheless, the performances reached by bio-based OSCs are still far from the state-of-the-art of the technology. The interest in the field of the scientific community is constantly growing and it is mainly focused on i) achieving fine control of the layer morphology and orientation and ii) reaching optimal energy alignment levels and charge transport features. The key efforts in this field are directed toward thin film fabrication techniques, surface functionalization, and peripheral functionalization of the aforementioned materials.

5.1.2. Charge Transporting Layer

Amino Acids: The presence of a polar amino group can be exploited to form a permanent interfacial dipole moment at the electrode interface, allowing for a better charge collection due to the reduction of the work function level of the ITO. This idea has recently been demonstrated by several groups. The reader could also read an excellent comprehensive overview on dipole effects at the interfaces reported by Nüesch.[287]

In 2015, Würfel's group did a pioneering work through numerical simulation of different solar cells architectures.[288] They explained that the essential requirement for efficient charge separation and further collection at the electrode is to create layers featuring highly dominant hole and electron conductivities near the anode and cathode, respectively. Hence, any increase of the concentration of the "wrong" type of charge carriers in proximity to the contact will, therefore, deteriorate the device performance. One year later, the same group and collaborators[49] introduced small molecules with permanent dipole to study how the alignment affects the collection efficiency of electron and holes. Noteworthy, three out of five molecules with permanent dipole were natural amino acids, namely histidine (His), phenylalanine (Phen), and sarcosine (Sarc). They built OSCs with four different donor polymers, i.e., P3HT, PCDTBT, PTB7-Th, and PffBT4T-2OD mixed with $PC_{71}BM$ or $PC_{61}BM$ and the device architecture was ITO/DL/active layer/MoO_3/Ag where DL indicates the interlayer with dipole (Figure 5). All of them enhanced the PV performances, mainly on V_{OC} and FF, while His showed the largest effect regardless of the active layer composition, reaching PCE = 7.4%; J_{SC} = 14.95 mA cm^{-2}; V_{OC} = 0.78 V, and FF = 63% (Table 1). Moreover, the His interlayer outperformed the more established interlayers, such as ZnO, TiO_x, or PFN. Thus, they proved that amino acids are highly effective in converting a nonselective electrode, like ITO, into an electron contact with a high degree of selectivity.

In the same year Li et al. successfully introduced L-arginine (L-Arg) as ETL into inverted OSCs with architecture: ITO/ZnO/L-Arg/PTB7:$PC_{71}BM$/MoO_3/Ag, directly spin coated at 2500 rpm for 40 s from a nontoxic water solution.[84] The device exhibited a PCE of 9.31%, J_{SC} of 17.49 mA cm^{-2}, a V_{OC} of 0.78 V, and a FF of 68%. This accounts to a PCE that is fivefold

© 2021 The Authors. Advanced Energy Materials published by Wiley-VCH GmbH

16146840, 2021, 43, Downloaded from https://onlinelibrary.wiley.com/doi/10.1002/aenm.202100520 by Universita Di Torino, Wiley Online Library on [21/02/2025]. See the Terms and Conditions (https://onlinelibrary.wiley.com/terms-and-conditions) on Wiley Online Library for rules of use; OA articles are governed by the applicable Creative Commons License

improved compared to the reference device without ETL. They also described a new aspect: the L-Arg films increased the lifetime of the OSCs. After 35 days, the average PCE of OSCs with ZnO/L-Arg double ETL feature a loss of 10%, while the reference device with only ZnO showed a PCE of ≈70% of the original value (Figure 5). The authors claimed that L-Arg films help to mitigate the native surface defects of ZnO layer and enhanced the efficient flow of electrons across the junction.

In 2019 Zhu et al.[289] demonstrated the versatility of this strategy implementing charge amino acids interlayers in non-fullerene based OSCs, i.e., ITO/ZnO(30 nm)/Gly/PM6:IT-4F/MoO_3 (10 nm)/Ag (100 nm), realizing PCEs of 14.0%, J_{SC}s of 22.0 mA cm^{-2}, V_{OC}s of 0.85 V, and FFs 75% (Table 1). In line with previous works, a glycine (Gly) modified ZnO film featured lower number of surface defects states and a lower work function. This facilitates both charge transport and collection. In addition, the surface ligand functionalization increased the hydrophobicity, enhancing the interfacial contact between the photoactive and the ETL layers.

Polypeptides: In 2018, Tang's group[290] firstly introduced a poly-amino acid, α-poly-L-Lysine (α-PLL) as effective electron extraction layer to improve the charge transport in fullerene-free OSC. They pointed how boosted PV performances could be obtained with an efficient interfacial doping between the α-PLL layer and the acceptor layer. Finally, they also demonstrated that an amino acid-based layer could be efficiently introduced also with a conventional architecture. This statement is supported by OSCs featuring fullerene- and nonfullerene-based acceptor layers as well as conventional/inverted structures. In all cases, the effect of α-PLL layer was always significantly positive. Among all the configurations tested, the device ITO/PEDOT:PSS/PBDB-T:IT-M/α-PLL (7 nm)/Al (140 nm) achieved the best performances, namely PCE of 11.9% and a J_{SC} of 17.13 mA cm^{-2}, with a V_{OC} of 0.94 V and a FF 74% (Table 1). One year later, Huang et al.[291] attempted for the first time to use two enantiomeric biopolymers, namely poly-L-lysine (PLL) and poly-D-lysine (PDL), as electron extraction layer. Although the consequence of the chiral nature of peptides is well-known in biology and medicine, the effect of the two enantiomers on the electrical performance of OSCs was not explored. They tuned the working function using various arrangements of the amino groups and correlating it with the polarity of the layer. The surface energy results suggested that the hydrophobic characteristic of PLL was favorable to improve the interfacial compatibility with the photoactive layer, while the blend of PLL and PDL led to lower surface potential. They tested the green poly-lysine electron extraction layer in fullerene- and nonfullerene-based OSCs. Regardless of the device, the performance was always boosted and, similar to L-Arg,[84] the integration of these biopolymers improved both thermal stabilities and photostabilities of the devices.

Recently, the same group[50] incorporated a poly-lysine layer as interlayer in ITO-free flexible OSCs based on a novel 100% bio-based polymer, polyethylene furandicarboxylate (PEF) vide infra. As expected, they observed a decreasing of working function of poly-lysine derived ZnO due to dipole formation arising from the arrangements of amino groups, resulting in well-defined blend morphologies to achieve high performance and long-term stability. They studied different anodic configurations, namely glass/ITO, glass/PEDOT:PSS and PEF/PEDOT:PSS and different photoactive layers, specifically PTB7-Th:$PC_{71}BM$, PBDB-T-2F:Y6, PBDB-T:ITIC, and PBDB-T-2Cl:IT-4F. The presence of the interlayer of PLL was always associated with an increase of V_{OC} and $J_{SC,}$ confirming that the work function shift leads to a better energetic alignment. Furthermore, the authors pointed out how the presence of these electron extracting layers exhibits a drastically effect on device stability. For instance, the reference device exhibited a dramatic decrease of PCE after 24 h, while the presence of the interlayers allows retaining 70% of the device performances after 400 h under operation conditions (Figure 5). This is related to the efficient blocking of spontaneous doping occurring at the interface between the active layer and the electrode vide supra. Finally, with regard to thermal-stability studies, the reference device (without interlayer) and the device with ZnO layer only retained 60% of the initial values upon 400 h at 100 °C, while devices with PLL held 80% of initial values.

Polysaccharides: In 2015, Chen's group[292] employed highly dispersed graphene sheets to modify ZnO electron transport layer to improve the PV response. Following up previous work, the authors used ethyl cellulose to obtain highly uniform graphene sheets via liquid ultrasound exfoliation.[293,294] Henceforth, a novel ZnO@graphene:ethylcellulose (ZnO@G:EC) nanocomposite was successfully prepared and implemented in inverted OSC with structure: ITO/ZnO@G:EC/active layer/MoO_3 (7 nm)/Ag (90 nm), in which the active layers were P3HT:$PC_{61}BM$ and PTB7:$PC_{71}BM$ (Table 1). Replacing the pure ZnO layer with ZnO@G:EC decreases the work function from 4.35 V to 3.78 eV, consequently enhancing the electron extraction and transport from the active layer. In addition, the presence of EC in the layer as stabilizer was proved to smoothen the surface, preventing the aggregation of ZnO onto the stacked graphene sheets. The two combined effects resulted mainly in an enhancement of conductivity and J_{SC} and in a consequent twofold improvement of PCE compare to bare ZnO-based devices.

Another inspiring work was carried out by Zhang et al. in 2017.[51] They solved the inhomogeneity of spin coated layers from chitosan solution via its chemical functionalization into an anionic polyelectrolyte *N,O*-carboxymethyl chitosan (NOCC) and a cationic polyelectrolyte quaternized chitosan (QCS). In this way, they took advantage of electrostatic layer-by-layer self-assembly to prepare continuous films. They studied the applications of chitosan as a cathode interlayer in an inverted OSC with architecture: ITO/NOCC:QCS8(7 nm)/PTB7:$PC_{71}BM$(210 nm)/MoO_3 (10 nm)/Ag (100 nm). The optimized OSCs exhibited a PCE of 10.2%, J_{SC} of 20.0 mA cm^{-2}, V_{OC} of 0.76 V, and FF of 67% (Table 1). These values represent an almost threefold improvement compared with reference devices without interlayer.

In 2018, Chueh's group systematically explored chitosan, methyl-cellulose, and dextrin as modifying interlayers for the ZnO electron-transporting layer in inverted OSCs.[201] They pointed out how the "β-type" glucose-based cellulose was the most efficient modifying interlayer for ZnO electron-transporting layer due to a smoother morphology of the thin layers (Table 1). While a similar energy alignment was expected, the authors also discussed that the glucose-based interlayers showed a capability to prevent the formation of aggregates in

© 2021 The Authors. Advanced Energy Materials published by Wiley-VCH GmbH

16146840, 2021, 43, Downloaded from https://onlinelibrary.wiley.com/doi/10.1002/aenm.202100520 by Universita Di Torino, Wiley Online Library on [21/02/2025]. See the Terms and Conditions (https://onlinelibrary.wiley.com/terms-and-conditions) on Wiley Online Library for rules of use; OA articles are governed by the applicable Creative Commons License

the photoactive layer prepared onto them to yield an ideal BHJ morphology.

In 2020, Ouyang and collaborators[295] pioneered the use of carboxymethyl cellulose sodium (CMC) as adhesive, stabilizer, and film former in PVs. They prepared a CMC layer from rice straws and used it as a co-modifying layer with ZnO for the transfer and collection of electrons in inverted OSCs. The best device architecture was ITO/ZnO/CMC/PBDB-T:IT-M(100 nm)/MoO_x (5 nm)/Ag (100 nm), showing PCEs of 11.96%, J_{SC}s of 17.87 mA cm^{-2}, V_{OC}s of 0.94 V, and FFs of 72% (Table 1). The presence of a ZnO/CMC bilayer diminishes the work function of ITO from 4.72 to 4.22 eV. In addition, the J_{SC} increased significantly, i.e., ≈8% higher than that of pristine ZnO-based devices, resulting an improvement in PCE up to 12%. Again, the increase in the current density was ascribed to the enhanced charge extraction from the active layer. All of the devices employing CMC as interlayer showed better performances than those with pristine ZnO interlayers, indicating a strong potential of CMC layer for the interfacial modification of OSCs.

DNA: In 2016, Brown's group successfully employed DNA isolated from salmon fish as electron extraction layer in ITO/DNA/PTB7:$PC_{70}BM$(80 nm)/MoO_3/Ag.[121] They firstly optimized the thickness of the DNA layer using spin-coating. Thin DNA layers led to dramatic enhancement in V_{OC} from 0.39 to 0.71 V, an increase in J_{SC} of almost 20%, and final PCEs ranging from 2.3% to 4.9% for devices without and with DNA layers, respectively. Thus, this work clearly settled the seminal use of DNA in OPVs. Especially, they highlighted the main benefits of using DNA: i) DNA as sodium salt can be processed from solution at room temperature, and ii) it can easily be functionalized with other molecular groups, ions, metal nanoparticles,[296] nanotubes,[297] or wires,[298] which can be used to tailor its electronic influence on PVs.

One year later, the same group' joint efforts with others research groups to further expand the use of DNA layers in OSCs.[83,262] They initially used a DNA nanolayer in concert with a ZnO nanoparticle-based electron transport layer in order to enhance charge separation/extraction efficiencies in OSCs. Since an annealing step was not required, they were able to transfer all layers from glass to flexible substrates. The inverted OSC with the structure: glass/ITO/ZnO/DNA/PTB7:$PC_{70}BM$/MoO_3 (5 nm)/Ag (100 nm) displayed PCEs of 8.31%, J_{SC}s of 18.90 mA cm^{-2}, V_{OC}s of 0.71 V, and FFs of 62%. The same architecture onto PET substrate achieved PCEs of 7.06%, J_{SC}s of 16.92 mA cm^{-2}, V_{OC}s of 0.72 V, and FFs of 58% (Table 1). Importantly, these devices were the most efficient OSCs at that time. The group explained that when DNA is deposited on the ZnO nanoparticles, the work function is lowered from 4.7 eV (bare ITO) to 4.27 eV (DNA–ZnO). In addition, the subsequent spin-coating of the photoactive blend allows the DNA to imprint a different long-range structure on the photoactive polymers with respect to the solar cells without DNA interlayer. The resulting structure is more efficient at extracting the initially formed excitons into separate polarons, improving mainly the J_{SC}.

In 2018, Elfwing et al. developed a new electron transport material based on a self-doped polyelectrolyte PEDOT-S, DNA and an ammonium surfactant, cetyltrimethylammonium chloride (CTMA) (**Figure 6**).[123] This blend effectively modified the work function of the cathode, showing a broad tolerance to thickness variation than other commercial materials, namely PCEs of 7.20% and 4.64% for 10 and 22 nm thick layers, respectively. Remarkably, devices with the thinnest layer exhibited comparable performance to that of devices based on the commonly used LiF/Al cathode (Table 1).

Catecholamine: Similar to the above-described works, another successful strategy to smooth ZnO films is the use of PDA. PDA exhibits strong adhesive properties, which ensure that the polymer is attachable to almost all the material interface.[299] O and N sites in PDA have a strong chelating capability toward metal ions; therefore, PDA can fix nanoparticles and prevent aggregation. Furthermore, the polymer has a strong reduction property that can be useful during the synthesis of metal nanoparticles from metal solution through atom-by-atom growth.[300] These appealing features, in concert with a good thermal stability, make PDA an appropriate interface material for optoelectronics.[232,301–303]

In 2017, Wang and Yan fabricated PDA/ZnO nanocomposites and used them as electron transport layer in OSCs.[244] The results showed that the strong adhesive property of PDA to ZnO nanoparticles is beneficial to prepare defect-free and uniform ZnO films. In addition, PDA has a strong chelating capability toward metal ions, and it partially forms a Zn-complex that enhances the electron transfer between ZnO and PDA. Devices with the architecture ITO/PDA–ZnO/PTB7:$PC_{70}BM$/MoO_3 (10 nm)/Al (100 nm) exhibited PCEs of 2.64%, J_{SC}s of 7.47 mA cm^{-2}, with a V_{OC}s of 0.67 V, and FFs of 53% (Table 1).

One year later, the same group exposed PDA powders and PDA films to electron beam to investigate the effect of radiation on morphology, structure, and band gap.[304] The electron beam irradiation modified PDA films combined with ZnO was used as charge transporting layer in OSCs. They pointed out a clear relationship between the irradiation dose and the polymerization degree of PDA. The changes in morphology, hydrophilicity, frontier orbitals, and bandgap were attributed to a different degree of conjugation upon irradiation due to distortion of phenyl rings and/or ring-opening. The modified PDA films showed a stronger binding affinity between ZnO and ITO substrates, leading to enhanced performances. The best device was ITO/100 kGy–PDA–ZnO/PTB7:$PC_{71}BM$/MoO_3/Al with PCEs of 3.82%, J_{SC}s of 13.70 mA cm^{-2}, V_{OC}s of 0.59 V, and FFs of 48% (Table 1).

In the same year, Yin and collaborators introduced another type of electron transport layers, namely a composite film mixing PDA and gold nanorods (AuNRs).[245] The doping with AuNRs is expected to improve the PCE due to their positive effects on light scattering, local electric fields, and charge transport. This was nicely corroborated in functional devices. For instance, the modification of ZnO layers with AuNRs increased the J_{SC} from 9.24 to 10.81 mA cm^{-2} and the PCE from 3.57% to 4.57%. Introduction of 50 kGy–PDA/AuNRs composite films further improved the device performance, resulting in PCEs of 5.66%, J_{SC}s of 12.75 mA cm^{-2}, V_{OC}s of 0.72 V, and FFs of 62% (Table 1).

In 2019, Tan et al. successfully used the PDA-based approach to overcome the limits of a novel class of electron transport oxide, aluminum-doped ZnO (AZO).[241] The inherent brittleness and low adhesion of this metal oxide layer had seriously limited charge transport and extraction in OSCs up to that time.[305–307] They pointed out that PDA can effectively passivate

© 2021 The Authors. Advanced Energy Materials published by Wiley-VCH GmbH

16146840, 2021, 43, Downloaded from https://onlinelibrary.wiley.com/doi/10.1002/aenm.202100520 by Universita Di Torino, Wiley Online Library on [21/02/2025]. See the Terms and Conditions (https://onlinelibrary.wiley.com/terms-and-conditions) on Wiley Online Library for rules of use; OA articles are governed by the applicable Creative Commons License

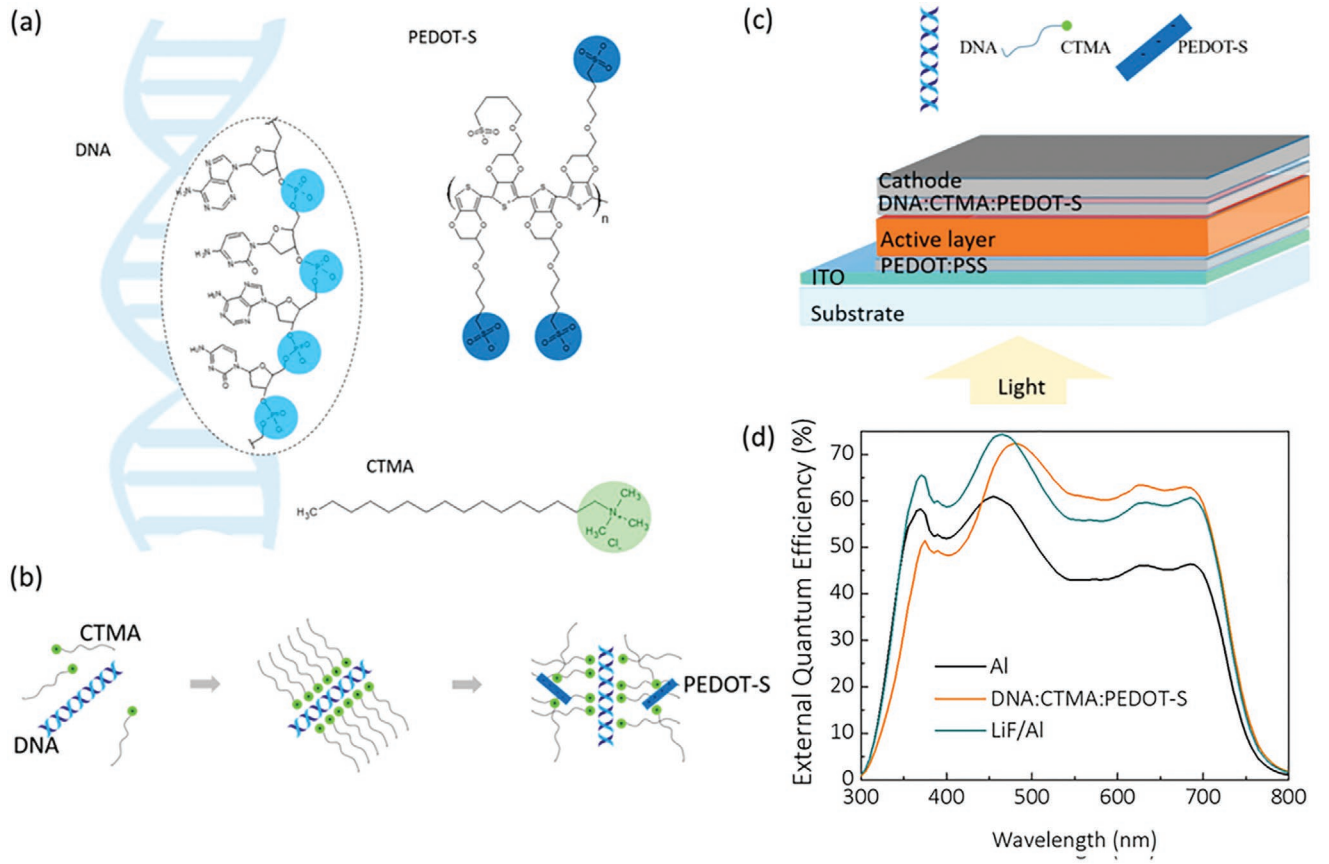

Figure 6. a) Molecular structures of DNA, CTMA, and PEDOT-S. b) Schematic representation of the fabrication of the layer. c) Schematic representation of the final OSC. d) EQE of devices interfaced with DNA:CTMA:PEDOT-S films and the reference devices. Reproduced with permission.[123] Copyright 2018, American Chemical Society.

surface defect sites of AZO through the formation of strong intermolecular hydrogen-bonding interactions. The modified nanoparticles exhibited superior features: i) high-transparency and conductivity, ii) enhanced flexural endurance of the inorganic ETL upon bending, and iii) endowed strong interfacial adhesion between the organic active layer and the inorganic one. The best device had the structure ITO/AZO:1.5% PDA/PBDB-T-2F:IT-4F/MoO_3/Al and exhibited PCEs of 12.5%, J_{SC}s of 21.62 mA cm^{-2}, V_{OC}s of 0.83 V, and FFs of 70% (Table 1).

In parallel, Ahmad et al. developed the idea of improving the performance of ZnO by introducing an very thin PDA layer between the glass/ITO electrode and the ZnO film.[308] They found that the introduction of a 10 nm film leads to improving PCE due to a better morphology given by the crystallinity and the crystal orientation in ZnO structure. These devices (ITO/PDA-10 nm/ZnO/PBDB-T-2F:ITIC/MoO_3/Al) exhibited PCEs of 11.1%, J_{SC}s of 17.86 mA cm^{-2}, V_{OC}s of 0.88 V, and FFs of 71% (Table 1). Recently, Yan and collaborators used PDA to modify the surface of gold nanoparticles (Au-NPs), improving their stability in thin film and effectively binding them to a ZnO electron transport layer in an OSC.[309] In fact, it is known that carrier recombination on the surface of exposed metal nanoparticles would result in an increase of the exciton quenching rate, with consequent degradation of the cell performance. Therefore, PDA coated Au-NPs were selected to prevent such phenomenon, as previously described for the PDA modification of ZnO ETL. These devices (ITO/Au@PDA–ZnO/PTB7:PC_{71}BM/MoO_3/Al) showed PCEs of 6.03%, J_{SC}s of 13.98 mA cm^{-2}, V_{OC}s of 0.74 V, and FFs of 59% (Table 1).

PEDOT:PSS is one of the most widely studied anode interface materials or hole transport materials over the past decades, although it shows several pivotal deficiencies, including a relatively modest work function and structural inhomogeneities.[310] Recently, Zeng et al. successfully doped with dopamine hydrochloride (DA * HCl) a PEDOT:PSS aqueous solution.[52] The dopamine reacted with PSS producing PSS–DA, as reported in literature.[311] This enhances the intermolecular stacking of the PSS–DA segments in PEDOT:PSS–DA, improving the regular aggregation of the PEDOT backbone and enhancing the electron conductivity of the resulting layer. They used the synthetized new hole transport material in OSCs with five different photoactive layers, namely PM6:Y6 as-cast, PM6:Y6 annealed, PBDB-T:ITIC, PM6:IDIC, and P3HT:PC_{61}BM. In all those cases, the performance of the devices with PEDOT:PSS–DA layer was superior with respect to the reference devices (Table 1).

Vitamins: In 2017, Zhang et al. treated PEDOT:PSS spin-coated film dropping 100 µL of vitamins B_1, B_3, B_6, and C water solutions (0.1 M).[312] They noticed a significantly enhancement in conductivity of PEDOT:PSS from 0.3 up to 1000 S cm^{-1}. Vitamins induce phase segregation between PEDOT and PSS

© 2021 The Authors. Advanced Energy Materials published by Wiley-VCH GmbH

16146840, 2021, 43, Downloaded from https://onlinelibrary.wiley.com/doi/10.1002/aenm.202100520 by Universita Di Torino, Wiley Online Library on [21/02/2025]. See the Terms and Conditions (https://onlinelibrary.wiley.com/terms-and-conditions) on Wiley Online Library for rules of use; OA articles are governed by the applicable Creative Commons License

Table 1. Figures of merit of bio-derived OSCs.

Compound	Function	Active layer	J_{SC} [mA cm^{-2}]	V_{OC} [V]	FF [%]	PCE [%]	Ref.
Ag-530/LHCII	Light harvesting	PIDTT-DFBT:$PC_{71}BM$	14.46	0.98	63	8.94	[105]
Ag-530/LHCII	Light harvesting	PBDT-DTNT:$PC_{71}BM$	15.50	0.85	67	8.89	[105]
Ag-530/LHCII	Light harvesting	PTB7-Th:$PC_{71}BM$	17.99	0.80	73	10.57	[105]
PSI	Active layer	PSI:C_{60}	3.47	0.36	33	0.52	[106]
PSI	Active Layer	–	0.96	0.25	31	0.07	[85]
DNA-fullerene conjugates	Active layer	–	–	0.67	–	0.2 (EQE)	[107]
β-Carotene	Active layer	β-Carotene:$PC_{71}BM$	3.51	0.46	33	0.53	[270]
Chlorophyll	Active layer	Lycopene:chlorophyll	0.23	0.85	23	0.045	[286]
His	Interlayer	P3HT: $PC_{61}BM$	9.90	0.62	62	3.80	[49]
His	Interlayer	PTB7-Th: $PC_{71}BM$	14.95	0.78	63	7.40	[49]
His	Interlayer	PCDTBT:$PC_{71}BM$	10.37	0.88	66	6.01	[49]
His	Interlayer	PffBT4T-2OD: $PC_{61}BM$	14.87	0.77	59	6.72	[49]
L-Arg	Interlayer	PTB7-Th: $PC_{71}BM$	17.49	0.78	68	9.31	[84]
Gly	Interlayer	PM6:IT-4F	22.00	0.85	75	14.0	[289]
α-PLL	Interlayer	PBDB-T:IT-M	17.13	0.94	74	11.92	[290]
α-PLL	Interlayer	PDCBT:ITIC	16.58	0.94	65	10.17	[290]
α-PLL	Interlayer	J52:IEICO-4F	25.95	0.72	63	11.74	[290]
PLL	Interlayer	PBDB-T-2Cl:IT-4F	19.77	0.85	60	9.86	[291]
PLL	Interlayer	PBDB-T:ITIC	16.80	0.84	53	7.39	[291]
PLL	Interlayer	PTB7-Th: $PC_{71}BM$	16.75	0.75	60	7.29	[291]
PLL (glass/PEDOT:PSS)	Interlayer	PTB7-Th: $PC_{71}BM$	12.95	0.77	46	4.59	[50]
PLL (PEF/PEDOT:PSS)	Interlayer	PBDB-T-2F:Y6	18.62	0.84	45	6.96	[50]
		PTB7-Th: $PC_{71}BM$	12.81	0.78	45	4.52	[50]
PLL (glass/ITO)	Interlayer	PTB7-Th: $PC_{71}BM$	17.48	0.77	62	8.29	[50]
		PBDB-T:ITIC	16.72	0.85	55	7.81	[50]
		PBDB-T-2Cl:IT-4F	20.58	0.85	70	12.32	[50]
		PBDB-T-2F:Y6	24.81	0.85	72	15.07	[50]
ZnO@G:EC	Interlayer	P3HT:$PC_{61}BM$	8.05	0.63	73	3.7	[292]
ZnO@G:EC	Interlayer	PTB7: $PC_{71}BM$	15.88	0.74	69	8.1	[292]
NOCC:QCS	Interlayer	PTB7-Th:$PC_{71}BM$	20.0	0.76	67	10.2	[51]
Chitosan	Interlayer	PTB7-Th:$PC_{71}BM$	16.45	0.78	59	7.54	[201]
Methyl-cellulose	Interlayer	PBDB-T:ITIC	16.93	0.87	67	9.89	[201]
Dextrin	Interlayer	PTB7-Th:$PC_{71}BM$	16.69	0.79	64	8.43	[201]
CMC	Interlayer	PBDB-T:IT-M	17.87	0.94	72	11.96	[295]
DNA	Interlayer	PTB7:$PC_{70}BM$	14.07	0.71	49	4.88	[121]
DNA (glass/ITO)	Interlayer	PTB7:$PC_{70}BM$	18.90	0.71	62	8.31	[83]
DNA (PET/ITO)	Interlayer	PTB7:$PC_{70}BM$	16.92	0.72	58	7.06	[83]
DNA	Interlayer	P3HT:$PC_{70}BM$	11.86	0.59	59	4.09	[262]
DNA:CTMA:PEDOT-S	Interlayer	PTB7:$PC_{71}BM$	13.52	0.76	70	7.20	[123]
PDA–ZnO	Interlayer	PTB7: $PC_{70}BM$	7.47	0.67	53	2.64	[244]
100 kGy–PDA–ZnO	Interlayer	PTB7:$PC_{71}BM$	13.70	0.59	48	3.82	[304]
50 kGy–PDA–Au–Nrs/ZnO	Interlayer	PTB7:$PC_{71}BM$	12.75	0.72	62	5.66	[245]
AZO:1.5% PDA	Interlayer	PBDB-T-2F:IT-4F	21.62	0.83	70	12.5	[241]
PDA–10 nm/ZnO	Interlayer	PBDB-T:ITIC	17.86	0.88	71	11.1	[308]
Au@PDA–ZnO	Interlayer	PTB7:$PC_{71}BM$	13.98	0.74	59	6.03	[309]
PEDOT:PSS–DA	Interlayer	PM6:Y6 (as-cast)	25.66	0.85	72	15.62	[52]
PEDOT:PSS–DA	Interlayer	PM6:Y6	25.52	0.84	77	16.55	[52]

© 2021 The Authors. Advanced Energy Materials published by Wiley-VCH GmbH

16146840, 2021, 43, Downloaded from https://onlinelibrary.wiley.com/doi/10.1002/aenm.202100520 by Universita Di Torino, Wiley Online Library on [21/02/2025]. See the Terms and Conditions (https://onlinelibrary.wiley.com/terms-and-conditions) on Wiley Online Library for rules of use; OA articles are governed by the applicable Creative Commons License

Table 1. Continued.

Compound	Function	Active layer	J_{SC} [mA cm^{-2}]	V_{OC} [V]	FF [%]	PCE [%]	Ref.
PEDOT:PSS–DA	Interlayer	PBDB-T:ITIC	16.93	0.90	72	10.92	[52]
PEDOT:PSS–DA	Interlayer	PM6:IDIC	17.52	0.95	66	10.96	[52]
PEDOT:PSS–DA	Interlayer	P3HT:$PC_{61}BM$	7.75	0.58	66	2.94	[52]
H:V–Mo (30 nm)	Interlayer	PB3T2:IT-M	16.2	0.96	68	10.5	[316]
H:V–Mo (150 nm)	Interlayer	PB3T2:IT-M	12.1	0.95	66	7.5	[316]
H:V–Mo	Interlayer	PBDB-TF:IT-4F	20.2	0.86	77	13.3	[316]
H:V–Mo	Interlayer	PBDB-TCl:IT-4F	20.7	0.87	78	14.2	[316]
Keratin	Substrate	P3HT:PC61BM	2.4	0.50	25	0.30	[330]
Newspaper	Substrate	CuPc/PTCBI	0.22	0.40	–	<0.30 (170 W m^{-2})	[81]
P10	Substrate	PTB7:$PC_{71}BM$	13.65	0.71	51	4.98	[335]
CNF	Substrate	P3HT:PC61BM	9.58	0.74	45	3.2	[331]
CNC	Substrate	PFDTBTP: $PC_{70}BM$	3.50	0.90	40	1.4	[332]
CNF	Substrate	PFDTBTP: $PC_{70}BM$	2.00	0.70	30	0.5	[332]
Cellophane	Substrate	PTB7-Th:$PC_{71}BM$	11.26	0.80	63	5.65	[333]
PEF	Substrate	PTB7-Th: $PC_{71}BM$	12.81	0.78	45	4.52	[50]
PEF	Substrate	PBDB-T-2F:Y6	18.62	0.84	45	6.96	[50]
Paper/PDMS	Light-trapping layer	TQ1: $PC_{71}BM$	11.29	0.85	58	5.50	[345]
CNP	Light-trapping layer	Y6:PM6	26.48	0.858	71.17	15.99	[346]
PEDOT:PSS:G:EC	Electrode	PBDTTT–EFT:$PC_{71}BM$	16.41	0.77	72	9.2	[86]
PEDOT:PSS:G:EC	Electrode	*p*-DTS$(FBTTh_2)_2$:$PC_{71}BM$	11.55	0.80	69	6.3	[86]
Cellulose-GnPs	Electrode	PffBT4T-2OD: $PC_{70}BM$	8.91	0.74	43	2.85	[350]
s-Ag grids/PDA	Electrode	PTB7-Th: $PC_{71}BM$	13.20	0.77	63	6.4	[351]
Ag mesh@PDA	Electrode	PBDB-T:IT-M	15.04	0.95	72	10.2	[352]
PDA@Ag grids	Electrode	PBDB-T:ITIC	16.90	0.85	63	9.1	[353]
PDA@Ag grids	Electrode	PBDB-T-2F:IT-4F	19.53	0.80	71	11.2	[353]
G-pNE	Electrode	PTB7-Th:$PC_{71}BM$	15.89	0.80	62	7.93	[242]

due to conformational changes in the PEDOT chain. As above explained, distancing PSS excess from the PEDOT chain is a method to improve conductivity and film morphology stability. Nevertheless, the typical chemical agents are poisonous and dangerous for environment.[313–315] Remarkably, vitamins A, D, E, K, B_2, and B_7 did not lead to an enhancement in the conductivity of PEDOT:PSS thin films, as they are not soluble in water. Despite the excellent results of Zhang et al., no functional OSCs have been fabricated employing this vitamin–PEDOT:PSS hole transport layers yet. One year later, Hou and co-workers used another characteristic of vitamin C, namely its reduction capability, to partially reduced Mo(VI) to Mo(V) realizing a n-type doping effect in the MoO_x anode interlayer (H:V–Mo).[316] Again, improving the conductivity of the interlayers through p- and n-type doping is a wide spread method to enhance their tolerance to the thickness variation in OSCs, reducing the device production costs.[307,317,318] They demonstrated how to control the doping effect merely varying the amount of vitamin C in the precursor water solution of ammonium heptamolybdate tetrahydrate, $(NH_4)_6Mo_7O_{24}$. Devices with architecture: ITO/H:V–Mo/active layer/PFN–Br/Al with the thickness of H:V–Mo layer spacing from 10 to 150 nm showed PCEs of 12–8% and J_{SC}s of 18.4–12.1 mA cm^{-2}, as well as a constant V_{OC} of 0.95 V and FF of 65% (Table 1). Although this is an effective method to control the hole transport capability of MoO_x, the light absorption nature of n-doped MoO_x will also lead to a non-negligible depletion of the sun energy, especially for thick layers(>100 nm).

To conclude, the presence of an electron extracting and transporting layer is crucial to achieve highly efficient OSCs. Bio-derived materials are rich in functional groups and they can be exploited to enhance the device performances, mainly due to a i) better level alignment, ii) enhanced morphology of the photoactive layer, and iii) faster dissociation of excitons in polarons. Among them, amino acids, DNA, and catecholamine have already outperformed synthetic materials. For instance, the presence of a His interlayer between ITO and photoactive materials led to almost eightfold enhancement of the PCE. DNA-based layer achieved comparable performances with respect to well-established electron transport materials, such as ZnO and LiF/Al, without requiring an annealing step. Henceforth, the development of DNA-based materials will be crucial to smooth the transition in flexible and wearable devices. Finally, the fine control of the electron conductivity of PEDOT:PSS through functionalization with DA has been demonstrated to be an easy-to-apply strategy. Through DA-based functionalization, at least 10% enhancement in all device has

© 2021 The Authors. Advanced Energy Materials published by Wiley-VCH GmbH

16146840, 2021, 43, Downloaded from https://onlinelibrary.wiley.com/doi/10.1002/aenm.202100520 by Universita Di Torino, Wiley Online Library on [21/02/2025]. See the Terms and Conditions (https://onlinelibrary.wiley.com/terms-and-conditions) on Wiley Online Library for rules of use; OA articles are governed by the applicable Creative Commons License

been demonstrated, regardless the active layer composition. Developing innovative production routes for these bio-derived materials will be a milestone to achieve fully sustainable OSC in the mid-term future.

5.1.3. Substrate

Flexible PVs has received an increasing attention from both the scientific and industrial communities due to the low thickness, lightweight, wearability, and up-scalable roll-to-roll fabrication technique.[319,320] Over the past decade, different kinds of polymers, e.g., PET,[321,322] polyethylene naphthalate (PEN), and[323–325] poly(ether sulfone) (PES)[326] have been developed as flexible substrates for solar cells. Less attention has been focused on renewable and biodegradable materials, such as cellulose.[327,328] In general, a proper substrate material has to guarantee: i) thermal stability, ii) mechanical stability, iii) surface smoothness, iv) high optical transmittance, v) chemical inertness, and vi) barrier properties. Often, the aforementioned polymers show a high CTE ≈10–80 × 10^{-6} K^{-1} that limits the electrode and active layers fabrication conditions, due to the growth and modification of the material under thermal stress. In addition, temperature fluctuations in a day- or year-timescale cause plastic substrates to expand and shrink severely, resulting in cracks and damage of the top coatings.[329] In this context, the development of flexible solar cells has significantly starting to flourish using sustainable and biocompatible substrates.

Proteins: In 2019, Posati et al. demonstrated for the first time the potential of keratin films (KF) as natural support for the fabrication of fully printable ITO-free OSCs.[330] They prepared keratin films from aqueous solution by adding glycerol as a plasticizer in order to improve their mechanical properties. As-cast KF and annealed KF80 samples were compared in terms of transparency, structure, morphology, thermal, and mechanical properties, in order to mimic and evaluate the impact of the processing conditions used for device fabrication. They obtained a free-standing, acidic water resistant, transparent, e.g., 87–90% transmittance in the visible region after annealing, and smooth film, i.e., RMS roughness of around 10 nm, which was successfully used as support for working OSCs. In particular, the annealed films showed better properties with respect to higher transparency and thermal stability, since the thermal annealing determines a transition from α-helix to β-sheet resulting in a more packed structure. Moreover, it was rehydrated at ambient conditions for 7 days, with a consequent decrease in the Young modulus to values typical of the nontreated film. Devices with structure KF/PEDOT:PSS/P3HT:PC_{61}BM/LiF/Al showed PCEs of 0.30%, J_{SC}s of 2.4 mA cm^{-2}, V_{OC}s of 0.50 V, and FFs of 25% (Table 1). Although this performance is not optimal compared to the state of the art, they were similar to those reported for the reference devices.

Polysaccharides: The first solar cell fabricated on a paper substrate was reported by Lamprecht et al. in 2005.[81] They coated a common newspaper with a film made of ORMOCER followed by parylene C film. The device PCE was <0.3% under 170 W m^{-2} irradiation with a J_{SC} of 0.22 mA cm^{-2} and a V_{OC} of 0.4 V. Since the device performance was not excellent, this paper did not attract the attention of the community for almost a decade. Indeed, almost no information about the optical and mechanical features of this substrate was provided.

In 2015, Nge's group produced optically transparent and conductive paper using CNF from wood pulps of Sitka spruce (*Picea sitchenis*) and silver nanowires synthesized via reduction of $AgNO_3$ in presence of poly(vinylpyrrolidone) in ethylene glycole.[331] Here, transmittance values of >90% across the visible range were the most remarkable figure of these films. OSCs were fabricated with the architecture: CNF/Ag nanowires/PEDOT:PSS/P3HT:PC_{61}BM/Al (60 nm), achieving a PCE of 3.2%, and a J_{SC} of 9.58 mA cm^{-2}, a V_{OC} of 0.74 V, and a FF of 45% (Table 1). Therefore, the device performance was definitely comparable to ITO–glass based solar cells, paving the way toward innovative highly transparent conductive paper for portable electronics.

One year later, Costa et al. successfully compared the PV performances of OSCs made on top of different cellulose-based substrates, namely CNC and CNF.[332] In both cases, the devices featured the structure substrate/Ag/ZnO:Al/PFDTBTP:PC_{70}BM/MoO_3/Ag. They pointed out how the PV response of CNC substrate was better than the one achieved by the traditional CNF-based substrate (Table 1). This was nicely correlated to the properties of the CNC films with respect to roughness, crystallinity, and homogeneity of the fibers. As the most relevant conclusion, they demonstrated how the cellulose fibers have to be precisely ordered in a nanocrystalline fashion in order to achieve high transmittances. Following up this work, Song and collaborators discovered that a reduction in substrate thickness from 150 to 25 μm is a mean to mitigate the strain stress in flexible SCs under folding with extremely curvature radius of micrometer.[333] They fabricated flexible polymer OSCs with a structure of cellophane/OMO/ZnO/PTB7-Th:PC_{71}BM/MoO_3/Al, where OMO is an emerging ultrathin Ag electrode with trilayer structure Oxide/Ag/Oxide,[334] and upon irradiation of AM1.5G, the devices exhibited PCEs of 5.65%, J_{SC}s of 11.26 mA cm^{-2}, V_{OC}s of 0.80 V, and FFs of 63% (Table 1). Noteworthy, the PV performances onto cellophane substrate were maintained upon 500 bending cycles, whereas the reference solar cells on PET/ITO failed only after a few cycles of bending. The same year, Zhang and co-workers fabricated a cellulose-based substrate for flexible solar cells utilizing seafood waste and cellulose pulp.[335] They performed homogenous etherification base-assisted of cellulose in NaOH/urea solution without extra catalyst, obtaining *O*-(2,3-dihydroxypropyl) cellulose (DHPC). In order to reinforce it, they added different amounts of rigid percolating tunicate cellulose nanocrystals (TCNCs) isolated from the mantles of sessile sea creatures. For the preparation of DHPC/TCNCs matrix, a suspension of the latter (3 wt%) was blended in an aqueous solution of the former (4 wt%) in accordance with the desired mass ratio. The mixed solution was cast on a glass mold and evaporated at 40 °C for 24 h. Thanks to the hydrogen bond interactions, the latter were homogeneously immobilized in DHPC matrix with a mass ratio DHPC/TCNCs 1:0.1 (P10). Noteworthy, without further treatments, a thin layer of ITO was directly deposited onto P10 using magnetron sputtering. The average roughness of P10-ITO was ≈4.4 nm, keeping the transparency of the ITO electrode. The OCS with

© 2021 The Authors. Advanced Energy Materials published by Wiley-VCH GmbH

16146840, 2021, 43, Downloaded from https://onlinelibrary.wiley.com/doi/10.1002/aenm.202100520 by Universita Di Torino, Wiley Online Library on [21/02/2025]. See the Terms and Conditions (https://onlinelibrary.wiley.com/terms-and-conditions) on Wiley Online Library for rules of use; OA articles are governed by the applicable Creative Commons License

architecture P10 (100 µm)/ITO (80 nm)/ZnO (30 nm)/PTB7-$PC_{71}BM$ (1:1.5 by weight, 100 nm)/MoO_3 (10 nm)/Ag (100 nm) exhibited PCEs of 4.98% under a P of 1000 W m^{-2} associated to J_{SC}s of 13.65 mA cm^{-2} and V_{OC}s of 0.71 V, and FFs of 51% (Table 1).

Recently, Chen's group[50] successfully introduced a novel 100% bio-based polymer, namely polyethylene furandicarboxylate (PEF), in the PV panorama. This polymer can be synthesized easily by monoethylene glycol (MEG) and 2,5-furandicarboxylic acid (2,5-FDCA), both moieties are able to be transformed from biomass components, such as lignocellulosic and agricultural wastes.[336–340] The ITO-free solar cells were fabricated with configuration: PEF/PEDOT:PSS/ZnO/poly-lysine/active layer/MoO_3/Ag. PEF retains the performances of glass-based reference devices, with PCE values around 4.7% in the presence of fullerene-based active layer and 7.14% with a non-fullerene one.

In conclusion, both proteins and polysaccharides used as substrates for OSCs have been disclosed. The most relevant aspect is the possibility to realize flexible and ITO-free devices that retain high transparency and conductivity features, even outperforming PET–ITO-based devices. On one hand, the research on proteins for this scope is still in its infancy, and a deeper optimization of such materials is necessary to reach state-of-the-art performances. On the other hand, the employment of polysaccharides is in a mature stage. The use of polysaccharide-based substrates has led to i) astonishing performances with regard of flexible devices (performances retained upon 500 bending cycles with cellophane substrate) and ii) successful valorization of biomass wastes (DHPC and PEF). In addition, huge effort has been made to investigate systematically the impact of the various hierarchical structures of cellulose derivatives onto the device performances. Remarkably, CNF must be precisely ordered, like in CNC, to retain high transmittance.

Besides, following the recent studies described therein, contributions in the direction of fully bio-derived polymers with suitable nanostructure for optical application are expected.

5.1.4. Light-Trapping Layers

In Section 3.1, it was pointed out how the PCEs of OSCs is still lower than that of the Si-SCs and PSCs owing to the limited absorption of the active layer.[341] In this regard, the development of novel materials and devices with enhanced light incoupling is highly desirable. Particularly, it will be a great help for developing solar windows, as fully transparent devices show lower performances due to the absence of a back-reflecting electrode, and a loss of photons to transmission.[342–344]

Polysaccharides: In 2015, Tang et al. combined a low-cost light trapping scheme with fully solution processed SCs.[345] In short, they fabricated an efficient device suitable for roll-to-roll process, demonstrating that a paper-based reflector could enhance the EQE by a factor of 2.5. The device structure was paper reflector/PDMS/glass/PEDOT:PSS/PEIE/TQ1:$PC_{71}BM$/PEDOT:PSS. Upon irradiation at 1 sun and AM1.5G conditions, the devices achieved PCEs of 5.50%, J_{SC}s of 11.29 mA cm^{-2}, V_{OC}s of 0.85 V, and FFs of 58% (Table 1). In 2020, Ouyang's group demonstrated the use of eco-friendly and water-resistant cellulose nanopaper (CNP) with high transparency and haze for efficient optical trapping.[346] The light trapping layer was prepared from tobacco stalk (agroforestry residues) and was cooked in a solution of ammonium sulfite and hydrolyzed with formic acid. CNP with thickness of 20 µm showed a haze above 75% from 300 to 1000 nm, with a corresponding transmittance over 90% (**Figure 7**). The conventional CNP-20/ITO/PEDOT:PSS/PM6:Y6/PDIN/Ag OSCs were fabricated using CNP as a light-trapping layer. They exhibited PCEs of 15.99% (AM1.5) with record J_{SC}s of 26.48 mA cm^{-2}, V_{OC}s of 0.86 V, and FFs of 72% (Table 1). This work demonstrated for the first time the successful utilization of biodegradable, renewable, and sustainable materials for light-trapping and wide-angle capture in OSCs.

5.1.5. Electrodes

Polysaccharides: In 2015, Chen's group did a pioneering work creating large-scale high conductive PEDOT:PSS:graphene:ethyl

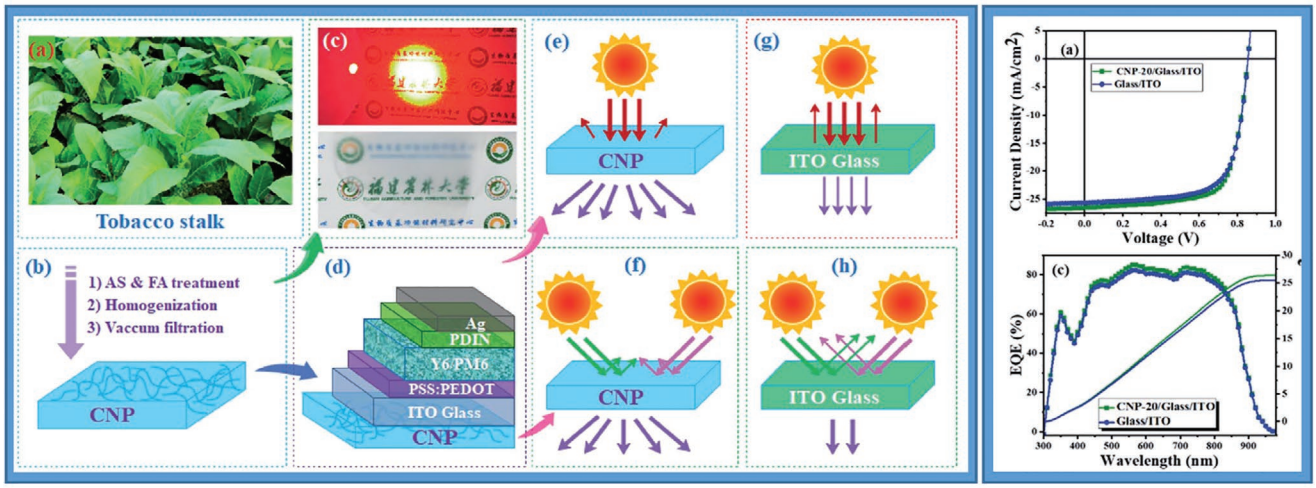

Figure 7. Right a) Tobacco stalk, b) CNP structure, c) transmittance of CNP under a red laser and daylight, d) final device architecture, e,f) schematic view of the processes of transmittance, scattering, and reflection of CNP and g,h) ITO glass under sunlight. Left (top): *J–V* curves; (bottom): dark *J–V* curves; and c) EQE values with integrated currents for glass/ITO. Reproduced with permission.[346] Copyright 2020, Royal Society of Chemistry.

© 2021 The Authors. Advanced Energy Materials published by Wiley-VCH GmbH

16146840, 2021, 43, Downloaded from https://onlinelibrary.wiley.com/doi/10.1002/aenm.202100520 by Universita Di Torino, Wiley Online Library on [21/02/2025]. See the Terms and Conditions (https://onlinelibrary.wiley.com/terms-and-conditions) on Wiley Online Library for rules of use; OA articles are governed by the applicable Creative Commons License

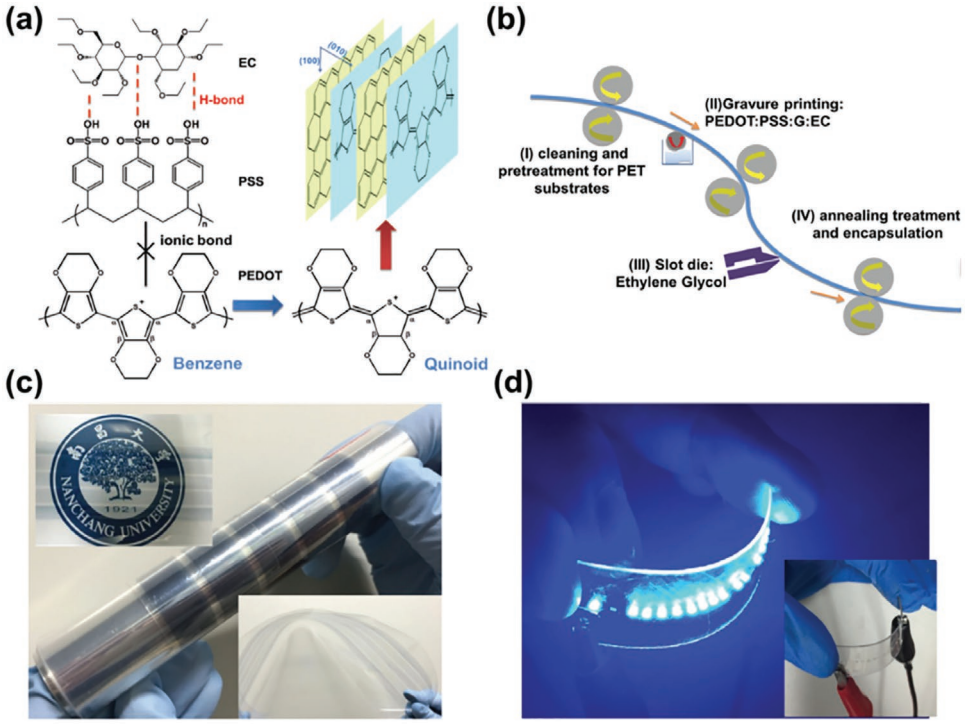

Figure 8. a) Schematic view of the structural rearrangement of PEDOT:PSS and G:EC, b) schematic roll-to-roll fabrication, c) pictures of the printed electrode, d) images of 20 LED etched onto the printed electrode. Reproduced with permission.[86] Copyright 2015, Wiley-VCH GmbH & Co. KGaA, Weinheim

cellulose (G:EC) electrodes (**Figure 8**).[86] The introduction of a G:CE suspension enables the increase of conductivity of the PEDOT:PSS composite, without the need of a strong acid treatment. In fact, the PSS interacts strongly with the ethyoxyl group of EC to realize a well phase separation between PEDOT and PSS chains, and the highly uniform and conductive G:EC enables the rearrangement of the PEDOT chains with more expended conformation surrounded by G:EC through the π–π interaction.[347,348] They successfully prepared ITO-free OLEDs, OSCs and organic photodetectors. Remarkably, in all cases reference ITO-based devices were outperformed. Concerning OSCs, they tested devices within the inverted structure concept, namely: PET/PEDOT:PSS:G:EC/PEIE/active layer/MoO_x/Ag, where the active layer was PBDTTT–EFT:$PC_{71}BM$ or *p*-DTS(FBTTh$_2$)$_2$:$PC_{71}BM$. The device based on a polymer PBDTTT–EFT:$PC_{71}BM$ blend featured PCE surprising values of 9.4% associated to V_{OC}s of 0.79 V, J_{SC}s of 16.52 mA·cm^{-2}, and FFs of 0.72 (Table 1).

Another key aspect that greatly benefits from the introduction of bio-derived materials is the realization of a solution-processed top electrode. In fact, the classical structure of evaporated MoO_3 and Ag or Al is not up-scalable and suffers mechanical unstability, under thermal aging.[349] The same approaches used to substituted ITO-based electrode are also suitable for this purpose. In detail, La Notte et al. fabricated the first fully sprayed flexible polymer solar cell with cellulose–graphene nanoplatelets (GnPs) electrodes. GnPs is a good candidate to confer conductivity to cellulose and its derivatives, and cellulose–graphene blends are achieving important results as flexible and printable material for optoelectronics.[350] The device with architecture PET/ITO–Ag–ITO/ZnO/PEIE/PffBT4T-2OD:PC70BM/V_2O_x/PEDOT/cellulose-GnPs achieved PCEs of 2.85%, J_{SC}s of 8.91 mA cm^{-2}, V_{OC}s of 0.74 V, and FFs of 43%, combining high efficiencies with remarkable resistance to bending (Table 1).

Catecholamine and Derivate: The aforementioned adhesive capability of PDA films could be helpful to overcome limits of metal meshes, such us poor adhesion and high temperature processing, allowing greener fabrication methods. In 2018, Wang et al. presented a novel s-Ag grids@PDA/PET electrode with ultraadhesion and mechanical flexibility that was successfully prepared by in situ growth at low temperature and fiber mask assisted acid etching.[351] OSCs with the structure PET/s-Ag grids@PDA/PEDOT:PSS/PTB7-Th:$PC_{71}BM$/Ca/Al showed PCEs of 6.4%, J_{SC}s of 13.20 mA cm^{-2}, V_{OC}s of 0.77 V, and FFs of 63% (Table 1). One year later, the same group collaborated in two interesting works,[352,353] where they again proposed again the same approach, that is, the preparation of a flexible metal-mesh electrode based on Ag mesh@PDA/PET, but they improved the preparation methods. At first, they combined electroless plating and inkjet printing. Significantly, electroless Ag plating was performed with the assistance of PDA and inkjet-printed polystyrene matrices, leading to an ultrathin film (50 nm) with highly homogeneous conductivity. The PET/Ag mesh@PDA/ZnO/PBDB-T:IT-M/MoO_3/Al showed PCE of 10.24%, J_{SC} of 15.04 mA cm^{-2}, V_{OC} of 0.95 V, and a FF 72%. This performance was on par with the PV response of the ITO-based reference device for the first time. In the second work, they combined ultraviolet nanoimprint lithography technology with the electroless deposition of metallic Ag on the exposed PDA, which guarantees superior conductivity and flexibility of PET/PDA@Ag grids and simultaneously improves the adhesion between the flexible substrate and Ag grids.

© 2021 The Authors. Advanced Energy Materials published by Wiley-VCH GmbH

16146840, 2021, 43, Downloaded from https://onlinelibrary.wiley.com/doi/10.1002/aenm.202100520 by Universita Di Torino, Wiley Online Library on [21/02/2025]. See the Terms and Conditions (https://onlinelibrary.wiley.com/terms-and-conditions) on Wiley Online Library for rules of use; OA articles are governed by the applicable Creative Commons License

Remarkably, the so-assembled different OSCs with configuration: PET/PDA@Ag grids/ZnO/Active Layer/MoO_3/Ag, where active layer is PBDB-T:ITIC or PBDB-T-2F:IT-4F, achieved higher performances than the ITO-based reference devices.

In 2018, Jung et al. successfully fabricated graphene electrode-based OSC by modifying the graphene surface via thin film coating of polymerized norepinephrine (pNE) as surface modifier.[242] NE is another derivate of catecholamine that functions as neurotransmitter and as hormone associated with stress or danger. It is composed of a hydrophobic benzene ring and a hydrophilic functional group, especially its 3,4-dihydroxybenzaldehyde unit suppresses the aggregation of pNE particles and yields a relatively smooth thin film.[354] By optimization of incubation time and annealing condition, pNE could effectively modify the hydrophobic surface of graphene, improve the overall film quality and induce doping of graphene with negligible change in the chemical composition and optical transmittance of the resulting film. The optimized graphene-based OSC with structure: G-pNE/PEDOT:PSS/PTB7-Th:$PC_{71}BM$/Al exhibited PCEs of 7.93%, J_{SC}s of 15.89 mA cm^{-2}, V_{OC}s of 0.80 V, and FFs of 62% (Table 1).

To conclude, the best candidates to replace ITO in PV devices are metal oxides, carbon materials, metallic nanomaterials, and conductive polymers. Each of them implies challenges to be solved before commercial applications. Nevertheless, it has been demonstrated that bio-derived materials perfectly fit with the next generation electrodes, as demonstrated by astonishing performances. For instance, cellulose–graphene blends are expected to play a crucial role in the close future toward a completely ITO-free optoelectronics in the close future. In addition, catecholamines are a versatile tool that can be used to effectively functionalize the aforementioned materials. Remarkably, the PET/PDA@Ag grid electrode developed by Chen's group led to a 10% enhancement of the corresponding OSC with regard to ITO-based reference.

5.2. Bio-PSCs

5.2.1. Charge Transport Layer

Aminoacids: Peptides have been successfully employed as additives to enhance the stability of PSCs. For instance, it was reported that the photovoltaic performance of PSCs could be improved through TiO_2 surface modification of the TiO_2/$CH_3NH_3PbI_3$ heterojunction interface with amino acids.[92,355–357] Usually, the carboxylic group of the amino acids binds to the titania surface, while the amino group can interact with the perovskite layer. Thus, the peptides are considered as an efficient monomolecular interlayer that enhances the electronic coupling between titania and perovskite layers. This depends on the molecular and electronic structures of the peptides. It has been, however, also pointed out that the amino acid has the ability to adsorb onto the TiO_2 surface in a zwitterionic form ($NH_3^+CH_nCOO^-$) through hydrogen bonds instead of the formerly indicated COO^- bidentate coordination.[358] This conformation is not beneficial to assist the electronic coupling between the titania and perovskite layers, reducing the carrier transport performance. These aspects are discussed as follows.

Shih et al. reported that PSC's performance could be improved through amphipathic monolayer located at the TiO_2/$CH_3NH_3PbI_3$ heterojunction interface using the amino acid glycine. This peptide reduces the surface defects formed during crystallization of perovskite.[355] The device architecture consisted in FTO/TiO_2/glycine/perovskite/Au. The average PCE of PSCs was increased from 6.99% to 9.48%, mainly due to the improvement of J_{SC} (Table 2). Without glycine, PbI_2 crystallized into a broader size range of 200–600 nm with more voids. In contrast, the PbI_2 grown on the glycine-treated TiO_2 displays less and smaller voids with a narrow crystal size range of 200–300 nm. Glycine was found to promote an even smoother PbI_2 crystal growth along the *c* axis of titania with the direction perpendicular to the TiO_2 surface.

In a follow-up contribution, they systematically explored the effects of different amino acids, namely glycine, *β*-alanine, L-alanine, and 5-aminovaleric acid, used to modify the TiO_2 electron transport layer, and its consequent effect on the crystalline features of the perovskite layer and the electrical properties of the interfacial charge transport.[92] The authors fabricated devices with the previously studied architecture. However, the FTO/TiO_2 electrodes were immersed in the amino acid solutions for over 10 h to ensure a full coverage of the electrode surface. All the amino acid-modified devices exhibited superior PCEs than the non-modified devices caused owing mainly to the rise in J_{SC}, while the V_{OC} and FF are slightly changed (Table 2). Among the tested amino acids, L-alanine, whose outward functional groups include $-NH_2$ and $-CH_3$, achieved the best performance with the highest average J_{SC} of 22.40 mA cm^{-2} and PCE of 14.22% (Table 2). This was accompanied by the lowest carrier lifetime, which is associated to faster charge diffusion and efficient charge transport at the TiO_2/perovskite interface.

Wu and collaborators also employed commercial L-leucine to improve electron injection from $CH_3NH_3PbI_3$ to the TiO_2 layer.[359] The group reported that the bipolar nature of L-leucine improves the quality of the perovskite films, promotes the charge transfer at the interface, and protects the films from H_2O/O_2 penetration. This is ascribed to the ability of L-leucine to form a passivation layer on the face of the perovskite film. PCEs reached a maximum of 18.2% in devices with the architecture ITO/PTAA/L-leucine/perovskite/C_{60}/BCP/Ag, with PTAA:poly(triaryl amine), BCP:bathocuproine. This strongly contrasts with the performance of the reference devices with PCEs of 16.1% due to mainly the lower J_{SC} values (Table 2).

The use of amino acids in inverted p–i–n PSCs was reported by Xu and collaborators.[360] The latter features an HTL commonly based on the PEDOT:PSS, which, can, however, cause degradation and hysteresis issues. Adding the amino acid L-alanine to pristine PEDOT:PSS proved beneficial to reconstruct the distribution of the $-SO_3^-$ and $-SO_3H$ groups, resulting an improvement of the charge collection and transport attributed to the weakened enrichment of $-SO_3H$. Here, when L-alanine is added to PEDOT:PSS, part of the sulfonyl groups ($-SO_3H$) of PSS easily react with $-NH_2$ groups, increasing the amount of $-SO_3^-$. Since PEDOT is a conjugated polymer and carries positive charges, charged macromolecules are formed via the "bridge" of $-SO_3^-$, resulting in an increase of conductivity. An optimized amount of L-alanine allowed for an improvement of

© 2021 The Authors. Advanced Energy Materials published by Wiley-VCH GmbH

16146840, 2021, 43, Downloaded from https://onlinelibrary.wiley.com/doi/10.1002/aenm.202100520 by Universita Di Torino, Wiley Online Library on [21/02/2025]. See the Terms and Conditions (https://onlinelibrary.wiley.com/terms-and-conditions) on Wiley Online Library for rules of use; OA articles are governed by the applicable Creative Commons License

the PCE from 12% (nonmodified PSC) to 15.5% (alanine-modified PSC) in devices with the architecture FTO/PEDOT:PSS/perovskite/PCBM/BCP/Ag, with PCBM: [6,6]-phenyl-C_{61}-butyric acid methyl ester. Additionally, the PSCs showed improved humidity-dependent stability, featuring a 70% of its maximum current value (21.77 mA cm^{-2}) after spending 8 h at 50% humidity, while the nonmodified PSC reached only a 56% (Table 2).

In 2018, He et al. implemented the amino acid cysteine in a Cu:NiO_x PSCs interlayer.[361] NiO was selected as electrode owing to its low cost and ultrahigh thermal stabilities and photostabilities, as well as its lower corrosion issues. However, improving the V_{OC} of the PSCs is still an open challenge. An effective strategy can be metal doping of the electrode (in this case, Cu doping). The ITO substrates covered by Cu:NiO_x were immersed in the cysteine solution for 12 h. The surface treatment slightly increased the surface energy and the wettability of the Cu:NiOx films, which facilitates the preparation of uniform and pinhole-free perovskite films. Therefore, J_{SC} and V_{OC} increased from 20 to 23.6 mA cm^{-2} and from 1.06 to 1.12 V, respectively (Table 2). A similar strategy was recently employed by Li and co-workers.[356] This group modified PSCs with the amino acid L-cysteine at the interface $TiO_2/CH_3NH_3PbI_3$. The incorporation of L-cysteine increased the PCE from 11.5% to 14.4% (Table 2). Here, spectroscopic studies showed that the electron injection from perovskite to mp-TiO_2 is enhanced due to the interactions between the functional groups (–COOH, $–NH_2$, and –SH) of cysteine and Ti^{4+} ions in mp-TiO_2 and unsaturated Pb^{2+} and I^- ions in the perovskite film. This accounts for an enhanced charge separation and collection, leading to higher J_{SC} values.

Proteins: Das et al. recently reported on how to enhance PSC's efficiencies through protein functionalization of the TiO_2 electrode.[362] In particular, the bacteriorhodopsin (bR) protein was immobilized on the TiO_2 surface by covalent attachment of the protein via cysteine groups. The bR molecules between TiO_2 and the perovskite layers have a key role in enhancing the photon absorption and hot carrier transfer, as the transfer of photogenerated electrons from the perovskite absorber to bR molecules through the Forster resonance energy transfer (FRET) process. Indeed, the excited state lifetime is significantly decreased upon the adsorption of bR on the TiO_2 film, which further confirms that bR can assist the charge carrier extraction from perovskite to the TiO_2 ETL. The champion cell with the TiO_2/bR electrode in a device architecture FTO/TiO_2/pervoskite:bR/spiro-OMeTAD/Au exhibited J_{SC}s of 22.61 mA cm^{-2}, FFs of 70.5%, V_{OC}s of 1.05 V, and PCEs of 17.02%. By contrast, reference devices without bR reached similar J_{SC}s (22.59 mA cm^{-2}) and V_{OC}s (1.02 V), but higher series resistances affecting the FFS (61.8%) and reducing the PCEs down to 14.59% (Table 2).

DNA: In 2016, Yusoff et al. demonstrated DNA–CTMA as HTL in inverted PSCs with the structure FTO/DNA–CTMA/$CH_3NH_3PbI_3$/PCBM/Al.[363] The group reported that spun-casted perovskite onto PEDOT:PSS produced incomplete surface coverage with pinholes, whereas spun-casted perovskite onto DNA–CTMA led to uniform and complete surface coverage. The devices with DNA–CTMA exhibited a PCE of 15.86% with J_{SC} of 20.85 mA cm^{-2}, V_{OC} of 1.04 V, and FF of 73.15% (Table 2). This represents a strong improvement compared to the reference device without DNA–CTMA – PCE of 12.49% with J_{SC} of 19.20 mA cm^{-2}, V_{OC} of 0.90 V, and FF of 72.27%. The authors attributed the performance improvement to the well-aligned energy of the perovskite valence band with the HOMO of DNA–CTMA. The HOMO orbitals located on the guanine and adenine units of the DNA–CTMA minimize energy loss for hole transfer and optimize the magnitude of the V_{OC}. The LUMO coefficients are located on the thymine and cytosine units, which efficiently blocks electrons, reducing the recombination and enhancing both J_{SC} and PCE of the device.

In 2020, Peng et al.[364] doped mesoporous TiO_2 with DNA by following a hydrothermal method. This consisted in spin coating onto a layer of compact titania a solution of hydrochloric acid, butyl titanate and DNA, The author observed an improved in the TiO_2 dispersion and uniformity in presence of the DNA. Importantly, the PCE of the cell with structure FTO/compact-TiO_2/meso-DNA:TiO_2/perovskite/spiro-OMeTAD/Ag with 0.2 mg mL^{-1} DNA doped meso-TiO_2 was remarkably boosted to 17.59% from 13.25%. The V_{OC}, J_{SC}, and FF were of 1.07 V, 22.90 mA cm^{-2}, and 71.9%.

Carbohydrates: In 2018, Hong's group reported a new bio-inspired hole transport material based on natural carbon components extracted from aloe-vera plant.[365] The aloe-vera gel was removed from leaves, dried for 24 h, carbonized, and crosslinked with carbon NPs. The obtained black powder was washed with HCl and water, dried, and thermal annealed at 1000 °C, then mixed with chlorobenzene and used as paste for screen printing. The resistivity of the screen-printed film and commercial colloidal carbon paste showed 6.99 and 78.72 Ω cm^{-2}, respectively. The devices with architecture FTO/Bl–TiO_2/mp–TiO_2/ZrO_2/$MAPbI_3$/aloe-vera HTL showed PCEs of 12.58%, J_{SC}s of 21.65 mA cm^{-2}, V_{OC}s of 0.99 V, and FFs of 59%. Noteworthy, the performances were retained without encapsulation for almost 1000 h, tenfold increase with respect of the reference device capped with the standard spiro-OMeTAD/Au cathode.

Catecholamine: In 2017, Huang et al. modified the HTL PEDOT:PSS of p–i–n PSCs with catechol derivatives, such as L-DOPA, norepinephrine, and 3,4-dihydroxybenzhydrazide (DOBD).[366] The average PCE increased to 13.68%, 13.23%, and 16.82% for PSCs based on DOPA–, norepinephrine–, and DOBD–PEDOT:PSS, respectively, while the nondoped PEDOT:PSS led to an average PCE of 13.53% (Table 2). While these results indicate that PEDOT:PSS can be replaced by catechol derivatives without affecting the device performance, this finding is not related to the electronic features of the catechol layers rather than to the changes in the perovskite layers. This was ascribed to the presence of bigger grains and fewer grain boundaries in the modified perovskites, which accounts for reduced carrier recombination.

Dopamine: They were mostly employed to functionalize the interfaces at, for example, the hole transport PEDOT:PSS layer in inverted PSCs and the metal oxide electron transport layer in planar PSCs. Cao's group modified PEDOT:PSS with dopamine semiquinone.[93] The modified material presented enhanced charge extraction capability. Additionally, the dopamine doping improved the quality of the perovskite films. This was ascribed to the ability of the amino and hydroxyl groups of the

© 2021 The Authors. Advanced Energy Materials published by Wiley-VCH GmbH

16146840, 2021, 43, Downloaded from https://onlinelibrary.wiley.com/doi/10.1002/aenm.202100520 by Universita Di Torino, Wiley Online Library on [21/02/2025]. See the Terms and Conditions (https://onlinelibrary.wiley.com/terms-and-conditions) on Wiley Online Library for rules of use; OA articles are governed by the applicable Creative Commons License

dopamine to interact with the under coordinated Pb atoms on the perovskite crystal, reducing charge-recombination rate, and increasing charge-extraction efficiency. The champion cells, i.e., ITO/dopamine-PEDOT:PSS/perovskite/PCBM/PN_4N/Ag architecture, with PN_4N being an amino-containing polymer[367] achieved V_{OC} of 1.08 V, PCE of 18.5%, compared to 1.01 V and 16.1% for the non-doped cells, respectively. In addition, only 20% PCE loss was noted after 250 h under operation conditions (Table 2).

In 2018, Hou et al. introduced dopamine as self-assembled interlayer between the perovskite sensitizer and the SnO_2 ETL interlayer.[368] This modification led to an enhanced crystallization of the perovskites, as well as a lower defect concentration and a faster electron transfer from the perovskite to the SnO_2 layer. This resulted in enhanced figures-of merit, reaching V_{OC}s, J_{SC}s, and PCEs of 1.05 V, 21.72 mA cm^{-2}, and 16.31% compared to 1.04 V, 19.07 mA cm^{-2}, and 12.63% for the non-modified devices (Table 2).

The same year, Zhai et al. covalently linked dopamine to anatase TiO_2 nanocrystals, optimizing the ratio between dopamine and TiO_2 to allow for a complete attachment of the former.[369] This type of interlayer successfully absorbs water molecules on its surface. This led to a lack of PbI_2 perovskite precursor isolation during the film forming process, as it creates hydrogen bonds with the inorganic salt. Finally, water, as well as PbI_2 processing solvent (DMSO, DMF) are removed in a drying step, leading to a mesoporous precursor PbI_2 layer, and, consequently, to a morphologically improved perovskite layer. The device was finalized with the architecture FTO/dopamine–TiO_2/perovskite/spiro-OMeTAD/Ag. Compared to the reference devices without dopamine, the device figures of merit enhanced, reaching a PCE of 16.36% that accounts for an increase of an absolute 2% in device efficiency (Table 2).

In 2019, Zhang et al. fabricated dopamine-capped TiO_2 nanoparticles as ETL interlayer for $Cs_{0.05}FA_{0.81}MA_{0.14}PbI_{2.55}Br_{0.45}$ PSCs.[90] In this follow-up work, the authors further exploited the strong electron-donating capability of dopamine. Dopamine-capped TiO_2 nanoparticles are therefore new hybrid systems, in which localized orbitals of surface-bound ligands are electronically coupled with the conduction band of TiO_2. This electronic coupling favors direct injection of photogenerated electron into the conduction band of the TiO_2,[370] resulting in effective charge transfer and reduced charge accumulation at the TiO_2/perovskite interface. The champion cell exhibited PCEs of 20.93% with negligible hysteresis. Moreover, unencapsulated devices retained 80% of their initial performance after 1200 h operation under constant full-sun illumination in nitrogen atmosphere, which represents an important step toward device commercialization. Finally, dopamine doping was also recently applied to the TiO_2 layer in planar PSCs.[371] The authors showed that in situ dopamine functionalization of titania leads to a tailoring of the energy level alignment and enhanced charge extraction, owing to reduced charge accumulation between titania and the perovskite layer. Overall, they achieved PCEs of 19.45% that are significantly higher to of the nondoped cells (16%) (Table 2).

Polydopamine: In 2017, Huang et al. used dopamine copolymerized PEDOT to obtain a water-resistant and high working function material (**Figure 9**).[89] They also replaced PSS by LS, to enhance the layer morphology. Thus, devices with the architecture ITO/PEDOT:PSS or dopamine–PEDOT:PSS/perovskite/PCBM/Al were compared. For reference devices, the V_{OC}, J_{SC}, and FF were 0.86 V, 20.62 mA cm^{-2}, and 67.5%, respectively, resulting in a PCE of 11.98%. These values were only slightly improved by using PDA:PEDOT:LS, i.e., V_{OC}, J_{SC}, and FF of 1.02 V, 18.19 mA cm^{-2}, and 65.14%, yielding a PCE of 12.05% (Table 2, Figure 9). However, the most relevant result was the significant enhancement toward water and irradiation resistances. As an example, after 32 days of aging under environmental conditions, the dopamine modified PSCs showed negligible changes in PCE, while this reduced to 58% for non-modified PSCs.

Likewise, Huang et al. copolymerized dopamine with PEDOT:PSS to obtain an improved hole extraction layer.[88]

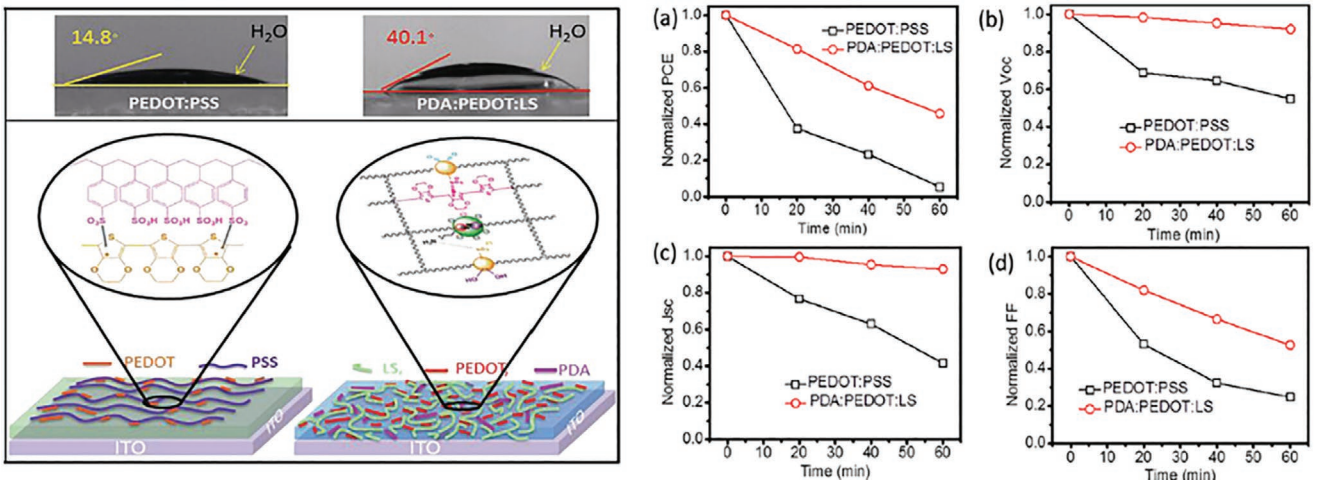

Figure 9. Top left: Contact angles of a drop of water on the surface of bare ITO substrate for bare PEDOT:PSS and PDA:PEDOT:LS (polydopamine-doped-PEDOT:PSS). Bottom left: Molecular packing and structure of PEDOT:PSS (left), and polydopamine-doped-PEDOT:PSS (right). Right: Normalized stability characteristics of the PSCs using PEDOT:PSS and PDA:PEDOT:LS as the HTL, with a) PCE; b) V_{OC}; c) J_{SC}; d) FF. Adapted with permission.[89] Copyright 2018, Royal Society of Chemistry.

© 2021 The Authors. Advanced Energy Materials published by Wiley-VCH GmbH

16146840, 2021, 43, Downloaded from https://onlinelibrary.wiley.com/doi/10.1002/aenm.202100520 by Universita Di Torino, Wiley Online Library on [21/02/2025]. See the Terms and Conditions (https://onlinelibrary.wiley.com/terms-and-conditions) on Wiley Online Library for rules of use; OA articles are governed by the applicable Creative Commons License

Table 2. Figures of merit of bio-derived PSCs.

Compound	Function	J_{SC} [mA cm^{-2}]	V_{OC} [mV]	FF [%]	PCE [%]	Ref.
L-Glycine	Interlayer	16.28	0.98	60	9.48	[355]
L-Glycine	Interlayer	21.37	0.96	64	13.14	[92]
L-Alanine	Interlayer	22.40	0.99	64	14.22	[92]
β-Alanine	Interlayer	21.36	0.99	64	13.27	[92]
5-Aminovaleric acid	Interlayer	18.41	0.96	60	11.72	[92]
L-Alanine	Interlayer	21.77	0.89	80	15.46	[360]
L-Cysteine	Interlayer	23.6	1.11	70	18.3	[361]
L-Cysteine	Interlayer	22.34	0.90	71	14.4	[356]
Bacteriorhodopsin	Interlayer	22.61	1.05	70.5	17.02	[362]
Aloe-vera extract	Interlayer	21.65	0.99	59	12.58	[365]
DNA	Interlayer	20.85	1.04	73	15.86	[363]
DNA	Interlayer	22.90	1.07	71.9	17.59	[364]
Dopamine semiquinone	Interlayer	22.0	1.08	77.5	18.5	[93]
Dopamine	Interlayer	21.55	–	–	19.45	[371]
Dopamine	Interlayer	21.72	1.05	71.8	16.31	[368]
Dopamine	Interlayer	23.65	1.16	76.3	20.93	[90]
Dopamine	Interlayer	20.58	1.07	77	16.94	[369]
DOPA	Interlayer	20.72	0.97	74.2	14.85	[366]
Norepinephrine	Interlayer	20.58	0.97	72	14.40	[366]
DOBD	Interlayer	21.45	1.04	78.6	17.46	[366]
Polydopamine	Interlayer	18.19	1.02	65.14	12.05	[89]
Polydopamine	Interlayer	20.63	1.08	78	16.6	[88]
Polydopamine semiquinone	Interlayer	19.97	0.97	75.36	14.60	[372]
Polydopamine	Interlayer	22.43	1.05	78.1	18.35	[243]
DNA	Sensitizer	23.46	1.12	78.9	20.63	[375]
L-lysine	Sensitizer	7.64	1.57	81	9.68	[357]
Glycine hydrocloride (*n*:8)	Sensitizer	22.19	1.08	75.08	18.06	[373]
Glycine hydrocloride (*n*:4)	Sensitizer	20.86	1.01	63.4	15.61	[373]
Ethyl cellulose	Sensitizer	22.89	1.1	77	19.41	[91]
CDHC	Sensitizer	17.73	0.96	61	10.38	[376]
HEC	Sensitizer	16.12	0.89	62	8.90	[376]
Chitin laminate composite	Substrate	17.41	0.98	74	12.52	[203]

In particular, the HOMO of the doped material was placed at –5.33 eV, compared to –5.1 eV for the nondoped HTL. Importantly, the doped layer also showed a higher pH of 5.2 (compared to 1.8 for the nondoped one), which can be linked to less corrosion issues. The PCE and J_{SC} retained 85.4% and 89.2% of their original values even after 28 days of aging as compared to 60.4% and 59.3%, respectively, for the PEDOT:PSS-based device. Devices based on dopamine–PEDOT:PSS, i.e., (ITO/dopamine–PEDOT:PSS/perovskite/$PC_{61}BM$/BCP/Ag exhibited a much higher V_{OC} of 1.08 eV and slightly decreased J_{SC} and FF as compared to PEDOT:PSS-based devices. Therefore, the PCE was enhanced to 16.6%, while PEDOT:PSS-based device only showed an efficiency of 15.2% associated to V_{OC}s of 0.97 V, J_{SC}s of 20.63 mA cm^{-2}, and FFs of 0.78 (Table 2). Dopamine semiquinone copolymerized PEDOT was also employed by Wang et al. in 2018 for heterojunction planar PSCs.[372] The authors reported that the working function of the modified PEDOT:PSS layer changed from 5.0 to 5.32 eV. This matches better with the HOMO energy level of the perovskite (–5.40 eV), rendering charge transfer more efficient. The average efficiency of twenty devices with modified PEDOT:PSS was increased to 14.16% from 10.67% with PEDOT:PSS (Table 2).

In 2019, Duan et al. employed polydopamine modified NiO for flexible PSCs with the architecture ITO/NiO:polydopamine/perovskite/PCBM/BCP/Ag.[243] The strong intramolecular interactions between polydopamine and the NiO allowed decreasing the inherent brittleness. Particularly, the crosslinked network NiO:polydopamine facilitates the releasing of mechanical stress, and thus the corresponding PSCs could hold >70% of the initial PCE after 1000 bending cycles. Moreover, the HOMO of the doped material (–5.35 eV) is more similar to the perovskite layers (–5.4 eV), improving charge transfer efficiency. Overall,

© 2021 The Authors. Advanced Energy Materials published by Wiley-VCH GmbH

16146840, 2021, 43, Downloaded from https://onlinelibrary.wiley.com/doi/10.1002/aenm.202100520 by Universita Di Torino, Wiley Online Library on [21/02/2025]. See the Terms and Conditions (https://onlinelibrary.wiley.com/terms-and-conditions) on Wiley Online Library for rules of use; OA articles are governed by the applicable Creative Commons License

champion devices showed PCEs of 18.35%, V_{OC}s of 1.05 V, and J_{SC}s of 22.49 mA cm^{-2}, compared to 15.87%, 0.97 V; and 21.90, respectively, for pure NiO-based PSCs (Table 2).

5.2.2. Sensitizer

Amino Acids: The positive effect of the amino acid L-lysine was also confirmed in inorganic PSCs based on cesium lead bromide ($CsPbBr_3$).[357] The latter presents outstanding environmental stability and low preparation cost. Therefore, it is regarded as one of the most promising perovskite sensitizers for commercial applications. However, the performance of $CsPbBr_3$ PSCs is highly sensitive to the presence of ionic defects at the grain boundaries of perovskite films, which generate high charge recombination and efficiency loss. Defects are usually originated when the precursor solution of CsBr is poured onto a $PbBr_2$ film, starting the crystallization process that leads to the formation of the perovskite layer. If L-lysine is incorporated into the $PbBr_2$ solution, it can considerably reduce the defect density upon crystallization, prolong the carrier lifetime, and heal the charge recombination centers (Pb^{2+},Cs^+, and Br^-) within perovskite films as well as it enhances the interfacial energy level alignment, which contributes to a remarkably enhanced charge extraction and transfer. Moreover, the addition of L-lysine delays the crystallization rate, enlarges grain size, and improves the crystallinity of $CsPbBr_3$ perovskite by modulating the surface morphology and crystallinity of $PbBr_2$ films, leading to reduced grain boundaries and improved quality of $CsPbBr_3$ films and thereby a suppressed charge recombination. The devices were fabricated with a standard configuration of FTO/TiO_2/L-lysine/perovskite/carbon. Overall, the V_{OC} could be improved of up to 61% compared to reference PSCs without L-lysine, reaching a high value of 1.56 V, accompanied by a PCE of 9.69% and a FF of 0.81 (Table 2). In this line, Chen and co-workers recently implemented amino acid derivatives in Ruddlesden–Popper (RP) perovskites.[373] In detail, they added glycine hydrochloride $[Gly_2(Cs_{0.05}FA_{0.95})_{n-1}Pb_nI_{3n-1}Cl_2]_{0.9}(FAPbBr_3)_{0.1}$, where n could be 4, 6, or 8. Due to the strong interaction between C=O and Pb^{2+}, the Gly^+ can become a nucleation center and be beneficial to uniform and fast growth of the Gly-based RP perovskites with larger grain sizes, leading to reduced grain boundary and increased carrier transport. The champion device with *n*:8 showed PCEs of 18.05%, V_{OC}s of 1.08 V, and J_{SC}s of 22.9 mA cm^{-2} (Table 2). Another interesting effect was recently reported by Lang et al.[374] The researchers investigated the effect of the amino acid L-lysine during the perovskite formation. While a comparable behavior was noticed, the authors also reported that amino acid additives strongly increase the perovskite stability in water. Unfortunately, the effects on the device figures of merit are still unknown.

DNA: In a preliminary work from Yusoff et al., DNA was incorporated as the separate layer underneath the perovskite layer, which resulted in insufficient interfacial coupling between DNA and perovskite. This issue was addressed by Hou et al. in 2019.[375] The authors developed a self-assembly process that can incorporate DNA strands into the perovskite nanocrystalline film. In detail, the bulk $CH_3NH_3PbI_3$ perovskite crystals were exfoliated by intercalation of methylamine molecules to form liquid intermediate consisting of 2D perovskite layers. The DNA–CTMA molecules were then introduced into the liquid perovskite intermediate, and the subsequent self-assembly of DNA–CTMA molecule with 2D perovskite layers finally resulted in a core–shell composite structure after spin-coating process. This results in the formation a core–shell heterostructure with DNA–CTMA molecules occupying the perovskite grain boundaries. The so-fabricated architecture allows the hole carriers to be effectively extracted from perovskite grains and then transferred to the HTL, while, simultaneously, the trap sites at grain boundaries are passivated by bonds between DNA molecules and the perovskite itself, thereby reducing the nonradiative recombination loss. The group built devices with the architecture FTO/compact TiO_2/mesoporous TiO_2/DNA–perovskite/spiro-OMeTAD/Au. The PSC devices based on the bio-based hybrid composite attained remarkable PCEs of 20.63%, and the V_{OC}, J_{SC}, and FF were 1.12 V, 23.46 mA cm^{-2}, and 78.9%, respectively.

By contrast, HTL-free PSC devices attained a PCE of 14.05%, which is nearly 65% higher compared with the pristine device. This represents one of the best device performances in the field of bio-photovoltaics and underlines the beneficial role of bio-derived materials.

Cellulose Derivatives: The use of ethyl cellulose for controlling the film quality of the perovskites was introduced by Bao and co-workers in 2019.[91] Indeed, the group highlights the fact that the use of a long polymer offers more stable and reliable interactions with the perovskite layers, serving as grain boundaries crosslinkers to reduce defects. The material was spin coated together with the precursors PbI_2 and CH_3NH_3I. Thanks to its hydroxyl and ethyl groups, the cellulose could coordinate the uncoordinated Pb^{2+} atoms via the lone pair on the oxygen atom, as confirmed by both XPS and FTIR measurements. The ethyl cellulose-passivated PSC in the planar n–i–p architecture (in which the perovskite is sandwiched between an ETL and an HTL), reaches an average PCE of 19.41%. The V_{OC}, J_{SC}, and FF were of 1.1 V, 22.89 mA cm^{-2}, and 0.77, respectively (Table 2). With regard to the stability, the device comprising EC retained 80% of the initial PCE value after 30 days in ambient air. At the same time, the reference PSC fully degraded.

The same year, Chu et al. implemented chlorodeoxyhydroxyethylcellulose (CDHC) and hydroxyethylcellulose (HEC) into organic inorganic inverted PSCs.[376] The dopants were directly added to the precursor CH_3NH_3I solution and were reported to improve film crystallinity by decreasing the number of grain boundary defects as well as increasing the crystal grain sizes, crystallinities, and absorption intensities of the modified perovskite films. The fabricated PSCs, whose device structure was indium tin oxide/PEDOT:PSS/$CH_3NH_3PbI_3$:cellulose derivative/[6,6]-phenyl–C_{61}–butyric acid methyl ester/Ag showed maximum J_{SC}s of 17.73/16.12 mA cm^{-2}, V_{OC}s of 0.96/0.89 V, FFs of 0.61/0.62, and PCEs of 10.38/8.90% for CDHC and HEC, respectively (Table 2).

5.2.3. Substrate

Chitin: The use of chitin nanofibers transparent laminate composite film (HCLaminate) for flexible PSCs was pioneered by

© 2021 The Authors. Advanced Energy Materials published by Wiley-VCH GmbH

16146840, 2021, 43, Downloaded from https://onlinelibrary.wiley.com/doi/10.1002/aenm.202100520 by Universita Di Torino, Wiley Online Library on [21/02/2025]. See the Terms and Conditions (https://onlinelibrary.wiley.com/terms-and-conditions) on Wiley Online Library for rules of use; OA articles are governed by the applicable Creative Commons License

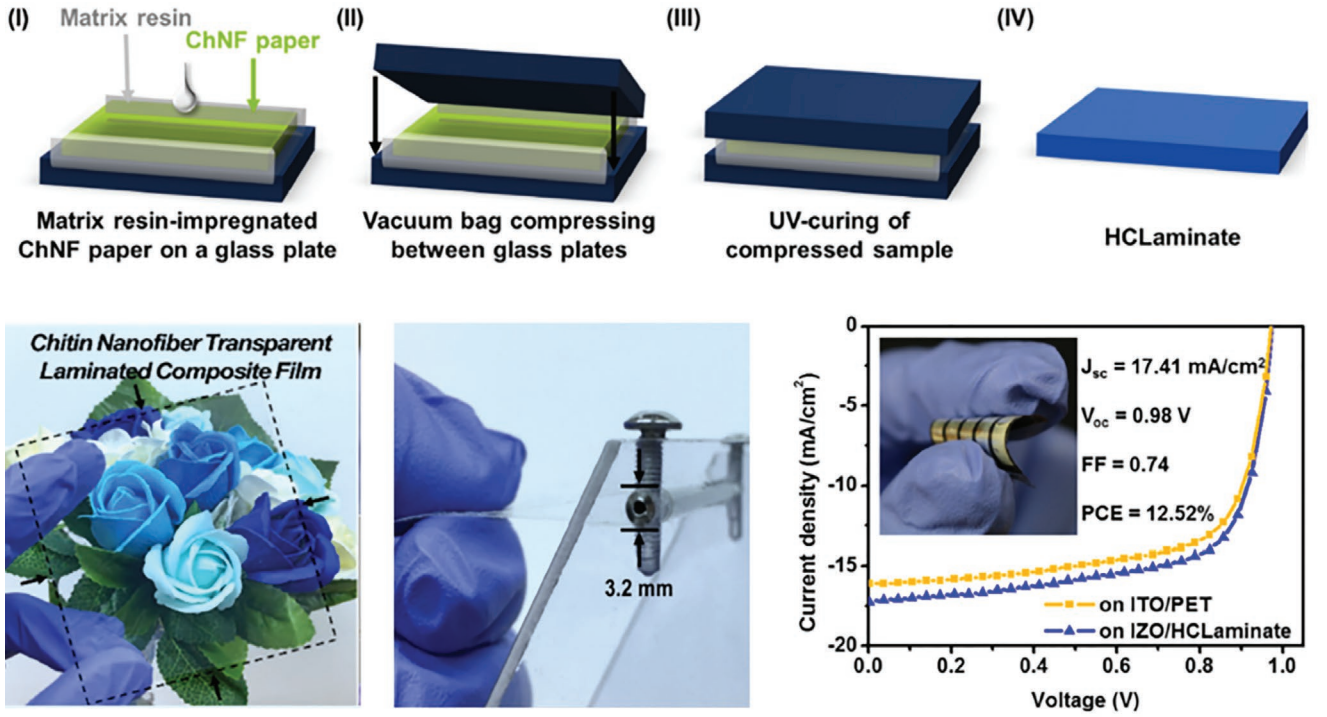

Figure 10. Top: Schematic illustration of the fabrication procedure of the HCLaminate. Bottom: digital photograph of the transparent HCLaminate (left), digital photograph showing the mandrel bend test of the HCLaminate (centre), and J-V curves of flexible PSC fabricated on the HCLaminate (right). Adapted with permission.[203] Copyright 2017, American Chemical Society.

Bae and collaborators.[203] These films presented a transparency >90% in all the visible range, as well as favorable mechanical properties, such as an higher elastic modulus of 6 GPa and very low CTE of only 22 ppm K^{-1} (PET, as an example, as a CTE of 24 ppm K^{-1}). Their proof-of-concept PSCs on CNL/ITO/PEDOT:PSS/perovskite/$PC_{60}BM$/Ag reached J_{SC}s of 17.41 mA cm^{-2}, V_{OC}s of 0.98 V, FFs of 74%, and PCEs of 12.52% that are comparable to those with standard PET (Table 2, **Figure 10**).

To summarize, the majority of contributions regarding the implementation of bio-derived materials in PSCs concerned the modification of the transport–perovskite interface or the perovskite with molecules possessing ambipolar moieties, such as amino acids, catecholamine, dopamine, and DNA. Noteworthy, other types of bio-derived materials led to impressive results, e.g., capsaicin,[377] betulin[378] and biopolymer heparin sodium interlayers.[379] Common to all of them is i) the improvement of the perovskite's morphology and its defect passivation, as well as ii) the enhancement of the charge extraction owing to a modified HTL/perovskite heterojunction. Additionally, these modifications are often accompanied by a simultaneous increase in device stability, which is essential in order to scale-up PSCs production. Importantly, the implementation of bio-derived materials usually leads to improved performances compared to the reference devices (Table 2). This is a key message as it is commonly accepted that performances can be within to a certain extent sacrificed in order to achieve greener devices, but, in the case of PSCs, a greener approach is becoming even essential to fabricate superior cells.

5.3. Bio-DSSCs

5.3.1. Photosensitizer

Proteins: In 2015, Molaeirad and Rezaeian immobilized for the first time a layer of bR onto a ZnO film and successfully built PV devices within DSSC concept.[165] In detail, they used a dip coating film deposition to sensitize the photoanonde with a monolayer of bR (**Figure 11**). The device was closed with a Pt-based counter electrode and filled the space between the two electrodes with iodine liquid electrolyte. The so-fabricated device showed poorly performances, namely PCE of 0.1%, J_{SC} of 0.39 mA cm^{-2}, V_{OC} of 0.50 V, and FF of 52% (Table 3). Despite these results, when comparing to literature data concerning protein-sensitized solar cells, this approach resulted in more efficient devices than the prior-art based on bR.[380,381] Some months later, Mohammadpour et al. further expanded the emergent field of protein-sensitized solar cells introducing for the first time green fluorescent proteins (GFP) as co-sensitizer of bR to enlarge the absorption spectra and enhance the PCE.[382] This devices consisted in a co-sensitized layer embedded between an FTO/TiO_2 photoanode and a FTO/Pt counter electrode with an iodine-based electrolyte (Figure 11), and led to PCE of 0.4%, J_{SC} of 1.2 mA cm^{-2}, V_{OC} of 0.68 V, and FF of 49%. Importantly, the authors confirmed the role of the proteins as photosensitizers, measuring an IPCE spectrum that resembles the absorption spectra of both proteins.

The following year, Chellamuthu et al. pointed out the limits of liquid electrolytes for protein-sensitized DSSCs due to the high recombination process that drastically reduces the

© 2021 The Authors. Advanced Energy Materials published by Wiley-VCH GmbH

16146840, 2021, 43, Downloaded from https://onlinelibrary.wiley.com/doi/10.1002/aenm.202100520 by Universita Di Torino, Wiley Online Library on [21/02/2025]. See the Terms and Conditions (https://onlinelibrary.wiley.com/terms-and-conditions) on Wiley Online Library for rules of use; OA articles are governed by the applicable Creative Commons License

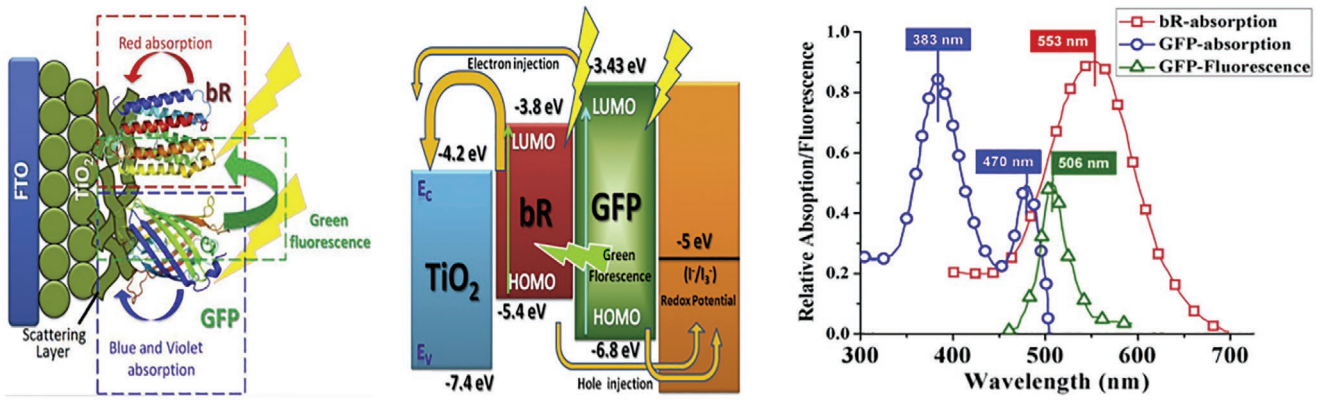

Figure 11. a) Schematic view of the co-sensitizing effect of GFP and bR, b) energy level diagram of the fabricated protein-based DSSC, c) absorption spectra of bR and absorption and emission spectra of GFP. Reproduced with permission.[382] Copyright 2016, Elsevier Ltd.

current density.[383] Thus, they applied a quasi-solid state electrolyte with an acetamide gel to a bR-based DSSC, achieving the record PCE of 0.5%, J_{SC} of 1.1 mA cm^{-2}, V_{OC} of 0.67 V, and FF of 58% (Table 3). In 2018, Srivastava et al. developed an innovative new class of bio-hybrid and biogenic material suitable for PV applications.[384] They successfully encapsulated *E. coli* cells, genetically modified to produce a photoactive dye, in TiO_2 mesoporous layer trough a tryptophan-mediated interface. When coupled with a Pt counter electrode and an I^-/I_3^- the so-fabricated DSSCS achieved PCE of 0.057%, J_{SC} of 0.69 mA cm^{-2}, V_{OC} of 0.29 V, and FF of 28% (Table 3).

Despite the modest results, the reported approach obviates the extraction and purifications steps for photosensitizers. As covalent linkages of the dyes are no longer required, genomic engineering could drastically enhance the yield of products and offer a green route toward the fabrication of DSSCs avoiding toxic solvents and chemicals.

In 2019, Cerdá's group further expanded the panorama of suitable proteins for PV devices fabricating a R-phycoerythrin red protein-based DSSCs.[385] Using raw extract from two different algae species *Anotrichium furcellatum* and *Palmaria decipiens*, without further purification, they built DSSCs that showed PCE of 0.11%, J_{SC} of 0.22 mA cm^{-2}, V_{OC} of 0.69 V, and FF of 62% (Table 3).

In the same year, Güzel et al. developed a bionanoferritin-based cages (FBNCs) and used it as interface modifier on TiO_2 layer, reporting a new concept of protein-based DSSCs.[386] The bionanoferritin-based particle were first mixed with graphene and then ITO coated with a TiO_2 layer was immersed in the dispersion. After coating, the photoanode was dried and the cell closed with a Pt-based counter electrode, finally iodine based liquid electrolyte was used to close the electrical circuit. This device achieved PCEs of 0.24%, J_{SC}s of 0.65 mA cm^{-2}, V_{OC}s of 0.54 V, and FFs of 72% (Table 3). Recently, the same group[387] used the same approach to prepare photosystem II bio-nanococktails (BCNs) and used it as photosensitizer of a TiO_2 layer. The resulting device exhibited PCE of 0.22%, J_{SC} of 0.88 mA cm^{-2}, V_{OC} of 0.37 V, and FF of 50% (Table 3).

In light of the above-mentioned, there are still many open questions about the efficiency of the charge transfer process from proteins to metal oxide electrodes, as well as the role of the protein functionalization and structure in the back electron transfer reactions. Thus, device efficiencies have remained poor up to date.

Natural Dyes: Different biological dyes, such as flavonoids, betalains, carotenoids, chlorophylls, and bacteria pigments, have been successfully employed as photosensitizer in DSSCs.[56] Up to date, their principal source of extraction from vegetables and a precisely final cost of the products is difficult to assess together with a proper life-cycles assessment analysis.[60] The promising results achieved by natural dyes in PVs required further efforts in developing new biosynthetic routes to obtain them in a more sustainable and up-scalable way. This was, for example, nicely highlighted by Lorquin and collaborators with respect to the application of carotenoids.[388]

Up to date, DSSCs sensitized with flavonoids have shown PCEs <1%,[389–391] mostly due to dye aggregation, electron recombination, and prominent undesired back electron transfer reactions. In 2017, Prabavathy et al. introduced two algae-derived buffer layers to functionalize the TiO_2–photoanode, improving the anchoring groups suitable for dye loading and the overall efficiency of the anthocyanin-based PVs.[166] The first buffer layer was made by sodium alginate, while the second one by *Spirulina*, i.e., green algae extract made of chlorophylls, xanthophylls, amino acid, and phycocyanin. Sodium alginate helps to produce more hydroxyl groups onto TiO_2 surface, and in turn, the dye concentration anchored to the semiconductor and its light-harvesting efficiency improved. The second buffer layer has different functions: i) xanthophylls (carotenoids family) broaden the absorption spectrum and dissipate the excess of energy from sunlight shielding from UV, ii) phycocyanin is an antioxidant that protect the SC from free radical, iii) chlorophylls help to improve the light harvesting, and iv) amino acids improve the interface between organic dyes and TiO_2. The synergistic effects of the various components led to an enhancement in device performances, namely PCE of 1.47%, J_{SC} of 5.8 mA cm^{-2}, V_{OC} of 0.60 V, and FF of 41% with an improvement of almost 185% compared to PCEs achieved by DSSCs sensitized with the same type of anthocyanines.[392]

Generally, the use of carotenoids as sensitizers has led to a very low PCEs, especially due to the lack of anchoring groups as demonstrated by Yamazaki et al.[268] Nevertheless, their use as co-sensitizers has showed promising results. For instance, Wang and collaborators used methyl 3-carboxy-3-devinyl-pyropheophorobide (PPB, a chlorophyll) as sensitizer in combination with 10% of spirilloxanthin (Spx) carotenoids from

© 2021 The Authors. Advanced Energy Materials published by Wiley-VCH GmbH

16146840, 2021, 43, Downloaded from https://onlinelibrary.wiley.com/doi/10.1002/aenm.202100520 by Universita Di Torino, Wiley Online Library on [21/02/2025]. See the Terms and Conditions (https://onlinelibrary.wiley.com/terms-and-conditions) on Wiley Online Library for rules of use; OA articles are governed by the applicable Creative Commons License

16146840, 2021, 43, Downloaded from https://onlinelibrary.wiley.com/doi/10.1002/aenm.202100520 by Universita Di Torino, Wiley Online Library on [21/02/2025]. See the Terms and Conditions (https://onlinelibrary.wiley.com/terms-and-conditions) on Wiley Online Library for rules of use; OA articles are governed by the applicable Creative Commons License

Rhodospirillum rubrum S1, reaching PCEs of 4.2%.[267] Unfortunately, no further improvements have been reported up to date.

Recently, two promising works reported on the use of carotenoids from non-photosynthetic UV-resistant Antarctic bacteria. In 2016, Órdenes-Aenishanslins et al. tested both the red- (*Hymenobacter*) and the yellow-pigments (*Chryseobacterium*) from Antarctic bacteria as sensitizers in DSSCs.[393] The PCEs were around 0.03% regardless of the pigment. The photostability of the isolated carotenoids was investigated from the decay in light absorbance at different exposure times, and it was evident that the UV-resistant carotenoids are stable under light exposure for longer times. Two years later, Montagni et al. improved the performance of the red-pigment-based DSSCs through the usage of polysaccharide co-sensitizers, which helped in improving bonding/anchoring of xanthophylls pigments onto the TiO_2 surface due to the presence of extra hydroxyl groups.[167] Noteworthy, this class of carotenoids from Antarctic bacteria has not been employed as co-sensitizer with other natural dyes yet, e.g., chlorophylls, suggesting that further improvements are easily at hand.

Despite the presence of a carboxylic group in betalains, only few reports have been published. Güzel et al. proposed a new betalain-based extract from stalk of pokeweed as natural sensitizer suitable for DSSCs.[394] Thanks to its broad absorption spectra spanning from 300 to 700 nm, the resulting devices showed PCE of 3.04%, J_{SC} of 9.08 mA cm^{-2}, V_{OC} of 0.63 V, and FF of 53%, This is the highest performances achieved by betalain-based DSSCs up to date (Table 3).

With regard to chlorophylls, there are no recent relevant progresses focused on their use as photosensitizer for DSSCs. The reader could use these exhaustive reviews to satisfy further curiosities.[56,59,60,389,390,395]

In conclusion, the research on proteins as photosensitizers has not led to outstanding performances yet. Nevertheless, remarkable progress has been achieved in the last 5 years: i) the panorama of suitable protein-based sensitizers has been expanded, ii) new concepts have been developed, and iii) interactions with other DSSC components have been disclosed. In particular, the PCE achieved by the bR-based DSSC fabricated by Jeganathan and collaborators represents a five-fold improvement with respect to the previous state-of-the-art. Concerning natural dyes: i) an almost threefold enhancement of flavonoid-based DSSC has been achieved and ii) the highest PCE has been achieved with betalain-based DSSCs. Noteworthy, the stability issues of proteins and natural dyes is still a challenge to be tackled in order to further optimize this type of photosensitizers. However, the beneficial impact of a buffer layer introduced by Prabavathy and co-workers has not been used with other classes of natural dyes yet. Overall, the use of bio-derived materials as photosensitizer in DSSCs is still very challenging.

5.3.2. Electrolytes

Polysaccharides: In 2017, Bella et al. proposed paper-based quasi-solid DSSCs, consisting of a cellulosic fiber based photoanode and nanoscale microfibrillated cellulose (NMFC) biopolymer electrolyte.[396] The latter was obtained from sulfite bleached spruce pulp using two stages refining process. Two oligomers, namely poly(ethylene glycol) diacrylate (PEGDA) and poly(ethylene glycol) methyl ether methacrylate (PEGMA), were mixed and added to the NMFC suspension. Through steps of drying, pressing, photocuring, and drying under vacuum, a final polymer membrane 100 μm thick was obtained, which was finally rapidly soaked into an I^-/I_3^- liquid electrolyte. The resulting DSSCs provided PCEs of 3.55% and 5.20% under 1 and 0.2 sun irradiations, respectively (Table 3). This bioinspired DSSC maintained a 96% of its PCE even after 1000 h of accelerated aging tests.

Later, Poskela et al. suggested the use of CNF, TEMPO-oxidized CNF (TOCNF), BC, and chitin nanofibers (ChNF) as bio-based cryogel membranes, acting as electrolyte holders in DSSCs. Through these membranes the electrolyte can be directly applied before sealing the cell, thereby preventing segregation effects (**Figure 12**). Among the candidates, BC was chosen as the most promising, yielding higher PCEs and longer stabilities, mainly due to residual components in CNF, e.g., lignine. DSSCs based on Z907 (Dyesol) and BC as cryogel membrane featured PCEs of 4.9%, FFs of 60%, V_{OC}s of 0.70 and J_{SC}s of 11.6 mA cm^{-2} (Table 3). The longest stability was, however, reported by Willgert et al. with CNC. They fabricated nanocomposites of CNC and polyethylene oxide (PEO) for a copper dye based DSSC featuring PCE of 1.09% that hold almost constant (15% loss) after 1440 h of aging (Table 3).

The high crystallinity of cellulose resulted in low ion conductivities. However, cellulose can easily be modified via chemical functionalization, plasticization, grafting, and blending with another polymers.[398] One of the most commonly employed derivatives is ethyl cellulose.

In 2015, Rudziah et al. studied biopolymer electrolytes based on carboxymethyl kappa-carrageenan (CMKC)/CMC blend for use as electrolytes in solid-state DSSCs.[399] The salts were then blended and doped with ammonium iodide/iodine (NH_4I/I_2). The so-fabricated gels exhibited a high conductivity of 2.41×10^{-3} S cm^{-1} for the CMKC/CMC containing 30 wt% of NH_4I. The DSSCs exhibited J_{SC} of 0.42 mA cm^{-2}, V_{OC} of 0.50 V, and FF of 0.64 that resulted in PCE of 0.13% (Table 3). The poor performance was attributed to the contact at the electrode–electrolyte interface. Two years later, Bella et al. employed CMC as electrolyte and 2-[{4-[4-(2,2-diphenylethenyl)phenyl]-1,2,3,3a,4,8b-hexahydrocyclopento[b]indole-7-yl}methylidene]-cyanoacetic acid (D131) as sensitizer.[53] The group fabricated a self-standing gel composed of 6.5 wt% CMC, aqueous NaI or KI, I_2. The best PCE (0.72%) was achieved in the presence of 5.5 wt% CMC and 5.5 M KI. More importantly, the stability performances were remarkable with a 93% of retained efficiency after 29 days of aging (Table 3).

Naceur Abouloula et al. applied oil palm waste based phtaloyl cellulose in N719-based DSSCs.[400] The gel was obtained in DMSO with the redox couple LiI/I_2. The group reported the presence of strong interactions between the Li^+ cations and the hydroxyl groups of the cellulose, as proved by Fourier transform infrared spectroscopy (FTIR) assays. Upon addition of 10 wt% LiI, the highest ionic conductivity in the electrolyte was obtained, and, therefore, the highest PCE of 3.29% evolved (Table 3). Selvanathan et al. employed phthaloyl starch and hydroxyethyl cellulose to fabricate ionic gels for N719-based

© 2021 The Authors. Advanced Energy Materials published by Wiley-VCH GmbH

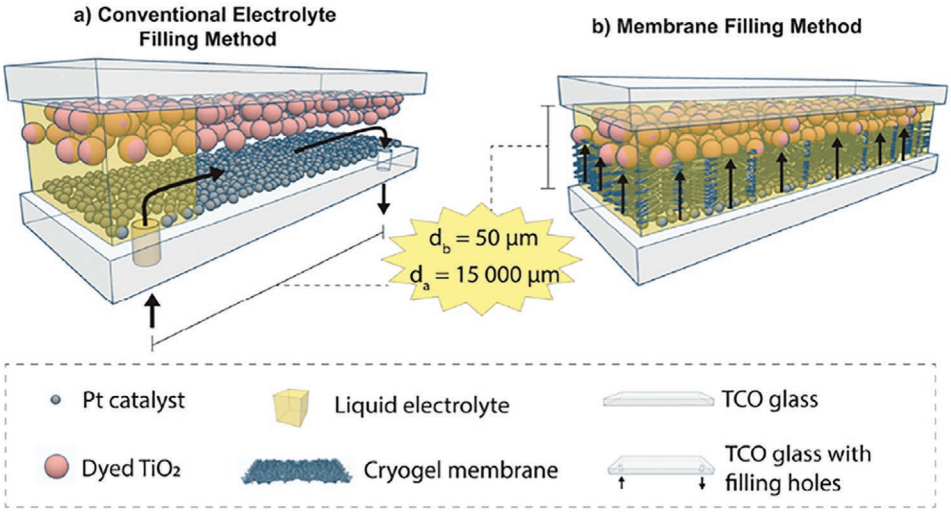

Figure 12. Conventional electrolyte filling method makes the electrolyte flow through the entire cell horizontally (10–20 mm distance) (left). By using an electrolyte membrane (right), the electrolyte can wet the photoelectrode vertically, reducing the diffusion length to 50 µm. Reproduced with permission.[397] Copyright 2019, American Chemical Society.

quasi-solid state DSSCs.[401] Devices containing gels with 70% and 30 wt% of phthaloyl starch and hydroxyethyl cellulose, respectively, showed the best mechanical and rheological properties, and also achieved the best device performances, namely PCE of 3.02%, J_{SC} of 9.02 mA cm^{-2}, V_{OC} of 0.57 V, and FF of 60% (Table 3).

Starch and Derivatives: In a first contribution, Yogananda et al. employed rice starch based aqueous gel electrolytes for DSSCs.[402] The gel was isolated from raw rice via an alkali treatment, while the electrolyte LiI/I_2 was used. The champion DSSC showed V_{OC} of 0.92 V, J_{SC} of 0.28 mA cm^{-2}, FF of 46%, and PCE of 0.35% (Table 3). In a follow-up work, the group focused on potato starch (PS) and potato starch nanocrystals (PSN).[403] Both electrolytes were obtained from raw potatoes via an alkali treatment. PSN was obtained by acid hydrolysis of PS and lyophilized to get a fine powder. The electrolyte gel was prepared by mixing PS or PSN with NaI/I_2 in DMSO. The latter showed slightly better performances than PS, achieving 5.59 mA cm^{-2}, V_{OC} of 0.72, PCE of 2.01%, and FF of 50% (Table 3).

In 2019, Lobregas and Camacho modified potato starch by grafting 1-glycidyl-3-methylimidazolium chloride (GMIC) ionic liquid onto the polysaccharide chain to afford a cationic starch.[213] The starch powder was added to a DMSO solution of the redox couple KI/I_2 to achieve a gel electrolyte. DSSCs based on N719 achieved PCE of 0.51% (Table 3). The group of Sambandam achieved a starch-based biopolymer gel electrolyte system by mixing LiI/I_2 with bare and citric acid crosslinked potato starches with glycerol as the plasticizing agent.[404] The gel is obtained by adding a gelation agent, namely starch, to the LiI/I_2 in DMSO solution. Crosslinked starch hinders the interaction of iodine with the starch polymer itself, thereby rendering the iodine more available for transport. The champion cell prepared with crosslinked starch and N719 as sensitizer featured PCE of 1.4%, FF of 82%, J_{SC} of 2.17 mA cm^{-2}, and V_{OC} of 0.67 V (Table 3).

Monosaccharides: In 2016, Sagaidak et al. explored the use of iodide salts and ionic liquids based on carbohydrate D-glucose or D-mannose core units as DSSC electrolytes.[405] The electrolytes based on D-glucose revealed excellent properties under environmental condition and accelerated aging test, reaching 1000 h in accelerated aging tests. The best solar cell performances were achieved with glucose methylimidazolium iodide, i.e., PCE of 7.3% compared to 8% for the benchmark electrolyte, using the ruthenium dye C106 as sensitizer. Recently, Boldrini et al. and Selvanathan et al. reported on sugar-based natural deep eutectic solvents (NADESs) as active electrolyte for DSSCs.[406,407] These were obtained by mixing different amounts of glucose, sorbitol, fructose, and mannose. The group furtherly implemented the glucose phenothiazine di-branched derivative PTZ–Glu as photosensitizer and a glucose-based co-adsorbent. The best devices were obtained with a glucose based electrolyte, sensitizer, and co-adsorbent, namely PCE of 1.4%, FF of 64%, V_{OC} of 0.53, and J_{SC} of 4 mA cm^{-2} (Table 3). The group highlighted how the interplay between the sugar-based sensitizer, the co-adsorbent, and the NADES are responsible for the highest device performance.

Gelatin: In 2015, Sharma et al. fabricated an Au/gelatin gel electrolyte for a set of quasi-solid-state DSSC.[408] The addition of Au NPs into a gel electrolyte facilitates the enhancement of ionic conductivity of the gel by providing a large active surface area.[409,410] To obtain the desired electrolyte, presynthesized Au nanocrystal dispersion was added to aqueous gelatin solution under vigorous stirring, and a crosslinker (glutaraldehyde) was added to the mixture. After curing at ≈60–70 °C, the mixture turned into the desired nanocrystal gel within a few minutes. A gel electrolyte was prepared by soaking dried Au/gelatin gel in the liquid electrolyte (LiI/I_2) for more than 96 h to reach absorption saturation. DSSCs exhibiting N719 as sensitizer and the Au/gelatin gel showed PCE of 1.97%, V_{OC} of 0.66 V, J_{SC} of 4.94 mA cm^{-2} and FF of 61% (Table 3). Two years later, Khannam et al. used graphene oxide immobilized into gelatin hydrogel as quasi-solid state gel electrolyte for DSSCs.[411] The graphene oxide was sonicated and dispersed in water and later added to the gelatin together with the glutaraldehyde crosslinker. The mixture was then cured to yield the desired hydrogel. The

© 2021 The Authors. Advanced Energy Materials published by Wiley-VCH GmbH

16146840, 2021, 43, Downloaded from https://onlinelibrary.wiley.com/doi/10.1002/aenm.202100520 by Universita Di Torino, Wiley Online Library on [21/02/2025]. See the Terms and Conditions (https://onlinelibrary.wiley.com/terms-and-conditions) on Wiley Online Library for rules of use; OA articles are governed by the applicable Creative Commons License

Table 3. Figures of merit of bio-derived DSSCs.

Compound	Function	Photosensitizer	J_{SC} [mA cm^{-2}]	V_{OC} [V]	FF [%]	PCE [%]	Ref.
bR	Photosensitizer	–	0.39	0.50	52	0.1	[165]
bR/GFP	Photosensitizer	–	1.2	0.68	49	0.4	[382]
bR+gel elctrolyte	Photosensitizer	–	1.1	0.67	58	0.5	[383]
cell@TiO_2	Photosensitizer	–	0.69	0.29	28	0.057	[384]
R-phycoerythrin	Photosensitizer	–	0.22	0.69	62	0.11	[385]
FBNCs	Photosensitizer	–	0.65	0.54	72	0.24	[386]
Spirulina	Buffer Layer	Anthocyanin	5.8	0.60	41	1.47	[166]
PPB + Spx	Photosensitizer	–	11.5	0.57	63	4.0	[267]
Yellow-pigment	Photosensitizer	–	0.13	0.55	48	0.032	[393]
Red-pigment	Photosensitizer	–	0.20	0.44	37	0.033	[393]
Red-pigment	Photosensitizer	–	0.13	0.46	51	0.03	[167]
Betalain	Photosensitizer	–	9.08	0.63	53	3.04	[394]
CMC	Electrolyte	N719	0.42	0.5	64	0.13	[399]
Cellulose	Electrolyte, substrate	N719	8.35	0.98	60	3.55	[396]
CMC	Electrolyte	D131	2.61	0.45	61	0.72	[396]
BC	Membrane	Z907	11.6	0.70	60	4.90	[397]
Phtaloyl cellulose	Electrolyte	N719	7.89	0.59	71	3.29	[400]
Phtaloyl starch, hydroxyethyl cellulose	Electrolyte	N719	9.02	0.57	60	3.02	[425]
Rice starch	Electrolyte	N719	0.28	0.92	46	0.35	[402]
Potato starch	Electrolyte	N719	5.44	0.68	51	1.88	[403]
Potato starch nanocrystals	Electrolyte	N719	5.59	0.72	50	2.01	[403]
Grafted starch	Electrolyte	Ruthenizer 535-bisTBA	–	–	–	0.51	[213]
Crosslinked starch	Electrolyte	N719	2.17	0.67	82	1.40	[404]
Glucose iodide salt	Electrolyte	C106	16.2	0.70	65	7.3	[405]
Glucose-NADES, glucose-phenothiazine, glucose co-adsorbent	Electrolyte, Sensitizer, Co-adsorbent	PtZ-Glu	4.0	0.53	64	1.4	[406]
Gelatin	Electrolyte	N719	4.94	0.66	61	1.98	[408]
Gelatin	Electrolyte	N719	3.06	0.68	63	1.31	[411]
TiO_2@GO-Tyr	Electrode	N719	8.190	0.69	73	4.13	[413]
PEDOT-G-SiCs	Electrode	N719	14.1	0.71	72	7.2	[414]
PEDOT-p	Electrode	N719	13.09	0.72	63	6.13	[161]
GDs/PEDOT:PSS-glass	Electrode	N719	14.7	0.72	70	7.36	[415]
GDs/PEDOT:PSS-paper	Electrode	N719	12.08	0.70	58	4.91	[415]
TiO_2/FBs/CMC	Electrode	N719	8.36	0.66	64	3.55	[396]
rGO-SCCh	Electrode	N719	12.30	0.74	69	6.36	[416]
CRCF	Electrode	N719	16.12	0.74	68	8.11	[160]
CN_x/CNT	Electrode	N719	16.3	0.73	61	7.38	[417]
DNA	Dispersing agent/ electrode	N719	16.8	0.72	70	8.3	[263]
C-DNA@TiO_2	Electrode	N719	15.53	0.79	64	7.88	[162]
W-DNA@TiO_2	Electrode	N719	16.98	0.82	65	9.01	[162]
CW-DNA@TiO_2	Electrode	N719	18.89	0.81	60	9.23	[162]
DNA	Dispersing agent/ electrode	–	0.34	0.51	39	0.68	[418]
DNA	Binding agent/electrode	N719	3.80	0.66	69	3.40	[54]
Rhodamine-doped Silk PC	Light-trapping Layer	N719	2.94	0.68	60	1.18	[420]
BC/NFC on polyurethane	Sealant	N719	–	–	–	3.25	[423]

© 2021 The Authors. Advanced Energy Materials published by Wiley-VCH GmbH

16146840, 2021, 43, Downloaded from https://onlinelibrary.wiley.com/doi/10.1002/aenm.202100520 by Universita Di Torino, Wiley Online Library on [21/02/2025]. See the Terms and Conditions (https://onlinelibrary.wiley.com/terms-and-conditions) on Wiley Online Library for rules of use; OA articles are governed by the applicable Creative Commons License

optimized graphene oxide/gelatin gel electrolyte (i.e., 0.1 wt% graphene oxide) was placed evenly in between the dye adsorbed NiO@TiO_2 based photoanodes and the Pt counter electrode. The champion cell featured PCE of 1.31%, V_{OC} of 0.68 V, J_{SC} of 3.06 mA cm^{-2}, and FFs of 63% (Table 3).

Following the electrolytes discussion, most of the contributions are focused on the implementation of quasi-solid or solid-state biopolymers.[412] In this context, the high polarity of poly- and mono-saccharides is ideal, as it improves the solvation process. In addition, they feature a low tendency to volatilize keeping good ion conductivities that lead to outstanding stabilities of >1000 h. However, more efforts are required in order to improve the PCE, which are usually lower than the ones achieved with conventional electrolytes.

5.3.3. Electrodes

Amino Acids: In 2017, Taki et al. demonstrated the use of amino acids for the reduction of graphene oxide and tune of the corresponding energy levels.[413] They incorporated the amino acids-functionalized graphene into TiO_2 layer in DSSCs, achieving a performance enhancement of about 4.1-fold for the device assembled with the tyrosine-functionalized graphene (Table 3). The electrical conductivity, electrocatalytic activity, and photovoltaic properties of the graphene-composite directly depend on the structure of the functional amino acids, realizing better performances with aromatic amino acids. Noteworthy, the amino acid-functionalized graphene nanosheets showed an HOMO–LUMO band gap correlated with the type of amino acid employed. Thus, the authors claimed that the graphene derivative acts as both sensitizer and electron transporting/collection material within the network of the photoanode.

Proteins: In 2018, Krishnamoorthy's group[414] identified silk cocoons (SiCs) as a competitive substrate for flexible DSSCs due to their intrinsic mechanical stability. They coated polyphenols from green tea on SiCs as a protective and reductive coating and then from a gold plating solution they deposited a metal film onto SiCs network. In order to obtain a functional counter-electrode, they finalized the fabrication trough electropolymerization of PEDOT:PSS (PEDOT-G-SiCs). SiCs display an insulating nature and require blending with conductive particles in order to be effectively incorporated in a functional electrode. Gold is an excellent candidate to this end due to its low electrocatalytic activity that avoids any interference with the real catalyst (PEDOT:PSS in this case). In addition, this fabrication method allows reducing the consumption of expensive gold. The DSSCs fabricated with architecture FTO/TiO_2/N719/PEDOT-G-SiCs achieved PCE of 7.2%, J_{SC} of 14.1 mA cm^{-2}, V_{OC} of 0.71 V, and FF of 72% that were comparable with those noted for Pt–FTO based references (PCE of 7.4%) (Table 3).

Polysaccharides: In 2015, Kurungot and co-workers successfully prepared a Pt- and TCO-free counter electrode for flexible DSSCs, taking advantage from the effective and up-scalable approach to prepare highly conducting PEDOT-impregnated cellulose paper (PEDOT-p).[161] In PEDOT-p the polymerization of ethelenedioxythiophene (EDOT) is confined over the cellulose fiber, which resulted in enhanced doping. The resulting DSSC with the structure: PET/ITO/N719/PEDOT-p showed PCE of 6.1%, J_{SC} of 13.09 mA cm^{-2}, V_{OC} of 0.72 V, and FF of 63% that were slightly below the performance observed for Pt–FTO based reference.

Two years later, Lee et al.[415] further improved the development of paper-based counter electrodes. They firstly synthesized graphene dots (GDs) from glucose and water in a sealed glass bottle heated in a microwave oven at 595 W for 9 min and then they added them to an aqueous solution of PEDOT:PSS. Afterward, they immersed a commercial A4 sized printing paper in the solution of GDs/PEDOT:PSS for 10 min to obtain the final composite counter electrode. DSSCs fabricated on glass substrate achieved PCEs of 7.36%, which is close to those realized in Pt-based reference DSSCs (8.46%). The PCE recorded by Lee and co-workers was the highest ever reported efficiency with PEDOT:PSS-based counter electrode (Table 3), confirming the beneficial effects of the addition of GDs. Noteworthy, flexible DSSCs with GDs/PEDOT:PSS paper-based counter electrodes achieved PCE of 4.91%, that was surprisingly higher with regards to the sputtered Pt paper electrode used as reference (1.70%). In addition, the performances of the flexible DSSC were retained upon 150 bending cycles. In the same year, Bella and collaborators fabricated the first two components paper-based DSSCs, comprising both bio-derived photoanode and electrolyte.[396] With regard to the photoanode, a bleached softwood pulp was beaten to obtain fibers (FBs) that were then mixed with CMC and TiO_2 nanopowder to gain a slurry. The suspension was filtered and dried; afterward the TiO_2-laden paper membrane was transferred and bonded onto the conductive substrate, namely FTO/glass. The resulting two components paper-based DSSC achieved a promising PCE of 3.55% (Table 3).

One year later, Feng and co-workers completed a further step in the expansion of bio-derived materials in the DSSCs panorama.[416] They realized S-doped chitin/graphene (rGO-SCCh) counter electrodes, enhancing both electrocatalytic and conductivity performances, reaching the state-of-the-art Pt-based counter electrodes. The presence of N- and S-doped graphenes onto a chitin structure improves the catalytic capability, while maintaining a high conductivity and an optimal charge carrier transfer. The resulting DSSCs with the architecture: FTO/TiO_2/N719/rGO-SCCh achieved PCEs of 6.36%, J_{SC}s of 12.30 mA cm^{-2}, V_{OC}s of 0.74 V, and FFs of 69% (Table 3). Finally, Ouyang's group successfully fabricated a novel counter electrode made of conductive regenerated cellulose film (CRCF).[160] In order to obtain CRCF, ITO was sputtered onto regenerated cellulose films. The fabricated DSSCs with the structure: FTO/TiO_2/N719/CRCF achieved PCE of 8.11%, J_{SC} of 16.12 mA cm^{-2}, V_{OC} of 0.74 V, and FF of 68% (Table 3).

Catecholamine: In 2017, Shrestha et al. demonstrated that polydopamine can be used successfully as nitrogen containing precursor to generate catalytically active nitrogen-doped carbon nanotubes (CN_x/CNT) with excellent activity toward the reduction of I_3^-.[417] The excellent adhesive properties of PDA have been beneficial to deposit it onto CNT surface and, upon carbonization, an highly catalytic and conductive CN_x/CNT has been obtained and employed as counter electrode in DSSCs. Again, the doping strategy has been established as a valuable method to increase the catalytic capability of carbon-based

© 2021 The Authors. Advanced Energy Materials published by Wiley-VCH GmbH

16146840, 2021, 43, Downloaded from https://onlinelibrary.wiley.com/doi/10.1002/aenm.202100520 by Universita Di Torino, Wiley Online Library on [21/02/2025]. See the Terms and Conditions (https://onlinelibrary.wiley.com/terms-and-conditions) on Wiley Online Library for rules of use; OA articles are governed by the applicable Creative Commons License

materials. The devices fabricated with this innovative counter electrode with architecture: FTO/TiO_2/N719/ CN_x/CNT reached PCE of 7.38%, J_{SC} of 16.30 mA cm^{-2}, V_{OC} of 0.73 V, and FF of 62%, superior to those noted for Pt-based DSSCs used as references (Table 3).

DNA: In 2015, Yu et al. created single-walled carbon nanotubes (SWNTs)@(TiO_2/Ag/Au) nanocomposites with a synthesis processes involving multifunctional DNA.[263] DNA works both, as a dispersing agent preventing SWNTs bundling and as a sacrificial mold assembling TiO_2, Ag and Au nanoparticles on the surface of the SWNTs. This material was used as photoanode for DSSCs. The plasmid DNA solution was mixed with SWNTs to achieve SWNT dispersion. The composite was then obtained by adding silver nitrate, chloro(trimethylphosphine) gold(I), and TiO_2 nanoparticles, and finally mixed with commercial TiO_2 paste to give rise to the improved photoanode. This resulted in N719-based DSSCs with PCE of 8.3%, J_{SC} of 16.8 mA cm^{-2}, V_{OC} of 0.72 V, and FF of 69.7% (Table 3).

In 2016, Sönmezoğlu's group reported for the first time on the application of DNA as interface modifier between TiO_2 layer and the sensitizer in DSSCs.[162] They pointed out how the introduction of DNA is beneficial in two ways: i) the binding of DNA to TiO_2 layer influences the energy Fermi level of the conduction band and prevent charge recombination at the interface by blocking of holes, enhancing V_{OC}, and ii) the DNA interlayer reduces the number of vacant Ti site and free anchoring group of dye molecules, reducing the aggregation behavior and enhancing J_{SC}. Furthermore, thanks to the phosphate moieties in the DNA double helix, the bond between DNA and TiO_2 is favorable without the usage of additional linkers. In their pioneering work, the authors extracted DNA from chickpea (C) and wheat (W) plants and then they spin coated the DNA aqueous suspension directly onto TiO_2 coated FTO substrates. The resulting DSSC was FTO/TiO_2/DNA/N719/Pt. The two different DNA molecules were used alone and in a mixture of them (CW) and the DSSC based on the latter achieved a PCEs of 9.23%, with an improvement of almost 50% compared to the reference device (Table 3).

Kundu and collaborators also exploited the idea of using DNA to promote the synthesis of an innovative photoanode material, namely Nb_2O_5 nanoassemblies.[418] The latter were obtained by dissolving niobium pentachloride in aqueous DNA solution and stirring for 30 min with intermittent microwave heating for about 3 min. Importantly, the different morphologies of Nb_2O_5 nanomaterials could be prepared by altering the concentration ratio of starting precursor solution and by optimizing other reaction parameters. Proof-of-concept DSSCs were fabricated and exhibited PCEs of 0.68%, J_{SC} of 0.34 mA cm^{-2}, V_{OC} of 0.51 V, and FF of 39% (Table 3).

In 2018, Shakir et al. fabricated DNA template gold wires (AuWs) on Pt sputtered ITO (Pt/ITO) substrates for their use as counter-electrode in DSSCs.[54] The group employed a previously developed method relying on the self-assembling properties of DNA–Ag/Au NP films prior to scribing.[419] The assembling process and the drying capillary force induce the NPs to form a metal–DNA pattern on the film. Enzymatic etching was finally applied to remove the unwanted DNA material to yield only the metal wire on the substrate. The so-fabricated AuWs/Pt/ITO counter electrode exhibited enhanced electrocatalytic activities and higher conductivities than conventional Pt/ITO electrodes due to the synergistic effect of Pt and AuWs network on ITO. The DSSCs fabricated using TiO_2 photoanode, N719 dye, I_3^-/I^- electrolyte, and AuWs/Pt/ITO counter-electrode showed a 36% increase in efficiency as compared to the cells made under same parameters but using conventional (Pt/ITO) counter-electrode (Table 3).

If the use of proteins as photosensitizer did not result in satisfying performances, their implementation in electrodes appear more than promising with overall PCEs around 7% and FFs of ≈70%, achieved with PEDOT-G-SiCs. In addition, there still is space for further improvement, especially with regard to replacement of gold as conductive component of the electrode. Following these inputs, innovative blends based either on graphene or on cheaper metals (Cu, Ag) are highly desired. As for the electrolyte, polysaccharide-derived materials are the most investigated categories. Paper-based counter electrodes have been demonstrated to be able to outperform the standard Pt-based counter electrode in flexible devices. The GDs/PEDOT:PSS paper-based counter electrode showed an almost threefold improvement of the performances with regard to the Pt-based reference. Furthermore, rGO-SCCh counter electrodes achieved on par performances with Pt-based reference also with the standard glass substrate. Moreover, PDA has been successfully used as nitrogen precursor to functionalize CNT. The resulting electrode exhibited excellent catalytic activity and adhesion property, leading to a DSSC outperforming the Pt-based reference. Several well operating devices were fabricated also with DNA-based electrodes, leading to an overall improvement of performances around 50%.

Anyway, the best results are related to proof-of-the-concept devices with N719 photosensitizer, whose toxicity is well-known. Therefore, a deeper research around the use of bio-based electrodes with non-Ru-based dyes is urgent.

5.3.4. Light-Trapping Layers

In 2019, Hu et al. built a silk-based "self-collimator" coupling fluorescence from doped Rhodamine 6G silk fibroin (SF) with the inverse opal photonic crystal (PC).[420] An SF solution was meso-doped with the dye and then used to infiltrated colloidal crystals prepared by Czochralski method.[421] After optimization of photonic bandgap and fluorescent emission, they pointed out that ten-layer rhodamine-doped silk PC increased the self-fluorescence by 50-fold. The integration of this so-fabricated light-trapping layer enhances the PCE of quasi-transparent N719-based DSSCs in different ways. First, offering reflected light by the presence of PCs. Second, converting the transmitted light of higher energy to the wavelength region where N719 displays maximum incident photo-to-current conversion efficiency (530–570 nm), through fluorescence that at the same time is greatly enhanced by the silk PC "self-collimator."

5.3.5. Sealant Films

Several attempts have been made to prolong the lifetime of the new emerging SCs, in particular by using encapsulations.

© 2021 The Authors. Advanced Energy Materials published by Wiley-VCH GmbH

16146840, 2021, 43, Downloaded from https://onlinelibrary.wiley.com/doi/10.1002/aenm.202100520 by Universita Di Torino, Wiley Online Library on [21/02/2025]. See the Terms and Conditions (https://onlinelibrary.wiley.com/terms-and-conditions) on Wiley Online Library for rules of use; OA articles are governed by the applicable Creative Commons License

Table 4. Selection of the best performing SCs with bio-derived materials.

Bio-derived material class	Advantages/disadvantages	PV device	Material	Function	PCE [%]	Remarks	Ref.
Monosaccharides	• High end-life value for biomass wastes • Good ion-solvating ability • High boiling point	OSC	–	–	–	–	–
	• Low conductivity	PSC	–	–	–	–	–
	• High crystalline nature	DSSC	Glucose iodide salt	Electrolyte	7.3	Green solvent	[405]
Cellulose and derivatives	• Inexpensiveness • Lightweight • Flexible	OSC	CNP	Light-trapping layer	15.99	Waste valorization	[346]
	• Poor solubility	PSC	Ethyl cellulose	Sensitizer	19.41	High stability	[91]
	• Required fine control of the nanostructures	DSSC	CRCF	Electrode	8.11	Waste valorization	[160]
Other polysaccharides	• High end-life value for biomass wastes • Lightweight • Easy functionalization	OSC	NOCC:QCS	Interlayer	10.2	Threefold improved PCE	[51]
	• Poor solubility	PSC	Chitin laminate composite	Substrate	12.52	Efficient flexible PSC	[203]
	• Limited industrial scale production	DSSC	rGO-SCCh	Electrode	6.36	Efficient metal-free CE	[416]
Amino acids	• High performing electron extraction layer • Good adhesion properties	OSC	Gly	Interlayer	14.0	10% enhanced PCE	[289]
	• Easy production	PSC	Glycine HCl (*n*:8)	Sensitizer	18.06	Long-term stability	[373]
	• Lack of well-established industrial plants	DSSC	TiO_2@GO–Tyr	Electrode	4.13	Fourfold enhanced PCE	[413]
Polypeptides	• Good surface modifiers	OSC	PLL	Interlayer	15.07	Long-term stability	[50]
	• Lightweight	PSC	–	–	–	–	–
	• Green production still not optimized	DSSC	PEDOT-G-SiCs	Electrode	7.2	Highly flexible	[414]
Proteins	• Inexpensiveness • Extremely high IQE • Easy industrial scale production	OSC	Ag-530/LHCII	Light harvesting	10.57	20% enhanced PCE	[105]
	• Poor stability	PSC	bR	Interlayer	17.02	20% enhanced PCE	[362]
	• Required high ordered systems	DSSC	bR	Sensitizer	0.5	Up-scalable production	[383]
Catecholamine and derivatives	• High adhesion properties • Easy functionalization	OSC	PEDOT:PSS-DA	Interlayer	16.55	>10% enhanced PCE	[52]
	• Long stability under ambient conditions	PSC	Dopamine	Interlayer	20.93	Long-term stability	[90]
	• Green production still not optimized	DSSC	CN_x/CNT	Electrode	7.38	10% improved PCE	[417]
DNA	• Good solubility • Excellent thermal stability	OSC	DNA	Interlayer	8.31	Smoother morphology	[83]
	• Easy functionalization	PSC	DNA-CTMA	Sensitizer	20.63	>10% improved PCE	[375]
	• Green production still not optimized	DSSC	CW-DNA@TiO_2	Electrode	9.23	50% enhanced PCE	[162]
Natural pigments	• Easy extraction • Inexpensiveness • High molar extinction coefficient in the VIS range	OSC	β-carotene	Active layer	0.53	30 nm thick active layer	[270]
	• Difficult purification	PSC	–	–	–	–	–
	• Poor performances	DSSC	Betalain	Sensitizer	3.04	Long-term stability of the pigment	[394]

Ideally, the specifications of encapsulating materials for electronic devices are water vapor transmission rate (WVTR) and oxygen transmission rate (OTR) values of $<10^{-6}$ g m^{-2} day^{-1} and $<10^{-5}$ cm^2 m^{-2} day^{-1} atm^{-1}, respectively.[422] Among the several types of polymeric materials, vinyl alcohol-based (co)polymers, such as PVA and EVOH, have been widely studied and developed for encapsulating organic electronic devices. This was encouraged by the reasonably low OTR values of PVA and EVOH compared to those of other common polymers. Several approaches were used to further optimize the barrier properties of the vinyl alcohol-based (co)polymers, such as applying ZnO nanopowder to the PVA matrix, and reinforcing EVOH with clay. It is noteworthy that when the clay was used, the barrier properties of the polymer were improved at the expense of its transmittance. This is considered a drawback of the system, taking into account the fact that light absorption of the active layer underneath the solar cell could be blocked or suppressed. In this regard, the use of nanofillers deserves a high consideration.

In 2017, Yuwawech et al. successfully demonstrated how to enhance the barrier properties of polyurethane-based sealant

© 2021 The Authors. Advanced Energy Materials published by Wiley-VCH GmbH

16146840, 2021, 43, Downloaded from https://onlinelibrary.wiley.com/doi/10.1002/aenm.202100520 by Universita Di Torino, Wiley Online Library on [21/02/2025]. See the Terms and Conditions (https://onlinelibrary.wiley.com/terms-and-conditions) on Wiley Online Library for rules of use; OA articles are governed by the applicable Creative Commons License

films for DSSC using cellulose derivatives, namely CNCs and esterified CNCs.[423] The encapsulated device showed a lifetime extended of almost 350 h, without losing the initial PCE. In addition, the transmittance of the device was maintained close to 90%. Another recent and ground-breaking work has been reported by Bonomo et al.,[424] in which the crucial role of polyurethane-based encapsulants for PSCs is illustrated. This underlines the relevance of polyurethane nanocomposites toward low-cost and long-life SCs.

6. Conclusion and Future Perspectives

This review has analyzed the intersection of different worlds (optoelectronics and biology) toward greener and more sustainable PVs. Throughout a brief historical survey, we pointed out how and when the PV scientific community was inspired by biology to fabricate innovative and eco-friendly solutions. Nowadays, scientists hold a complete understanding of the operation mechanisms of the different classes of emerging PVs, knowing strengths and weaknesses of each type of SCs. In addition, progress in nanotechnology has allowed mastering hierarchically natural structures. Henceforth, a mature stage of knowledge to merge efficiently bio-derived materials and PVs toward bio-based solar energy conversion devices has been reached. We have, indeed, shown that several groups have demonstrated that it is possible to take advantages from biology, managing to keep the device performance achieved by standard device components, and even outperforming the state-of-the-art. In principle, all components of PV devices (active layer/photosensitizers, carrier transport layers, electrolytes, substrates, electrodes, light-trapping layers, and sealant films) could be substituted with bio-derived materials. However, this represents a long-term goal in the field. To aid the reader to select the best bio-derived materials for each device component in the third generation photovoltaic technologies (Section 5), **Table 4** provides an eye-catching summary.

With regard to OSCs, the performances reached by bio-based active layers are still far from the state-of-the-art, but the interest in the field of the scientific community is constantly growing. A deeper knowledge of biological materials as well as of their interaction with inorganic component (ZnO, ITO) will lead to an optimum device design with respect to energy level alignment and morphology. Specifically, the orientation of the bulky bio-photoactive systems has been proved to be crucial to guarantee satisfying charge carrier mobility within the active layer. The best PCE (0.58%) was achieved with a β-carotene electron donor in an active layer constituted by β-carotene:$PC_{71}BM$.[270] More importantly, the solvent choice plays a fundamental role: higher boiling point solvents, such as chlorobenzene, induce a crystallization in the active layer that leads to improved efficiencies. This is a key point that must be taken into consideration when planning future work in the field. In general, however, much higher efficiencies were reached by modifying the interlayer (e.g., PEDOT:PSS) with bio-derived materials, such as dopamine (PCE = 16.55%) (Table 4).[52] The dopamine doping was found to improve the regular aggregation of the PEDOT backbone and the electron conductivity of PEDOT:PSS. The morphology of the thin films plays a key role in determining the hole extraction efficiency at the interface between interlayer and active layer. Interestingly, this strategy also led to excellent results in PSCs.[88,93,372] Another interesting aspect is the possibility to realize ITO-free and flexible devices that keep high transparency and electronic conductivity features, even outperforming PET–ITO based devices. In this context, both proteins and polysaccharides have been already successfully implemented (Table 4).[346,426] As leading examples, OSCs with bio-derived PEF reached over 7% in devices that maintained the 80% efficiency under the high bending radius of 3 mm. Cellulose achieved good results when employed as substrate and excellent results as light-scattering layer. The implementation of cellulose nanopaper from agroforestry residues led to OSCs with an efficiency higher than 16%.[346] The success is attributed to the different refractive indices of amorphous and crystalline regions in cellulose, which results in a wide-angle light trapping. However, the manufacture of raw cellulose to obtain a material with the right transparency, homogeneity, and suitable mechanical properties for photovoltaics still poses some difficulties as far as the reproducibility and up-scalability of the synthetic methods are concerned. The use of polysaccharides certainly requires further in-depth studies concerning their thermal, optical, and mechanical features, as well as the development of new strategies to achieve functionalized structures with tailored properties. Finally, several groups have actively tested bio-derived materials to replace conventional electrodes. Interesting results were reported by Zhou et al. in 2019 with PDA-modified PET/Ag grids (PCE 11.6%).[353] These were prepared by electroless deposition of metallic Ag on PDA through coordination-bond interactions, which show better results in bending tests and lower sheet resistance with comparison to the commercial PET/ITO. However, the presence of silver renders the material neither biocompatible nor recyclable. Further efforts have to be devoted to achieve 100% bio-based electrodes.

With regard to PSCs, the results achieved through the implementation of bio-derived materials are highly encouraging. Usually, either the TiO_2/PEDOT:PSS interlayer or the perovskite itself is modified with the biomaterial, but the aim is similar, that is, improving the charge collection through superior morphology and defect passivation at the interface HTL/perovskite. The best PCE (20.93%) was obtained by employing dopamine-capped TiO_2 nanoparticles with suppressed charge recombination at the interface and improved binding with the perovskite layer (Table 4). Those, along with similar results with amino acids and catecholamine, were achieved by following a widely known procedure with proved positive effects on the charge collection, perovskite grain morphology, and improved water resistance and stability. A similar result (PCE of 20.63%) was realized by directly modifying the perovskite with the HTL material DNA–CTMA (Table 4).[375] This produces the same effect as the dopamine-doping of the TiO_2 layer, that is, improved charge collection and defect passivation (65% with respect to the reference). This *per se* justifies the implementation of bio-derived materials as a relevant green concept toward enhanced devices. A further take home message is their effect as modifiers as a universal strategy to enhance PSCs regardless of the device architecture. Finally, it is

© 2021 The Authors. Advanced Energy Materials published by Wiley-VCH GmbH

16146840, 2021, 43, Downloaded from https://onlinelibrary.wiley.com/doi/10.1002/aenm.202100520 by Universita Di Torino, Wiley Online Library on [21/02/2025]. See the Terms and Conditions (https://onlinelibrary.wiley.com/terms-and-conditions) on Wiley Online Library for rules of use; OA articles are governed by the applicable Creative Commons License

important to underline that numerous contributions reported on the increase of the humidity resistance and stability of PSCs following implementation of bio-derived materials, such as amino acids, DNA, dopamine, and catecholamines (Table 4). As leading example, a DNA–PSC retained 90% of its initial conversion efficiency after more than 700 h of use.[375] This effect was also reported for doped PEDOT:PSS layer (e.g., 85% of the PCE retained after more than 670 h of use).[88] This is particularly important considering that PSCs are still heavily affected by their low stability under ambient operation and storage conditions. The quick success in bio-based PSCs must be considered as very striking since i) so far, a vast majority of bio-derived materials has still to be explored, e.g., polysaccharides were not considered yet, and ii) it has mostly concerned interfacial TiO_2/perovskite and perovskite/HTL interfaces, while green electrodes or substrates are scarcely reported. In this context, promising results have been reported by Bae and collaborators,[203] which fabricated chitin nanofiber-based substrates for PSCs that featured comparable PCEs (≈13%) to those fabricated on PET. Similar to other photovoltaic technologies, the field is far from providing fully bio-based PSCs. Indeed, the perovskite itself has been strongly criticized owing to its toxicity and non-recyclability. Although the use of bio-derived materials plays an essential role in modifying the characteristics of the device, they do not render the device more "environmental friendly," as they are usually added as an additional component. This represents the major challenge in the field.

As far as DSSCs are concerned, research on natural dyes has led to very poor efficiencies, while a bacterial up-scalable production of the suitable sensitizers also remains as the major challenge. Noteworthy, data are often obtained under different conditions and device set-ups and, as such, it is difficult to provide direct comparisons. The majority of the employed photosensitizers belong to different chemical classes, which contain mainly carotenoids, betalains, flavonoids, or chlorophyll (Table 4). The best PCE (3%) involves betalain, which displays a broad absorption spectrum and a good chemical stability. Overall, the stability of natural pigments is still an open question.[427] Many research groups focused on the implementation of bio-based electrolytes aiming at replacing or diminishing the amount of the commonly employed iodine-based electrolytes, which are toxic, difficult to dispose, and corrosive. In general, biopolymer-based electrolytes shine in competitiveness with respect to the nonsustainable counterparts, achieving thousands of hours of stabilities. Biopolymers used for the solid-state and quasi-solid state electrolyte preparation are mostly mono- or poly-saccharide (Table 4). They are appealing candidates as their high polarity ensured high ion conductivity and their low T_g guarantees a high ion conduction. Mono- and poly-saccharides possess structural similarities with slight variations, which lead in the resulting gels to differences in ion conductivity and performances.[169] As a rule of thumb, the ion diffusion, and conductivity increase proportionally to the number of free polar groups available in the biopolymer. The most efficient device (PCE = 7.3%) was reported by Sauvage and co-workers in 2016.[405] They used a glucose 1,3-dimethylimidazolium iodide salt as quasi-solid state electrolyte and the polypyridyl Ruthenium C106 dye as sensitizer, which combined high conductivity and chemical stability with low viscosity and low volatility. As a result, the PCE of reference devices with 1,3-dimethylimidazolium iodide was only slightly higher (8%), which is an encouraging result. However, despite their large number of polar groups present on their backbones, biopolymers are considered a very poor conductive material, owing to the intermolecular secondary bonding between the polymer chains, high crystalline nature, and high activation energy barrier for ion transportation.[53,428] In addition, the limitations in the solvent selection is a bottleneck with respect to device fabrication. A viable solution is the replacement of hydroxyl or amino groups with more polar groups, such as carboxymethyl, hexanoyl, and cyanoethyl groups, in order to provide more active sites for ion transportation.[425,429] Regarding the fabrication of a bio-based electrodes for flexible DSSCs, CRCF and DNA have been identified as the best candidates (Table 4). As the most relevant result, DNA–TiO_2 photoelectrodes have led to PCE of 9.23%.[162] DNA possesses phosphate groups of nucleotides along the double helix structure that readily react with TiO_2 surface. The presence of DNA influences both the valence band of the semiconductor and the undesired recombination processes, as it blocks holes from accessing recombination centers on the TiO_2 surface. Nevertheless, the high PCEs are achieved by employing Ru-based photosensitizer (N719), which is toxic and unsustainable. Bio-inspired materials have also been tested as sealants, imposing themselves as co-actors of traditional encapsulation systems. They are, however, often combined with nondegradable agents and polymers.[424] Thus, efforts are needed i) to optimize the new high performing encapsulants in the presence of biodegradable agents, and ii) to move toward fully bio-based solutions.

In general, solar cells must be considered as multifactorial systems, whose performance is truly depending on the optimization of every single constituent of the device. Most of the studies therein proposed followed mono- or bi-component approaches consisting in the implementation of one or two bio-derived elements in the solar cell architecture. We rationally recognize that this behavior perfectly suits the needs of evaluating the possible implementation of the aforementioned components in the device, comparing it with reference items. Anyway, an effort toward a fully bio-based device is now required, since the applicability of bio-derived materials has been investigated and confirmed in every respect. We strongly believe the scientific community is ready to fulfil this milestone in a close future.

Acknowledgements

R.D.C. acknowledges the European Union's Horizon 2020 research and innovation FET-OPEN under grant agreement ARTIBLED No 863170, the ERC-Co InOutBioLight No. 816856, and the MSCA-ITN STiBNite No. 956923.

Open access funding enabled and organized by Projekt DEAL.

Conflict of Interest

The authors declare no conflict of interest.

© 2021 The Authors. Advanced Energy Materials published by Wiley-VCH GmbH

16146840, 2021, 43, Downloaded from https://onlinelibrary.wiley.com/doi/10.1002/aenm.202100520 by Universita Di Torino, Wiley Online Library on [21/02/2025]. See the Terms and Conditions (https://onlinelibrary.wiley.com/terms-and-conditions) on Wiley Online Library for rules of use; OA articles are governed by the applicable Creative Commons License

Keywords

bio-based energy devices, bio-derived materials, green photonics, photovoltaics, sustainable optoelectronics

Received: February 12, 2021
Revised: March 26, 2021
Published online: May 6, 2021

[1] International Energy Agency, International Renewable Energy Agency, Perspectives for the Energy Transition: Investment Needs for a Low-Carbon Energy System, **2017**.
[2] P. Moriarty, D. Honnery, *Renewable Sustainable Energy Rev.* **2012**, *16*, 244.
[3] P. M. Voroshilov, C. R. Simovski, P. A. Belov, A. S. Shalin, *J. Appl. Phys.* **2015**, *117*, 203101.
[4] M. Sharmina, C. McGlade, P. Gilbert, A. Larkin, *Mar. Policy* **2017**, *84*, 12.
[5] S. Chu, A. Majumdar, *Nature* **2012**, *488*, 294.
[6] Fraunhofer Institute for Solar Energy Systems, ISE, *Photovoltaics Report*, **2020**.
[7] M. A. Green, E. D. Dunlop, J. Hohl-Ebinger, M. Yoshita, N. Kopidakis, X. Hao, *Prog. Photovoltaics Res. Appl.* **2020**, *28*, 629.
[8] K. Yoshikawa, H. Kawasaki, W. Yoshida, T. Irie, K. Konishi, K. Nakano, T. Uto, D. Adachi, M. Kanematsu, H. Uzu, K. Yamamoto, *Nat. Energy* **2017**, *2*, 17032.
[9] Silicon Metal | CRM Alliance, https://www.crmalliance.eu/silicon-metal (accessed: March 2021).
[10] L. Zong, B. Zhu, Z. Lu, Y. Tan, Y. Jin, N. Liu, Y. Hu, S. Gu, J. Zhu, Y. Cui, *Proc. Natl. Acad. Sci. USA* **2015**, *112*, 13473.
[11] E. Commission, Critical raw materials | Internal Market, Industry, Entrepreneurship and SMEs, https://ec.europa.eu/growth/sectors/raw-materials/specific-interest/critical_en (accessed: January 2021).
[12] X. Hu, Z. Huang, X. Zhou, P. Li, Y. Wang, Z. Huang, M. Su, W. Ren, F. Li, M. Li, Y. Chen, Y. Song, *Adv. Mater.* **2017**, *29*, 1703236.
[13] R. Li, X. Xiang, X. Tong, J. Zou, Q. Li, *Adv. Mater.* **2015**, *27*, 3831.
[14] Z. Yang, J. Deng, X. Sun, H. Li, H. Peng, *Adv. Mater.* **2014**, *26*, 2643.
[15] S. Rahmany, M. Layani, S. Magdassi, L. Etgar, *Sustainable Energy Fuels* **2017**, *1*, 2120.
[16] F. Guo, P. Kubis, T. Stubhan, N. Li, D. Baran, T. Przybilla, E. Spiecker, K. Forberich, C. J. Brabec, *ACS Appl. Mater. Interfaces* **2014**, *6*, 18251.
[17] C. Gao, S. Yuan, K. Cui, Z. Qiu, S. Ge, B. Cao, J. Yu, *Sol. RRL* **2018**, *2*, 1800175.
[18] M. Li, Y. Li, S. Sasaki, J. Song, C. Wang, H. Tamiaki, W. Tian, G. Chen, T. Miyasaka, X.-F. Wang, *ChemSusChem* **2016**, *9*, 2862.
[19] Y. Liu, N. Qi, T. Song, M. Jia, Z. Xia, Z. Yuan, W. Yuan, K.-Q. Zhang, B. Sun, *ACS Appl. Mater. Interfaces* **2014**, *6*, 20670.
[20] T. Ameri, G. Dennler, C. Lungenschmied, C. J. Brabec, *Energy Environ. Sci.* **2009**, *2*, 347.
[21] J. Kim, Z. Hong, G. Li, T. Song, J. Chey, Y. S. Lee, J. You, C.-C. Chen, D. K. Sadana, Y. Yang, *Nat. Commun.* **2015**, *6*, 6391.
[22] S. Essig, C. Allebé, T. Remo, J. F. Geisz, M. A. Steiner, K. Horowitz, L. Barraud, J. S. Ward, M. Schnabel, A. Descoeudres, D. L. Young, M. Woodhouse, M. Despeisse, C. Ballif, A. Tamboli, *Nat. Energy* **2017**, *2*, 17144.
[23] S. He, L. Qiu, L. K. Ono, Y. Qi, *Mater. Sci. Eng., R* **2020**, *140*, 100545.
[24] P. Chen, Z. Wang, S. Wang, M. Lyu, M. Hao, M. Ghasemi, M. Xiao, J. H. Yun, Y. Bai, L. Wang, *Nano Energy* **2020**, *69*, 104392.
[25] J. Xu, C. C. Boyd, Z. J. Yu, A. F. Palmstrom, D. J. Witter, B. W. Larson, R. M. France, J. Werner, S. P. Harvey, E. J. Wolf, W. Weigand, S. Manzoor, M. F. A. M. van Hest, J. J. Berry, J. M. Luther, Z. C. Holman, M. D. McGehee, *Science* **2020**, *367*, 1097.
[26] D. Kim, H. J. Jung, I. J. Park, B. W. Larson, S. P. Dunfield, C. Xiao, J. Kim, J. Tong, P. Boonmongkolras, S. G. Ji, F. Zhang, S. R. Pae, M. Kim, S. B. Kang, V. Dravid, J. J. Berry, J. Y. Kim, K. Zhu, D. H. Kim, B. Shin, *Science* **2020**, *368*, 155.
[27] T. Duong, H. Pham, T. C. Kho, P. Phang, K. C. Fong, D. Yan, Y. Yin, J. Peng, M. A. Mahmud, S. Gharibzadeh, B. A. Nejand, I. M. Hossain, M. R. Khan, N. Mozaffari, Y. Wu, H. Shen, J. Zheng, H. Mai, W. Liang, C. Samundsett, M. Stocks, K. McIntosh, G. G. Andersson, U. Lemmer, B. S. Richards, U. W. Paetzold, A. Ho-Ballie, Y. Liu, D. Macdonald, A. Blakers, J. Wong-Leung, T. White, K. Weber, K. Catchpole, *Adv. Energy Mater.* **2020**, *10*, 2002139.
[28] A. Hagfeldt, G. Boschloo, L. Sun, L. Kloo, H. Pettersson, *Chem. Rev.* **2010**, *110*, 6595.
[29] S. M. Feldt, E. A. Gibson, E. Gabrielsson, L. Sun, G. Boschloo, A. Hagfeldt, *J. Am. Chem. Soc.* **2010**, *132*, 16714.
[30] B. O'Regan, M. Grätzel, *Nature* **1991**, *353*, 737.
[31] D. Y. Lyon, P. J. J. Alvarez, *Environ. Sci. Technol.* **2008**, *42*, 8127.
[32] H. Schmidt, H. Flügge, T. Winkler, T. Bülow, T. Riedl, W. Kowalsky, *Appl. Phys. Lett.* **2009**, *94*, 243302.
[33] M. P. Ramuz, M. Vosgueritchian, P. Wei, C. Wang, Y. Gao, Y. Wu, Y. Chen, Z. Bao, *ACS Nano* **2012**, *6*, 10384.
[34] G. Lockitch, *Clin. Biochem.* **1993**, *26*, 371.
[35] D. A. Gidlow, *Occup. Med.* **2004**, *54*, 76.
[36] B. Toussaint, B. Raffael, A. Angers-Loustau, D. Gilliland, V. Kestens, M. Petrillo, I. M. Rio-Echevarria, G. Van den Eede, *Food Addit. Contam., Part A* **2019**, *36*, 639.
[37] E. Fresta, V. Fernández-Luna, P. B. Coto, R. D. Costa, *Adv. Funct. Mater.* **2018**, *28*, 1707011.
[38] S. Coda, P. Siersema, G. Stamp, A. Thillainayagam, *Endosc. Int. Open* **2015**, *03*, E380.
[39] B. T. Dotta, K. S. Saroka, M. A. Persinger, *Neurosci. Lett.* **2012**, *513*, 151.
[40] M. Kobayashi, D. Kikuchi, H. Okamura, *PLoS One* **2009**, *4*, e6256.
[41] C. G. England, E. B. Ehlerding, W. Cai, *Bioconjugate Chem.* **2016**, *27*, 1175.
[42] A. P. F. Turner, *Chem. Soc. Rev.* **2013**, *42*, 3184.
[43] S. Tadepalli, J. M. Slocik, M. K. Gupta, R. R. Naik, S. Singamaneni, *Chem. Rev.* **2017**, *117*, 12705.
[44] V. Fernández-Luna, J. P. Fernández-Blázquez, M. A. Monclús, F. J. Rojo, R. Daza, D. Sanchez-Dealcazar, A. L. Cortajarena, R. D. Costa, *Mater. Horiz.* **2020**, *7*, 1790.
[45] A. Aires, V. Fernández-Luna, J. Fernández-Cestau, R. D. Costa, A. L. Cortajarena, *Nano Lett.* **2020**, *20*, 2710.
[46] S. Tekoglu, M. Held, M. Bender, G. N. Yeo, A. Kretzschmar, M. Hamburger, J. Freudenberg, S. Beck, U. H. F. Bunz, G. Hernandez-Sosa, *Adv. Sustainable Syst.* **2020**, 2000203.
[47] D. F. Williams, *Biomaterials* **2009**, *30*, 5897.
[48] W. D. Jang, J. H. Hwang, H. U. Kim, J. Y. Ryu, S. Y. Lee, *Microb. Biotechnol.* **2017**, *10*, 1181.
[49] U. Würfel, M. Seßler, M. Unmüssig, N. Hofmann, M. List, E. Mankel, T. Mayer, G. Reiter, J.-L. Bubendorff, L. Simon, M. Kohlstädt, *Adv. Energy Mater.* **2016**, *6*, 1600594.
[50] K.-T. T. Huang, C.-P. P. Chen, B.-H. H. Jiang, R.-J. J. Jeng, W.-C. C. Chen, *Org. Electron.* **2020**, *87*, 105924.
[51] K. Zhang, R. Xu, W. Ge, M. Qi, G. Zhang, Q. H. Xu, F. Huang, Y. Cao, X. Wang, *Nano Energy* **2017**, *34*, 164.
[52] M. Zeng, X. Wang, R. Ma, W. Zhu, Y. Li, Z. Chen, J. Zhou, W. Li, T. Liu, Z. He, H. Yan, F. Huang, Y. Cao, *Adv. Energy Mater.* **2020**, *10*, 2000743.

© 2021 The Authors. Advanced Energy Materials published by Wiley-VCH GmbH

16146840, 2021, 43, Downloaded from https://onlinelibrary.wiley.com/doi/10.1002/aenm.202100520 by Universita Di Torino, Wiley Online Library on [21/02/2025]. See the Terms and Conditions (https://onlinelibrary.wiley.com/terms-and-conditions) on Wiley Online Library for rules of use; OA articles are governed by the applicable Creative Commons License

[53] F. Bella, S. Galliano, M. Falco, G. Viscardi, C. Barolo, M. Grätzel, C. Gerbaldi, *Green Chem.* **2017**, *19*, 1043.
[54] S. Shakir, Y. Y. Foo, N. Rizan, H. M. Abd-ur-Rehman, K. Yunus, P. S. Moi, V. Periasamy, *J. Mater. Sci.: Mater. Electron.* **2018**, *29*, 4602.
[55] L. Valentini, *Mater. Lett.* **2015**, *148*, 204.
[56] G. Calogero, A. Bartolotta, G. Di Marco, A. Di Carlo, F. Bonaccorso, G. Di Marco, A. Di Carlo, F. Bonaccorso, *Chem. Soc. Rev.* **2015**, *44*, 3244.
[57] D. Ha, Z. Fang, N. B. Zhitenev, *Adv. Electron. Mater.* **2018**, *4*, 1700593.
[58] S. Peter, N. Lyczko, D. Gopakumar, H. J. Maria, A. Nzihou, S. Thomas, *Waste Biomass Valorization* **2020**, https://doi.org/10.1007/s12649-020-01244-6.
[59] H. A. Maddah, V. Berry, S. K. Behura, *Renewable Sustainable Energy Rev.* **2020**, *121*, 109678.
[60] N. Mariotti, M. Bonomo, L. Fagiolari, N. Barbero, C. Gerbaldi, F. Bella, C. Barolo, *Green Chem.* **2020**, *22*, 7168.
[61] F. Jiang, T. Li, Y. Li, Y. Zhang, A. Gong, J. Dai, E. Hitz, W. Luo, L. Hu, *Adv. Mater.* **2018**, *30*, 1703453.
[62] Y. Shchipunov, I. Postnova, *Adv. Funct. Mater.* **2018**, *28*, 1705042.
[63] R. Williams, *J. Chem. Phys.* **1960**, *32*, 1505.
[64] B. Parida, S. Iniyan, R. Goic, *Renewable Sustainable Energy Rev.* **2011**, *15*, 1625.
[65] D. M. Chapin, C. S. Fuller, G. L. Pearson, *J. Appl. Phys.* **1954**, *25*, 676.
[66] M. Wolf, *IEEE Trans. Compon., Hybrids, Manuf. Technol.* **1980**, *3*, 464.
[67] D. E. Carlson, C. R. Wronski, *Appl. Phys. Lett.* **1976**, *28*, 671.
[68] K. Mitchell, C. Eberspacher, J. Ermer, D. Pier, *Conf. Rec IEEE Photovoltaic Spec. Conf.*, IEEE, New York **1988**, pp. 1384–1389.
[69] N. S. Sariciftci, L. Smilowitz, A. J. Heeger, F. Wudl, *Science* **1992**, *258*, 1474.
[70] J. Guo, J. Min, *Adv. Energy Mater.* **2019**, *9*, 1802521.
[71] D. Weber, *Z. Naturforsch., B: J. Chem. Sci.* **1978**, *33*, 1443.
[72] C. R. Kagan, D. B. Mitzi, C. D. Dimitrakopoulos, *Science* **1999**, *286*, 945.
[73] S. A. Veldhuis, P. P. Boix, N. Yantara, M. Li, T. C. Sum, N. Mathews, S. G. Mhaisalkar, *Adv. Mater.* **2016**, *28*, 6804.
[74] A. Kojima, K. Teshima, T. Miyasaka, Y. Shirai, *ECS Meet. Abstr.* **2006**, *MA2006-02*, 397.
[75] Best Research-Cell Efficiency Chart | Photovoltaic Research | NREL, https://www.nrel.gov/pv/cell-efficiency.html (accessed: November **2020**).
[76] H. Minoura, D. Zhang, N. Yamamoto, T. Yoshida, *Trans. MRS J.* **2002**, *27*, 811.
[77] S. Ananth, P. Vivek, T. Arumanayagam, P. Murugakoothan, *Spectrochim. Acta, Part A* **2014**, *128*, 420.
[78] K.-H. Park, T.-Y. Kim, S. Han, H.-S. Ko, S.-H. Lee, Y.-M. Song, J.-H. Kim, J.-W. Lee, *Spectrochim. Acta, Part A* **2014**, *128*, 868.
[79] M. A. M. Al-Alwani, A. B. Mohamad, A. A. H. Kadhum, N. A. Ludin, *Asian J. Chem.* **2014**, *26*, 6285.
[80] F. Bella, L. Porcarelli, D. Mantione, C. Gerbaldi, C. Barolo, M. Grätzel, D. Mecerreyes, *Chem. Sci.* **2020**, *11*, 1485.
[81] B. Lamprecht, R. Thünauer, M. Ostermann, G. Jakopic, G. Leising, *Phys. Status Solidi A* **2005**, *202*, R50.
[82] X. F. Wang, L. Wang, Z. Wang, Y. Wang, N. Tamai, Z. Hong, J. Kido, *J. Phys. Chem. C* **2013**, *117*, 804.
[83] J. Dagar, G. Scavia, M. Scarselli, S. Destri, M. De Crescenzi, T. M. Brown, *Nanoscale* **2017**, *9*, 19031.
[84] J. Li, N. Wang, Y. Wang, Z. Liang, Y. Peng, C. Yang, X. Bao, Y. Xia, *Sol. Energy* **2020**, *196*, 168.
[85] S. Kazemzadeh, G. Riazi, R. Ajeian, *ACS Sustainable Chem. Eng.* **2017**, *5*, 9836.
[86] X. Hu, L. Chen, T. Ji, Y. Zhang, A. Hu, F. Wu, G. Li, Y. Chen, *Adv. Mater. Interfaces* **2015**, *2*, 1500445.
[87] T. Uchiyama, T. Sano, Y. Okada-Shudo, V. Vohra, *J. Mater. Chem. C* **2020**, *8*, 7162.
[88] J. Huang, K. X. Wang, J. J. Chang, Y. Y. Jiang, Q. S. Xiao, Y. Li, *J. Mater. Chem. A* **2017**, *5*, 13817.
[89] J. Huang, C. Wang, Z. Liu, X. Qiu, J. Yang, J. Chang, *J. Mater. Chem. C* **2018**, *6*, 2311.
[90] Y. Zhang, X. Liu, P. Li, Y. Duan, X. Hu, F. Li, Y. Song, *Nano Energy* **2019**, *56*, 733.
[91] J. Yang, S. Xiong, T. Qu, Y. Zhang, X. He, X. Guo, Q. Zhao, S. Braun, J. Chen, J. Xu, Y. Li, X. Liu, C. Duan, J. Tang, M. Fahlman, Q. Bao, *ACS Appl. Mater. Interfaces* **2019**, *11*, 13491.
[92] Y.-C. Shih, Y.-B. Lan, C.-S. Li, H.-C. Hsieh, L. Wang, C.-I. Wu, K.-F. Lin, *Small* **2017**, *13*, 1604305.
[93] Q. Xue, M. Liu, Z. Li, L. Yan, Z. Hu, J. Zhou, W. Li, X. F. Jiang, B. Xu, F. Huang, Y. Li, H. L. Yip, Y. Cao, *Adv. Funct. Mater.* **2018**, *28*, 14.
[94] F. Momeni, J. Ni, *Renewable Energy* **2018**, *122*, 35.
[95] M. Cai, Y. Wu, H. Chen, X. Yang, Y. Qiang, L. Han, *Adv. Sci.* **2017**, *4*, 1600269.
[96] N. Gasparini, X. Jiao, T. Heumueller, D. Baran, G. J. Matt, S. Fladischer, E. Spiecker, H. Ade, C. J. Brabec, T. Ameri, *Nat. Energy* **2016**, *1*, 16118.
[97] P. Bi, X. Hao, *Sol. RRL* **2019**, *3*, 1800263.
[98] A. Wadsworth, M. Moser, A. Marks, M. S. Little, N. Gasparini, C. J. Brabec, D. Baran, I. McCulloch, *Chem. Soc. Rev.* **2019**, *48*, 1596.
[99] L. Zuo, J. Yu, X. Shi, F. Lin, W. Tang, A. K.-Y. Jen, *Adv. Mater.* **2017**, *29*, 1702547.
[100] N. Li, D. Baran, K. Forberich, F. Machui, T. Ameri, M. Turbiez, M. Carrasco-Orozco, M. Drees, A. Facchetti, F. C. Krebs, C. J. Brabec, *Energy Environ. Sci.* **2013**, *6*, 3407.
[101] A. J. Heeger, *Adv. Mater.* **2014**, *26*, 10.
[102] Y. Lin, Y. Li, X. Zhan, *Chem. Soc. Rev.* **2012**, *41*, 4245.
[103] J. S. Wu, S. W. Cheng, Y. J. Cheng, C. S. Hsu, *Chem. Soc. Rev.* **2015**, *44*, 1113.
[104] J. Jensen, M. Hösel, A. L. Dyer, F. C. Krebs, *Adv. Funct. Mater.* **2015**, *25*, 2073.
[105] K. Yao, H. Jiao, Y. X. Xu, Q. He, F. Li, X. Wang, *J. Mater. Chem. A* **2016**, *4*, 13400.
[106] A. Zeynali, T. S. Ghiasi, G. Riazi, R. Ajeian, *Org. Electron.* **2017**, *51*, 341.
[107] P. Ensslen, S. Gärtner, K. Glaser, A. Colsmann, H.-A. Wagenknecht, *Angew. Chem., Int. Ed.* **2016**, *55*, 1904.
[108] K. Sun, S. Zhang, P. Li, Y. Xia, X. Zhang, D. Du, F. H. Isikgor, J. Ouyang, *J. Mater. Sci.: Mater. Electron.* **2015**, *26*, 4438.
[109] D. Li, W.-Y. Lai, Y.-Z. Zhang, W. Huang, *Adv. Mater.* **2018**, *30*, 1704738.
[110] Y. Li, G. Xu, C. Cui, Y. Li, *Adv. Energy Mater.* **2018**, *8*, 1701791.
[111] J. A. G. Williams, *Top. Curr. Chem.* **2007**, *281*, 205.
[112] A. Sharma, R. Kroon, D. A. Lewis, G. G. Andersson, M. R. Andersson, *ACS Appl. Mater. Interfaces* **2017**, *9*, 10929.
[113] F. Wang, K. Nakano, H. Yoshida, K. Hashimoto, H. Segawa, C. S. Hsu, K. Tajima, *J. Mater. Chem. A* **2018**, *6*, 22889.
[114] Z. Zheng, Q. Hu, S. Zhang, D. Zhang, J. Wang, S. Xie, R. Wang, Y. Qin, W. Li, L. Hong, N. Liang, F. Liu, Y. Zhang, Z. Wei, Z. Tang, T. P. Russell, J. Hou, H. Zhou, *Adv. Mater.* **2018**, *30*, 1801801.
[115] C. P. Chen, Y. D. Chen, S. C. Chuang, *Adv. Mater.* **2011**, *23*, 3859.
[116] Z. George, Y. Xia, A. Sharma, C. Lindqvist, G. Andersson, O. Inganäs, E. Moons, C. Müller, M. R. Andersson, *J. Mater. Chem. A* **2016**, *4*, 2663.
[117] T. P. Le, Z. Shang, L. Wang, N. Li, S. Vajjala Kesava, J. W. O'Connor, Y. Chang, C. Bae, C. Zhu, A. Hexemer, E. W. Gomez, A. Salleo, M. A. Hickner, E. D. Gomez, *Macromolecules* **2015**, *48*, 5162.
[118] S. Nam, J. Seo, S. Woo, W. H. Kim, H. Kim, D. D. C. Bradley, Y. Kim, *Nat. Commun.* **2015**, *6*, 8929.

© 2021 The Authors. Advanced Energy Materials published by Wiley-VCH GmbH

16146840, 2021, 43, Downloaded from https://onlinelibrary.wiley.com/doi/10.1002/aenm.202100520 by Universita Di Torino, Wiley Online Library on [21/02/2025]. See the Terms and Conditions (https://onlinelibrary.wiley.com/terms-and-conditions) on Wiley Online Library for rules of use; OA articles are governed by the applicable Creative Commons License

[119] A. Karl, A. Osvet, A. Vetter, P. Maisch, N. Li, H. Egelhaaf, C. J. Brabec, *Prog. Photovoltaics Res. Appl.* **2019**, *27*, 460.
[120] S. Izawa, N. Shintaku, M. Hiramoto, *J. Phys. Chem. Lett.* **2018**, *9*, 2914.
[121] J. Dagar, M. Scarselli, M. De Crescenzi, T. M. Brown, *ACS Energy Lett.* **2016**, *1*, 510.
[122] F. Toschi, D. Catone, P. O'Keeffe, A. Paladini, S. Turchini, J. Dagar, T. M. Brown, *Adv. Funct. Mater.* **2018**, *28*, 1870181.
[123] A. Elfwing, W. Cai, L. Ouyang, X. Liu, Y. Xia, Z. Tang, O. Inganäs, *ACS Appl. Mater. Interfaces* **2018**, *10*, 9579.
[124] M. Zhu, T. Li, C. S. Davis, Y. Yao, J. Dai, Y. Wang, F. AlQatari, J. W. Gilman, L. Hu, *Nano Energy* **2016**, *26*, 332.
[125] J. S. Kim, J. H. Park, J. H. Lee, J. Jo, D. Y. Kim, K. Cho, *Appl. Phys. Lett.* **2007**, *91*, 112111.
[126] Y. Wang, Z. Liang, J. Qin, J. Tong, P. Guo, X. Cao, J. Li, Y. Xia, *IEEE J. Photovoltaics* **2019**, *9*, 1678.
[127] S. Luo, W. A. Daoud, *J. Mater. Chem. A* **2015**, *3*, 8992.
[128] G. Niu, X. Guo, L. Wang, *J. Mater. Chem. A* **2015**, *3*, 8970.
[129] M. Jeong, I. W. Choi, E. M. Go, Y. Cho, M. Kim, B. Lee, S. Jeong, Y. Jo, H. W. Choi, J. Lee, J. H. Bae, S. K. Kwak, D. S. Kim, C. Yang, *Science* **2020**, *369*, 1615.
[130] P. K. Nayak, S. Mahesh, H. J. Snaith, D. Cahen, *Nat. Rev. Mater.* **2019**, *4*, 269.
[131] M. Bidikoudi, E. Fresta, R. D. Costa, *Chem. Commun.* **2018**, *54*, 8150.
[132] N. G. Park, *Mater. Today* **2015**, *18*, 65.
[133] A. K. Jena, A. Kulkarni, T. Miyasaka, *Chem. Rev.* **2019**, *119*, 3036.
[134] M. U. Rothmann, W. Li, J. Etheridge, Y.-B. Cheng, *Adv. Energy Mater.* **2017**, *7*, 1700912.
[135] L. K. Ono, Y. Qi, S. (Frank) Liu, *Joule* **2018**, *2*, 1961.
[136] N. Elumalai, M. Mahmud, D. Wang, A. Uddin, *Energies* **2016**, *9*, 861.
[137] H. Zhang, H. Xu, X. Ji, J. Liang, Q. Yu, *Energy Fuels* **2020**, *34*, 6624.
[138] M. Saliba, J.-P. Correa-Baena, M. Grätzel, A. Hagfeldt, A. Abate, *Angew. Chem.* **2018**, *130*, 2582.
[139] J. P. Correa-Baena, M. Saliba, T. Buonassisi, M. Grätzel, A. Abate, W. Tress, A. Hagfeldt, *Science* **2017**, *358*, 739.
[140] Y. Zhang, J. Liu, Z. Wang, Y. Xue, Q. Ou, L. Polavarapu, J. Zheng, X. Qi, Q. Bao, *Chem. Commun.* **2016**, *52*, 13637.
[141] I. Deretzis, E. Smecca, G. Mannino, A. La Magna, T. Miyasaka, A. Alberti, *J. Phys. Chem. Lett.* **2018**, *9*, 3000.
[142] I. Deretzis, A. La Magna, *Nanoscale* **2017**, *9*, 5896.
[143] J. Bisquert, E. J. Juarez-Perez, *J. Phys. Chem. Lett.* **2019**, *10*, 5889.
[144] S. Ito, S. Tanaka, K. Manabe, H. Nishino, *J. Phys. Chem. C* **2014**, *118*, 16995.
[145] Q. Fu, X. Tang, B. Huang, T. Hu, L. Tan, L. Chen, Y. Chen, *Adv. Sci.* **2018**, *5*, 1700387.
[146] S. Emami, L. Andrade, A. Mendes, U. Porto, *J. Eng.* **2018**, *1*, 52.
[147] S. C. Yun, S. Ma, H. C. Kwon, K. Kim, G. Jang, H. Yang, J. Moon, *Nano Energy* **2019**, *59*, 481.
[148] Q. Tai, F. Yan, *Adv. Mater.* **2017**, *29*, 1700192.
[149] N. J. Cherepy, G. P. Smestad, M. Grätzel, J. Z. Zhang, *J. Phys. Chem. B* **1997**, *101*, 9342.
[150] V. Novelli, N. Barbero, C. Barolo, G. Viscardi, M. Sliwa, F. Sauvage, *Phys. Chem. Chem. Phys.* **2017**, *19*, 27670.
[151] A. Fakharuddin, R. Jose, T. M. Brown, F. Fabregat-Santiago, J. Bisquert, *Energy Environ. Sci.* **2014**, *7*, 3952.
[152] S. Mozaffari, M. R. Nateghi, M. B. Zarandi, *Renewable Sustainable Energy Rev.* **2017**, *71*, 675.
[153] Y. Cao, Y. Liu, S. M. Zakeeruddin, A. Hagfeldt, M. Grätzel, *Joule* **2018**, *2*, 1108.
[154] H. Yuan, W. Wang, D. Xu, Q. Xu, J. Xie, X. Chen, T. Zhang, C. Xiong, Y. He, Y. Zhang, Y. Liu, H. Shen, *Sol. Energy* **2018**, *165*, 233.
[155] J. Gong, J. Liang, K. Sumathy, *Renewable Sustainable Energy Rev.* **2012**, *16*, 5848.
[156] R. Boaretto, S. Carli, S. Caramori, C. A. Bignozzi, D. Saccone, C. Magistris, C. Barolo, G. Viscardi, *Dalton Trans.* **2017**, *46*, 16390.
[157] F. Bella, C. Gerbaldi, C. Barolo, M. Grätzel, *Chem. Soc. Rev.* **2015**, *44*, 3431.
[158] S. Venkatesan, W.-H. Lin, H. Teng, Y.-L. Lee, *ACS Appl. Mater. Interfaces* **2019**, *11*, 42780.
[159] Y. S. Tingare, N. S. Vinh, H.-H. Chou, Y.-C. Liu, Y.-S. Long, T.-C. Wu, T.-C. Wei, C.-Y. Yeh, *Adv. Energy Mater.* **2017**, *7*, 1700032.
[160] J. Li, H. Yang, K. Huang, S. Cao, Y. Ni, L. Huang, L. Chen, X. Ouyang, *Cellulose* **2018**, *25*, 5113.
[161] B. Anothumakkool, I. Agrawal, S. N. Bhange, R. Soni, O. Game, S. B. Ogale, S. Kurungot, *ACS Appl. Mater. Interfaces* **2016**, *8*, 553.
[162] Ö. Ateş Sönmezoğlu, S. Akın, B. Terzi, S. Mutlu, S. Sönmezoğlu, *Adv. Funct. Mater.* **2016**, *26*, 8776.
[163] Y. Numata, S. Zhang, X. Yang, L. Han, *Chem. Lett.* **2013**, *42*, 1328.
[164] C. Qin, Y. Numata, S. Zhang, X. Yang, A. Islam, K. Zhang, H. Chen, L. Han, *Adv. Funct. Mater.* **2014**, *24*, 3059.
[165] A. Molaeirad, N. Rezaeian, *Biotechnol. Appl. Biochem.* **2015**, *62*, 489.
[166] N. Prabavathy, S. Shalini, R. Balasundaraprabhu, Dhayalan Velauth apillai, S. Prasanna, G. Balaji, N. Muthukumarasamy, *Int. J. Energy Res.* **2018**, *42*, 790.
[167] T. Montagni, P. Enciso, J. J. Marizcurrena, S. Castro-Sowinski, C. Fontana, D. Davyt, M. F. Cerdá, *Environ. Sustainability* **2018**, *1*, 89.
[168] J. Wu, Z. Lan, J. Lin, M. Huang, Y. Huang, L. Fan, G. Luo, *Chem. Rev.* **2015**, *115*, 2136.
[169] M. M. Hasan, M. D. Islam, T. U. Rashid, *Energy Fuels* **2020**, *34*, 15634.
[170] P. Semalti, S. N. Sharma, *J. Nanosci. Nanotechnol.* **2019**, *20*, 3647.
[171] C. Yan, S. Barlow, Z. Wang, H. Yan, A. K. Y. Jen, S. R. Marder, X. Zhan, *Nat. Rev. Mater.* **2018**, *3*, 18003.
[172] R. W. Miles, K. M. Hynes, I. Forbes, *Prog. Cryst. Growth Charact. Mater.* **2005**, *51*, 1.
[173] G. Chen, Y. Li, M. Bick, J. Chen, *Chem. Rev.* **2020**, *120*, 3668.
[174] F. Zhang, H. Lu, J. Tong, J. J. Berry, M. C. Beard, K. Zhu, *Energy Environ. Sci.* **2020**, *13*, 1154.
[175] A. Gok, *Reliability and Ecological Aspects of Photovoltaic Modules* IntechOpen **2020**.
[176] C. Stylianopoulos, *Encycl. Hum. Nutr.* **2012**, *1–4*, 265.
[177] S. Choudhury, S. Stalin, D. Vu, A. Warren, Y. Deng, P. Biswal, L. A. Archer, *Nat. Commun.* **2019**, *10*, 4398.
[178] H. Bi, X. Wang, H. Liu, Y. He, W. Wang, W. Deng, X. Ma, Y. Wang, W. Rao, Y. Chai, H. Ma, R. Li, J. Chen, Y. Wang, M. Xue, *Adv. Mater.* **2020**, *32*, 2000074.
[179] R. Carter, L. Oakes, A. Douglas, N. Muralidharan, A. P. Cohn, C. L. Pint, *Nano Lett.* **2017**, *17*, 1863.
[180] Y. Wu, J. P. Cao, Z. Zhou, X. Y. Zhao, Q. Q. Zhuang, Y. L. Wei, M. Zhao, Y. P. Zhao, H. C. Bai, *Int. J. Hydrogen Energy* **2020**, *45*, 31367.
[181] M. A. Yassin, I. M. A. Mohamed, F. S. Al-Mubaddel, N. A. M. Barakat, *Mater. Lett.* **2017**, *201*, 22.
[182] T. Shintani, *Fermentation* **2019**, *5*, 47.
[183] A. T. Vicente, A. Araújo, M. J. Mendes, D. Nunes, M. J. Oliveira, O. Sanchez-Sobrado, M. P. Ferreira, H. Águas, E. Fortunato, R. Martins, *J. Mater. Chem. C* **2018**, *6*, 3143.
[184] F. Brunetti, A. Operamolla, S. Castro-Hermosa, G. Lucarelli, V. Manca, G. M. Farinola, T. M. Brown, *Adv. Funct. Mater.* **2019**, *29*, 1806798.
[185] H. Águas, T. Mateus, A. Vicente, D. Gaspar, M. J. Mendes, W. A. Schmidt, L. Pereira, E. Fortunato, R. Martins, *Adv. Funct. Mater.* **2015**, *25*, 3592.

© 2021 The Authors. Advanced Energy Materials published by Wiley-VCH GmbH

16146840, 2021, 43, Downloaded from https://onlinelibrary.wiley.com/doi/10.1002/aenm.202100520 by Universita Di Torino, Wiley Online Library on [21/02/2025]. See the Terms and Conditions (https://onlinelibrary.wiley.com/terms-and-conditions) on Wiley Online Library for rules of use; OA articles are governed by the applicable Creative Commons License

[186] C. Zhong, *Front. Bioeng. Biotechnol.* **2020**, *8*, 1425.
[187] F. Esa, S. M. Tasirin, N. A. Rahman, *Agric. Agric. Sci. Procedia* **2014**, *2*, 113.
[188] H. Zhu, W. Luo, P. N. Ciesielski, Z. Fang, J. Y. Zhu, G. Henriksson, M. E. Himmel, L. Hu, *Chem. Rev.* **2016**, *116*, 9305.
[189] R. Martins, I. Ferreira, E. Fortunato, *Phys. Status Solidi RRL* **2011**, *5*, 332.
[190] G. Guhados, W. Wan, J. L. Hutter, *Langmuir* **2005**, *21*, 6642.
[191] K. Crews, C. Huntley, D. Cooley, B. Phillips, M. Curry, *Int. J. Polym. Sci.* **2016**, *2016*, 1.
[192] J. D. Schiffman, C. L. Schauer, *Polym. Rev.* **2008**, *48*, 317.
[193] N. Lavoine, I. Desloges, A. Dufresne, J. Bras, *Carbohydr. Polym.* **2012**, *90*, 735.
[194] R. Zhao, X. Zhang, J. Xu, Y. Yang, G. He, *RSC Adv.* **2013**, *3*, 23178.
[195] Y. Zhang, N. Hao, X. Lin, S. Nie, *Carbohydr. Polym.* **2020**, *234*, 115888.
[196] D. Elieh-Ali-Komi, M. R. Hamblin, *Int. J. Adv. Res.* **2016**, *4*, 411.
[197] J. Pal, H. O. Verma, V. K. Munka, S. K. Maurya, D. Roy, J. Kumar, *Int. J. Fish. Aquat. Stud.* **2014**, *1*, 104.
[198] M. Rinaudo, *Prog. Polym. Sci.* **2006**, *31*, 603.
[199] A. E. C. Fai, T. C. M. Stamford, T. M. Stamford-Arnaud, P. D. Santa-Cruz, M. C. F. da Silva, G. M. Campos-Takaki, T. L. M. Stamford, *Molecules* **2011**, *16*, 7143.
[200] L. Berger, T. Stamford, T. Stamford-Arnaud, S. de Alcântara, A. da Silva, A. da Silva, A. do Nascimento, G. de Campos-Takaki, *Int. J. Mol. Sci.* **2014**, *15*, 9082.
[201] P. C. Lin, Y. T. Wong, Y. A. Su, W. C. Chen, C. C. Chueh, *ACS Sustainable Chem. Eng.* **2018**, *6*, 14621.
[202] D. E. Azofeifa, H. J. Arguedas, W. E. Vargas, *Opt. Mater.* **2012**, *35*, 175.
[203] D. Lee, Y. W. Lim, H. G. Im, S. Jeong, S. Ji, Y. H. Kim, G. M. Choi, J. U. Park, J. Y. Lee, J. Jin, B. S. Bae, *ACS Appl. Mater. Interfaces* **2017**, *9*, 24161.
[204] W. Stelte, C. Clemons, J. K. Holm, J. Ahrenfeldt, U. B. Henriksen, A. R. Sanadi, *Ind. Crops Prod.* **2011**, *34*, 1053.
[205] D. S. Bajwa, G. Pourhashem, A. H. Ullah, S. G. Bajwa, *Ind. Crops Prod.* **2019**, *139*, 111526.
[206] W. G. Glasser, *Front. Chem.* **2019**, *7*, 1.
[207] Y. Wu, J. Wang, X. Qiu, R. Yang, H. Lou, X. Bao, Y. Li, *ACS Appl. Mater. Interfaces* **2016**, *8*, 12377.
[208] S. Gillet, M. Aguedo, L. Petitjean, A. R. C. Morais, A. M. Da Costa Lopes, R. M. Łukasik, P. T. Anastas, *Green Chem.* **2017**, *19*, 4200.
[209] A. Khan, J. C. Colmenares, R. Gläser, in *Lignin Chemistry* (Eds: L. Serrano, R. Luque, B. F. Sels), Springer International Publishing, Cham **2020**, pp. 1–31.
[210] J. F. Robyt, *Glycoscience*, Springer Berlin Heidelberg, Berlin **2008**, pp. 1437–1472.
[211] R. P. Ellis, M. P. Cochrane, M. F. B. Dale, C. M. Duffus, A. Lynn, I. M. Morrison, R. D. M. Prentice, J. S. Swanston, S. A. Tiller, *J. Sci. Food Agric.* **1998**, *77*, 289.
[212] A. S. Ayoub, S. S. H. Rizvi, *J. Plast. Film Sheeting* **2009**, *25*, 25.
[213] M. O. S. Lobregas, D. H. Camacho, *Electrochim. Acta* **2019**, *298*, 219.
[214] H. Jeong, S. Baek, S. Han, H. Jang, S. H. Kim, H. S. Lee, *Adv. Funct. Mater.* **2018**, *28*, 1704433.
[215] C. Sano, *Am. J. Clin. Nutr.* **2009**, *90*, 728S.
[216] M. Ikeda, S. Nakagawa, *Appl. Microbiol. Biotechnol.* **2003**, *62*, 99.
[217] M. D'Este, M. Alvarado-Morales, I. Angelidaki, *Biotechnol. Adv.* **2018**, *36*, 14.
[218] J. Hiraki, T. Ichikawa, S. I. Ninomiya, H. Seki, K. Uohama, H. Seki, S. Kimura, Y. Yanagimoto, J. W. Barnett, *Regul. Toxicol. Pharmacol.* **2003**, *37*, 328.
[219] D. Mazia, G. Schatten, W. Sale, *J. Cell Biol.* **1975**, *66*, 198.
[220] Z. Kadlecova, Y. Rajendra, M. Matasci, L. Baldi, D. L. Hacker, F. M. Wurm, H. A. Klok, *J. Controlled Release* **2013**, *169*, 276.
[221] Y. Jiang, P. Arounleut, S. Rheiner, Y. Bae, A. V. Kabanov, C. Milligan, D. S. Manickam, *J. Controlled Release* **2016**, *231*, 38.
[222] S. Nozohouri, A. E. Sifat, B. Vaidya, T. J. Abbruscato, *Drug Discovery Today* **2020**, *25*, 535.
[223] J. Xia, Z. Xu, H. Xu, J. Liang, S. Li, X. Feng, *Bioresour. Technol.* **2014**, *164*, 241.
[224] D. A. LaVan, J. N. Cha, *Proc. Natl. Acad. Sci. USA* **2006**, *103*, 5251.
[225] J. Barber, B. Andersson, *Nature* **1994**, *370*, 31.
[226] R. E. Blankenship, D. M. Tiede, J. Barber, G. W. Brudvig, G. Fleming, M. Ghirardi, M. R. Gunner, W. Junge, D. M. Kramer, A. Melis, T. A. Moore, C. C. Moser, D. G. Nocera, A. J. Nozik, D. R. Ort, W. W. Parson, R. C. Prince, R. T. Sayre, *Science* **2011**, *332*, 805.
[227] M. C. Hanna, A. J. Nozik, *J. Appl. Phys.* **2006**, *100*, 074510.
[228] G. S. Engel, T. R. Calhoun, E. L. Read, T. K. Ahn, T. Mančal, Y. C. Cheng, R. E. Blankenship, G. R. Fleming, *Nature* **2007**, *446*, 782.
[229] P. Singh, S. Singh, N. Jaggi, K. H. Kim, P. Devi, *Nano Energy* **2021**, *79*, 105482.
[230] A. Laisk, V. Oja, H. Eichelmann, L. Dall'Osto, *Biochim. Biophys. Acta, Bioenerg.* **2014**, *1837*, 315.
[231] H. Lee, S. M. Dellatore, W. M. Miller, P. B. Messersmith, *Science* **2007**, *318*, 426.
[232] Y. Liu, K. Ai, L. Lu, *Chem. Rev.* **2014**, *114*, 5057.
[233] J. Wünsche, F. Cicoira, C. F. O. Graeff, C. Santato, *J. Mater. Chem. B* **2013**, *1*, 3836.
[234] Z. Khan, R. Shanker, D. Um, A. Jaiswal, H. Ko, *Bioinspired Polydopamine and Composites for Biomedical Applications. In Electrically Conductive Polymer and Polymer Composites* (Eds: A. Khan, M. Jawaid, A. A. Parwaz Khan, A. M. Asiri) **2018**, https://doi.org/10.1002/9783527807918.ch1.
[235] V. Ball, *Front. Bioeng. Biotechnol.* **2018**, *6*, 109.
[236] M. H. Ryou, Y. M. Lee, J. K. Park, J. W. Choi, *Adv. Mater.* **2011**, *23*, 3066.
[237] H. Jiang, L. Yang, C. Li, C. Yan, P. S. Lee, J. Ma, *Energy Environ. Sci.* **2011**, *4*, 1813.
[238] Q. Liu, B. Yu, W. Ye, F. Zhou, *Macromol. Biosci.* **2011**, *11*, 1227.
[239] C. Zong, K. Ai, G. Zhang, H. Li, L. Lu, *Anal. Chem.* **2011**, *83*, 3126.
[240] Li Qi, Zhang Yong, *Acta Phys. Sin.* **2017**, *66*, 198201.
[241] L. Tan, Y. Wang, J. Zhang, S. Xiao, H. Zhou, Y. Li, Y. Chen, Y. Li, *Adv. Sci.* **2019**, *6*, 1801180.
[242] S. Jung, H. Kim, J. Lee, G. Jeong, H. Kim, J. Park, H. Park, *ACS Appl. Energy Mater.* **2018**, *1*, 6463.
[243] X. Duan, Z. Huang, C. Liu, J. Yang, L. Tan, Y. Chen, *Chem. Commun.* **2019**, *55*, 3666.
[244] H. Wang, L. Yan, *Colloids Surf., A* **2017**, *531*, 198.
[245] X. Gao, L. Yan, R. Xu, X. Sun, *J. Mater. Sci.: Mater. Electron.* **2018**, *29*, 19976.
[246] H. U. Blaser, H. J. Federsel, *Asymmetric Catalysis on Industrial Scale: Challenges, Approaches and Solutions*, 2nd ed., Wiley, Hoboken, NJ **2010**.
[247] K. Min, K. Park, D. H. Park, Y. J. Yoo, *Appl. Microbiol. Biotechnol.* **2015**, *99*, 575.
[248] E. Vilanova, A. Manjon, J. L. Iborra, *Biotechnol. Bioeng.* **1984**, *26*, 1306.
[249] M. C. Simon, D. I. Gray, N. Cook, *Appl. Environ. Microbiol.* **1996**, *62*, 822.
[250] J. Nizioł, K. Makyła-Juzak, M. M. Marzec, R. Ekiert, M. Marzec, E. Gondek, *Opt. Mater.* **2017**, *66*, 344.
[251] M. Muskovich, C. J. Bettinger, *Adv. Healthcare Mater.* **2012**, *1*, 248.
[252] M. Irimia-Vladu, N. S. Sariciftci, S. Bauer, *J. Mater. Chem.* **2011**, *21*, 1350.
[253] A. J. Steckl, *Nat. Photonics* **2007**, *1*, 3.

© 2021 The Authors. Advanced Energy Materials published by Wiley-VCH GmbH

16146840, 2021, 43, Downloaded from https://onlinelibrary.wiley.com/doi/10.1002/aenm.202100520 by Universita Di Torino, Wiley Online Library on [21/02/2025]. See the Terms and Conditions (https://onlinelibrary.wiley.com/terms-and-conditions) on Wiley Online Library for rules of use; OA articles are governed by the applicable Creative Commons License

[254] J. A. Hagen, W. Li, A. J. Steckl, J. G. Grote, *Appl. Phys. Lett.* **2006**, *88*, 171109.
[255] P. Zalar, D. Kamkar, R. Naik, F. Ouchen, J. G. Grote, G. C. Bazan, T. Q. Nguyen, *J. Am. Chem. Soc.* **2011**, *133*, 11010.
[256] Y. Zhang, M. Wang, S. D. Collins, H. Zhou, H. Phan, C. Proctor, A. Mikhailovsky, F. Wudl, T.-Q. Nguyen, *Angew. Chem.* **2014**, *126*, 248.
[257] Y. Zhang, P. Zalar, C. Kim, S. Collins, G. C. Bazan, T.-Q. Nguyen, *Adv. Mater.* **2012**, *24*, 4255.
[258] Z. Deng, C. Mao, *Nano Lett.* **2003**, *3*, 1545.
[259] P. Stadler, K. Oppelt, T. B. Singh, J. G. Grote, R. Schwödiauer, S. Bauer, H. Piglmayer-Brezina, D. Bäuerle, N. S. Sariciftci, *Org. Electron.* **2007**, *8*, 648.
[260] D. Pramanik, P. K. Maiti, *ACS Appl. Mater. Interfaces* **2017**, *9*, 35287.
[261] A. K. Manna, S. K. Pati, *J. Mater. Chem. B* **2013**, *1*, 91.
[262] F. Toschi, D. Catone, P. O'Keeffe, A. Paladini, S. Turchini, J. Dagar, T. M. Brown, *Adv. Funct. Mater.* **2018**, *28*, 1707126.
[263] M. Yu, J. Zhang, S. Li, Y. Meng, J. Liu, *RSC Adv.* **2015**, *5*, 5604.
[264] S. Sabagh, M. Izadyar, F. Arkan, *Int. J. Quantum Chem.* **2020**, *120*, e26171.
[265] G. Calogero, G. Di Marco, S. Cazzanti, S. Caramori, R. Argazzi, A. Di Carlo, C. A. Bignozzi, *Int. J. Mol. Sci.* **2010**, *11*, 254.
[266] S. Deckers, S. Vandendriessche, D. Cornelis, F. Monnaie, G. Koeckelberghs, I. Asselberghs, T. Verbiest, M. A. van der Veen, *Chem. Commun.* **2014**, *50*, 2741.
[267] X. F. Wang, J. Xiang, P. Wang, Y. Koyama, S. Yanagida, Y. Wada, K. Hamada, S. I. Sasaki, H. Tamiaki, *Chem. Phys. Lett.* **2005**, *408*, 409.
[268] E. Yamazaki, M. Murayama, N. Nishikawa, N. Hashimoto, M. Shoyama, O. Kurita, *Sol. Energy* **2007**, *81*, 512.
[269] Y. Koyama, Y. Kakitani, H. Nagae, *Molecules* **2012**, *17*, 2188.
[270] V. Vohra, T. Uchiyama, S. Inaba, Y. Okada-Shudo, *ACS Sustainable Chem. Eng.* **2019**, *7*, 4376.
[271] Z. Zhang, P. H. Lambrev, K. L. Wells, G. Garab, H.-S. Tan, *Nat. Commun.* **2015**, *6*, 7914.
[272] Z. Liu, H. Yan, K. Wang, T. Kuang, J. Zhang, L. Gui, X. An, W. Chang, *Nature* **2004**, *428*, 287.
[273] I. Oda, M. Iwaki, D. Fujita, Y. Tsutsui, S. Ishizaka, M. Dewa, M. Nango, T. Kajino, Y. Fukushima, S. Itoh, *Langmuir* **2010**, *26*, 13399.
[274] K. R. Catchpole, A. Polman, *Appl. Phys. Lett.* **2008**, *93*, 191113.
[275] H. A. Atwater, A. Polman, *Materials for Sustainable Energy: A Collection of Peer-Reviewed Research and Review Articles from Nature Publishing Group*, World Scientific Publishing Co., Singapore **2010**, pp. 3–11.
[276] M. Rycenga, C. M. Cobley, J. Zeng, W. Li, C. H. Moran, Q. Zhang, D. Qin, Y. Xia, *Chem. Rev.* **2011**, *111*, 3669.
[277] E. Darby, G. Leblanc, E. A. Gizzie, K. M. Winter, G. K. Jennings, D. E. Cliffel, *Langmuir* **2014**, *30*, 8990.
[278] G. LeBlanc, E. Gizzie, S. Yang, D. E. Cliffel, G. K. Jennings, *Langmuir* **2014**, *30*, 10990.
[279] P. I. Gordiichuk, G.-J. J. A. H. Wetzelaer, D. Rimmerman, A. Gruszka, J. W. De Vries, M. Saller, D. A. Gautier, S. Catarci, D. Pesce, S. Richter, P. W. M. Blom, A. Herrmann, *Adv. Mater.* **2014**, *26*, 4863.
[280] P. O. Saboe, E. Conte, S. Chan, H. Feroz, B. Ferlez, M. Farell, M. F. Poyton, I. T. Sines, H. Yan, G. C. Bazan, J. Golbeck, M. Kumar, *J. Mater. Chem. A* **2016**, *4*, 15457.
[281] P. O. Saboe, C. E. Lubner, N. S. McCool, N. M. Vargas-Barbosa, H. Yan, S. Chan, B. Ferlez, G. C. Bazan, J. H. Golbeck, M. Kumar, *Adv. Mater.* **2014**, *26*, 7064.
[282] S. Sezi, H. A. Wagenknecht, *Chem. Commun.* **2013**, *49*, 9257.
[283] P. Ensslen, Y. Fritz, H. A. Wagenknecht, *Org. Biomol. Chem.* **2015**, *13*, 487.
[284] J.-J. Yun, H.-S. Jung, S.-H. Kim, E.-M. Han, V. Vaithianathan, S. A. Jenekhe, *Appl. Phys. Lett.* **2005**, *87*, 123102.
[285] R. Tange, K. Inai, T. Sagawa, S. Yoshikawa, *J. Mater. Res.* **2011**, *26*, 306.
[286] T. Zhuang, S. Sasaki, T. Ikeuchi, J. Kido, X.-F. Wang, *RSC Adv.* **2015**, *5*, 45755.
[287] F. A. Nüesch, *Chim. Int. J. Chem.* **2013**, *67*, 796.
[288] U. Wurfel, A. Cuevas, P. Wurfel, *IEEE J. Photovoltaics* **2015**, *5*, 461.
[289] X. Zhu, B. Guo, J. Fang, T. Zhai, Y. Wang, G. Li, J. Zhang, Z. Wei, S. Duhm, X. Guo, M. Zhang, Y. Li, *Org. Electron.* **2019**, *70*, 25.
[290] Z. Zheng, R. Wang, H. Yao, S. Xie, Y. Zhang, J. Hou, H. Zhou, Z. Tang, *Nano Energy* **2018**, *50*, 169.
[291] K.-T. T. Huang, C.-C. C. Shih, B.-H. H. Jiang, R.-J. J. Jeng, C.-P. P. Chen, W.-C. C. Chen, *J. Mater. Chem. C* **2019**, *7*, 12572.
[292] A. Hu, Q. Wang, L. Chen, X. Hu, Y. Zhang, Y. Wu, Y. Chen, *ACS Appl. Mater. Interfaces* **2015**, *7*, 16078.
[293] Y. T. Liang, M. C. Hersam, *J. Am. Chem. Soc.* **2010**, *132*, 17661.
[294] E. B. Secor, S. Lim, H. Zhang, C. D. Frisbie, L. F. Francis, M. C. Hersam, *Adv. Mater.* **2014**, *26*, 4533.
[295] J. Wu, Y. Liu, A. Islam, Q. Zheng, J. Li, W. Ji, L. Chen, X. Ouyang, *Adv. Sci.* **2020**, *7*, 1902269.
[296] R. Elghanian, J. J. Storhoff, R. C. Mucic, R. L. Letsinger, C. A. Mirkin, *Science* **1997**, *277*, 1078.
[297] M. Zheng, A. Jagota, E. D. Semke, B. A. Diner, R. S. Mclean, S. R. Lustig, R. E. Richardson, N. G. Tassi, *Nat. Mater.* **2003**, *2*, 338.
[298] E. Braun, Y. Eichen, U. Sivan, G. Ben-Yoseph, *Nature* **1998**, *391*, 775.
[299] H. Lee, J. Rho, P. B. Messersmith, *Adv. Mater.* **2009**, *21*, 431.
[300] H. W. Chien, W. H. Kuo, M. J. Wang, S. W. Tsai, W. B. Tsai, *Langmuir* **2012**, *28*, 5775.
[301] S. A. Mian, L. M. Yang, L. C. Saha, E. Ahmed, M. Ajmal, E. Ganz, *Langmuir* **2014**, *30*, 6906.
[302] C. Zhang, Y. Ou, W. X. Lei, L. S. Wan, J. Ji, Z. K. Xu, *Angew. Chem., Int. Ed.* **2016**, *55*, 3054.
[303] M. V. Rapp, G. P. Maier, H. A. Dobbs, N. J. Higdon, J. H. Waite, A. Butler, J. N. Israelachvili, *J. Am. Chem. Soc.* **2016**, *138*, 9013.
[304] L. Wang, L. Yan, X. Gao, *Int. J. Energy Res.* **2018**, *42*, 3496.
[305] M. Gaceur, S. Ben Dkhil, D. Duché, F. Bencheikh, J.-J. Simon, L. Escoubas, M. Mansour, A. Guerrero, G. Garcia-Belmonte, X. Liu, M. Fahlman, W. Dachraoui, A. K. Diallo, C. Videlot-Ackermann, O. Margeat, J. Ackermann, *Adv. Funct. Mater.* **2016**, *26*, 243.
[306] L. K. Jagadamma, M. Al-Senani, A. El-Labban, I. Gereige, G. O. Ngongang Ndjawa, J. C. D. Faria, T. Kim, K. Zhao, F. Cruciani, D. H. Anjum, M. A. McLachlan, P. M. Beaujuge, A. Amassian, *Adv. Energy Mater.* **2015**, *5*, 1500204.
[307] X. Liu, X. Li, Y. Li, C. Song, L. Zhu, W. Zhang, H. Q. Wang, J. Fang, *Adv. Mater.* **2016**, *28*, 7405.
[308] N. Ahmad, X. Zhang, S. Yang, D. Zhang, J. Wang, S. U. Zafar, Y. Li, Y. Zhang, S. Hussain, Z. Cheng, A. Kumaresan, H. Zhou, S. Uz Zafar, Y. Li, Y. Zhang, S. Hussain, Z. Cheng, A. Kumaresan, H. Zhou, *J. Mater. Chem. C* **2019**, *7*, 10795.
[309] M. Xu, L. Yan, Y. Zhu, Y. Li, X. Song, L. Yin, *J. Mater. Sci. Mater. Electron.* **2020**, *31*, 6698.
[310] L. Chen, C. Xie, Y. Chen, *Adv. Funct. Mater.* **2014**, *24*, 3986.
[311] W. Liang, L. Xu, S. Sun, L. Lan, X. Qiu, R. Chen, Y. Li, *ACS Sustainable Chem. Eng.* **2017**, *5*, 460.
[312] S. Zhang, Y. Xia, J. Ouyang, *Org. Electron.* **2017**, *45*, 139.
[313] Y. Xia, K. Sun, J. Ouyang, *Adv. Mater.* **2012**, *24*, 2436.
[314] Y. H. Kim, C. Sachse, M. L. MacHala, C. May, L. Müller-Meskamp, K. Leo, *Adv. Funct. Mater.* **2011**, *21*, 1076.
[315] H. Shi, C. Liu, Q. Jiang, J. Xu, *Adv. Electron. Mater.* **2015**, *1*, 1500017.

© 2021 The Authors. Advanced Energy Materials published by Wiley-VCH GmbH

16146840, 2021, 43, Downloaded from https://onlinelibrary.wiley.com/doi/10.1002/aenm.202100520 by Universita Di Torino, Wiley Online Library on [21/02/2025]. See the Terms and Conditions (https://onlinelibrary.wiley.com/terms-and-conditions) on Wiley Online Library for rules of use; OA articles are governed by the applicable Creative Commons License

[316] B. Yang, Y. Chen, Y. Cui, D. Liu, B. Xu, J. Hou, *Adv. Energy Mater.* **2018**, *8*, 1800698.
[317] C. Girotto, E. Voroshazi, D. Cheyns, P. Heremans, B. P. Rand, *ACS Appl. Mater. Interfaces* **2011**, *3*, 3244.
[318] F. Xie, W. C. H. Choy, C. Wang, X. Li, S. Zhang, J. Hou, *Adv. Mater.* **2013**, *25*, 2051.
[319] C. Roldán-Carmona, O. Malinkiewicz, A. Soriano, G. Mínguez Espallargas, A. Garcia, P. Reinecke, T. Kroyer, M. I. Dar, M. K. Nazeeruddin, H. J. Bolink, *Energy Environ. Sci.* **2014**, *7*, 994.
[320] R. Wang, H. Yu, M. Dirican, L. Chen, D. Fang, Y. Tian, C. Yan, J. Xie, D. Jia, H. Liu, J. Wang, F. Tang, A. M. Asiri, X. Zhang, J. Tao, *ACS Appl. Energy Mater.* **2020**, *3*, 785.
[321] Y. Li, L. Meng, Y. (Michael) Yang, G. Xu, Z. Hong, Q. Chen, J. You, G. Li, Y. Yang, Y. Li, *Nat. Commun.* **2016**, *7*, 10214.
[322] Y. Chen, Y. Mei, R. Kaltofen, J. I. Mönch, J. Schumann, J. Freudenberger, H.-J. Klauß, O. G. Schmidt, *Adv. Mater.* **2008**, *20*, 3224.
[323] S. S. Shin, W. S. Yang, J. H. Noh, J. H. Suk, N. J. Jeon, J. H. Park, J. S. Kim, W. M. Seong, S. Il Seok, *Nat. Commun.* **2015**, *6*, 7410.
[324] Y. Guo, W. Sato, K. Shoyama, E. Nakamura, *J. Am. Chem. Soc.* **2016**, *138*, 5410.
[325] B. J. Kim, D. H. Kim, Y. Y. Lee, H. W. Shin, G. S. Han, J. S. Hong, K. Mahmood, T. K. Ahn, Y. C. Joo, K. S. Hong, N. G. Park, S. Lee, H. S. Jung, *Energy Environ. Sci.* **2015**, *8*, 916.
[326] B. Abdollahi Nejand, P. Nazari, S. Gharibzadeh, V. Ahmadi, A. Moshaii, *Chem. Commun.* **2017**, *53*, 747.
[327] J. J. Pacheco, M. E. Davis, *Proc. Natl. Acad. Sci. USA* **2014**, *111*, 8363.
[328] D. Klemm, B. Heublein, H.-P. Fink, A. Bohn, *Angew. Chem., Int. Ed.* **2005**, *44*, 3358.
[329] C. Jia, X. Zhao, Y. H. Lai, J. Zhao, P. C. Wang, D. S. Liou, P. Wang, Z. Liu, W. Zhang, W. Chen, Y. H. Chu, J. Li, *Nano Energy* **2019**, *60*, 476.
[330] T. Posati, A. Aluigi, A. Donnadio, G. Sotgiu, M. Mosconi, M. Muccini, G. Ruani, R. Zamboni, M. Seri, *Adv. Sustainable Syst.* **2019**, *3*, 1900080.
[331] M. Nogi, M. Karakawa, N. Komoda, H. Yagyu, T. T. Nge, *Sci. Rep.* **2015**, *5*, 17254.
[332] S. V. Costa, P. Pingel, S. Janietz, A. F. Nogueira, *J. Appl. Polym. Sci.* **2016**, *133*, 43679.
[333] H. Li, X. Liu, W. Wang, Y. Lu, J. Huang, J. Li, J. Xu, P. Fan, J. Fang, W. Song, *Sol. RRL* **2018**, *2*, 1800123.
[334] H. Kang, S. Jung, S. Jeong, G. Kim, K. Lee, *Nat. Commun.* **2015**, *6*, 6503.
[335] Q. Cheng, D. Ye, W. Yang, S. Zhang, H. Chen, C. Chang, L. Zhang, *ACS Sustainable Chem. Eng.* **2018**, *6*, 8040.
[336] J.-Y. Lam, C.-C. Shih, W.-Y. Lee, C.-C. Chueh, G.-W. Jang, C.-J. Huang, S.-H. Tung, W.-C. Chen, *Macromol. Rapid Commun.* **2018**, *39*, 1800271.
[337] A. J. J. E. Eerhart, A. P. C. Faaij, M. K. Patel, *Energy Environ. Sci.* **2012**, *5*, 6407.
[338] S. K. Burgess, O. Karvan, J. R. Johnson, R. M. Kriegel, W. J. Koros, *Polymer* **2014**, *55*, 4748.
[339] A. Pellis, K. Haernvall, C. M. Pichler, G. Ghazaryan, R. Breinbauer, G. M. Guebitz, *J. Biotechnol.* **2016**, *235*, 47.
[340] J.-G. Rosenboom, D. K. Hohl, P. Fleckenstein, G. Storti, M. Morbidelli, *Nat. Commun.* **2018**, *9*, 2701.
[341] Y. Xie, L. Huo, B. Fan, H. Fu, Y. Cai, L. Zhang, Z. Li, Y. Wang, W. Ma, Y. Chen, Y. Sun, *Adv. Funct. Mater.* **2018**, *28*, 1800627.
[342] Y. Zhou, T. M. Khan, J. W. Shim, A. Dindar, C. Fuentes-Hernandez, B. Kippelen, *J. Mater. Chem. A* **2014**, *2*, 3492.
[343] W. Yu, L. Shen, P. Shen, Y. Long, H. Sun, W. Chen, S. Ruan, *ACS Appl. Mater. Interfaces* **2014**, *6*, 599.
[344] Z. Tang, A. Elfwing, J. Bergqvist, W. Tress, O. Inganäs, *Adv. Energy Mater.* **2013**, *3*, 1606.
[345] Z. Tang, A. Elfwing, A. Melianas, J. Bergqvist, Q. Bao, O. Inganäs, *J. Mater. Chem. A* **2015**, *3*, 24289.
[346] J. Wu, X. Che, H. C. Hu, H. Xu, B. Li, Y. Liu, J. Li, Y. Ni, X. Zhang, X. Ouyang, *J. Mater. Chem. A* **2020**, *8*, 5442.
[347] A. M. Nardes, M. Kemerink, M. M. de Kok, E. Vinken, K. Maturova, R. A. J. Janssen, *Org. Electron.* **2008**, *9*, 727.
[348] N. Kim, S. Kee, S. H. Lee, B. H. Lee, Y. H. Kahng, Y. R. Jo, B. J. Kim, K. Lee, *Adv. Mater.* **2014**, *26*, 2268.
[349] W. Greenbank, N. Rolston, E. Destouesse, G. Wantz, L. Hirsch, R. Dauskardt, S. Chambon, *J. Mater. Chem. A* **2017**, *5*, 2911.
[350] L. La Notte, P. Cataldi, L. Ceseracciu, I. S. Bayer, A. Athanassiou, S. Marras, E. Villari, F. Brunetti, A. Reale, *Mater. Today Energy* **2018**, 7, 105.
[351] Q. Wang, X. Hu, X. Yang, G. Liu, X. Meng, Y. Xie, Y. Xiao, J. Liu, L. Tan, Y. Chen, *Org. Electron.* **2018**, *61*, 296.
[352] X. Meng, Y. Xu, Q. Wang, X. Yang, J. Guo, X. Hu, L. Tan, Y. Chen, *Langmuir* **2019**, *35*, 9713.
[353] H. Zhou, H. Mao, X. Meng, Q. Wang, L. Tan, Y. Chen, *Org. Electron.* **2019**, *75*, 105408.
[354] S. Hong, J. Kim, Y. S. Na, J. Park, S. Kim, K. Singha, G. Il Im, D. K. Han, W. J. Kim, H. Lee, *Angew. Chem., Int. Ed.* **2013**, *52*, 9187.
[355] Y. C. Shih, L. Y. Wang, H. C. Hsieh, K. F. Lin, *J. Mater. Chem. A* **2015**, *3*, 9133.
[356] P. Wu, X. Ma, B. Zhao, C. Liu, Y. Chen, G. Yang, X. Li, *Sustainable Energy Fuels* **2020**, *4*, 878.
[357] W. Zhang, X. Liu, B. He, J. Zhu, X. Li, K. Shen, H. Chen, Y. Duan, Q. Tang, *ACS Appl. Mater. Interfaces* **2020**, *12*, 36092.
[358] R. Tonner, *ChemPhysChem* **2010**, *11*, 1053.
[359] W. Zhang, X. Lei, J. Liu, J. Dong, X. Yan, W. Gao, H. Dong, C. Ran, Z. Wu, *Phys. Status Solidi RRL* **2019**, *13*, 1.
[360] H. Li, C. Zhang, Y. Ma, Y. Mai, Y. Xu, *Org. Electron.* **2018**, *62*, 468.
[361] J. He, Y. Xiang, F. Zhang, J. Lian, R. Hu, P. Zeng, J. Song, J. Qu, *Nano Energy* **2018**, *45*, 471.
[362] S. Das, C. Wu, Z. Song, Y. Hou, R. Koch, P. Somasundaran, S. Priya, B. Barbiellini, R. Venkatesan, *ACS Appl. Mater. Interfaces* **2019**, *11*, 30728.
[363] A. R. b. M. Yusoff, J. Kim, J. Jang, M. K. Nazeeruddin, *ChemSusChem* **2016**, *9*, 1736.
[364] X. Peng, H. Lu, J. Zhuang, X. Liu, Z. Ma, H. Wang, Z. Guo, Q. Wang, H. Zhang, S. Zhao, *Sol. Energy* **2020**, *206*, 855.
[365] S. S. Mali, H. Kim, J. V Patil, C. K. Hong, *ACS Appl. Mater. Interfaces* **2018**, *10*, 31280.
[366] P. Huang, Y. Liu, K. Zhang, L. Yuan, D. Li, G. Hou, B. Dong, Y. Zhou, B. Song, Y. Li, *J. Mater. Chem. A* **2017**, *5*, 24275.
[367] Q. Xue, Z. Hu, J. Liu, J. Lin, C. Sun, Z. Chen, C. Duan, J. Wang, C. Liao, W. M. Lau, F. Huang, H. L. Yip, Y. Cao, *J. Mater. Chem. A* **2014**, *2*, 19598.
[368] M. Hou, H. Zhang, Z. Wang, Y. Xia, Y. Chen, W. Huang, *ACS Appl. Mater. Interfaces* **2018**, *10*, 30607.
[369] P. Zhai, R. Cheng, L. Ren, Y.-T. Huang, H. Lee, S.-P. Feng, *Sol. RRL* **2018**, *2*, 1800103.
[370] I. A. Shkrob, A. D. Liu, M. C. Sauer, A. D. Trifunac, *J. Phys. Chem. A* **2001**, *105*, 7211.
[371] C. Liu, H. Su, C. Wei, K. Xie, H. Wang, P. Zhai, M. Guo, J. Zhang, L. Liu, *Electrochim. Acta* **2020**, *354*, 136720.
[372] C. Wang, Y. Li, C. Zhang, L. Shi, S. Tong, B. Guo, J. Zhang, J. He, Y. Gao, C. Su, J. Yang, *J. Power Sources* **2018**, *390*, 134.
[373] H. Zheng, W. Wu, H. Xu, F. Zheng, G. Liu, X. Pan, Q. Chen, *Adv. Funct. Mater.* **2020**, *30*, 2000034.
[374] A. Lang, I. Polishchuk, E. Seknazi, J. Feldmann, A. Katsman, B. Pokroy, *Adv. Funct. Mater.* **2020**, *30*, 2005136.
[375] Y. Hou, K. Wang, D. Yang, Y. Jiang, N. Yennawar, K. Wang, M. Sanghadasa, C. Wu, S. Priya, *ACS Energy Lett.* **2019**, *4*, 2646.

© 2021 The Authors. Advanced Energy Materials published by Wiley-VCH GmbH

16146840, 2021, 43, Downloaded from https://onlinelibrary.wiley.com/doi/10.1002/aenm.202100520 by Universita Di Torino, Wiley Online Library on [21/02/2025]. See the Terms and Conditions (https://onlinelibrary.wiley.com/terms-and-conditions) on Wiley Online Library for rules of use; OA articles are governed by the applicable Creative Commons License

[376] H. Y. Chu, J. Y. Hong, C. F. Huang, J. Y. Wu, T. L. Wang, T. M. Wu, R. H. Lee, *Cellulose* **2019**, *26*, 9229.
[377] S. Xiong, Z. Hou, S. Zou, X. Lu, J. Yang, T. Hao, Z. Zhou, J. Xu, Y. Zeng, W. Xiao, W. Dong, D. Li, X. Wang, Z. Hu, L. Sun, Y. Wu, X. Liu, L. Ding, Z. Sun, M. Fahlman, Q. Bao, *Joule* **2021**, *5*, 467.
[378] S. Xiong, T. Hao, Y. Sun, J. Yang, R. Ma, J. Wang, S. Gong, X. Liu, L. Ding, M. Fahlman, Q. Bao, *J. Energy Chem.* **2021**, *55*, 265.
[379] S. You, H. Wang, S. Bi, J. Zhou, L. Qin, X. Qiu, Z. Zhao, Y. Xu, Y. Zhang, X. Shi, H. Zhou, Z. Tang, *Adv. Mater.* **2018**, *30*, 1706924.
[380] S. Y. Zaitsev, D. O. Solovyeva, I. Nabiev, *Adv. Colloid Interface Sci.* **2012**, *14*, 183.
[381] S. Janfaza, A. Molaeirad, R. Mohamadpour, M. Khayati, J. Mehrvand, *Bionanoscience* **2014**, *4*, 71.
[382] R. Mohammadpour, S. Janfaza, M. Zeinoddini, *Biomass Bioenergy* **2016**, *87*, 35.
[383] J. Chellamuthu, P. Nagaraj, S. G. Chidambaram, A. Sambandam, A. Muthupandian, *J. Photochem. Photobiol., B* **2016**, *162*, 208.
[384] S. K. Srivastava, P. Piwek, S. R. Ayakar, A. Bonakdarpour, D. P. Wilkinson, V. G. Yadav, *Small* **2018**, *14*, 1800729.
[385] J. G. Yañuk, F. M. Cabrerizo, F. G. Dellatorre, M. F. Cerdá, *Energy Rep.* **2020**, *6*, 25.
[386] R. Güzel, Y. S. Ocak, Ş. N. Karuk, A. Ersöz, R. Say, *J. Power Sources* **2019**, *440*, 227119.
[387] R. Güzel, F. Yediyıldız, Y. S. Ocak, F. Yılmaz, A. Ersöz, R. Say, *J. Photochem. Photobiol., A* **2020**, *401*, 112743.
[388] J. Lorquin, F. Molouba, B. L. Dreyfus, *Appl. Environ. Microbiol.* **1997**, *63*, 1151.
[389] N. T. R. N. Kumara, A. Lim, C. M. Lim, M. I. Petra, P. Ekanayake, *Renewable Sustainable Energy Rev.* **2017**, *78*, 301.
[390] M. Z. Iqbal, S. R. Ali, S. Khan, *Sol. Energy* **2019**, *181*, 490.
[391] N. Aziz, N. A. Mat Nor, A. K. Arof, *Opt. Quantum Electron.* **2020**, *52*, 24.
[392] N. Gokilamani, N. Muthukumarasamy, M. Thambidurai, A. Ranjitha, D. Velauthapillai, T. S. Senthil, R. Balasundaraprabhu, *J. Mater. Sci.: Mater. Electron.* **2013**, *24*, 3394.
[393] N. Órdenes-Aenishanslins, G. Anziani-Ostuni, M. Vargas-Reyes, J. Alarcón, A. Tello, J. M. Pérez-Donoso, *J. Photochem. Photobiol., B* **2016**, *162*, 707.
[394] E. Güzel, B. S. Arslan, V. Durmaz, M. Cesur, Ö. F. Tutar, T. Sarı, M. İşleyen, M. Nebioğlu, İ. Şişman, *Sol. Energy* **2018**, *173*, 34.
[395] S. Shalini, R. Balasundara Prabhu, S. Prasanna, T. K. Mallick, S. Senthilarasu, *Renewable Sustainable Energy Rev.* **2015**, *51*, 1306.
[396] F. Bella, D. Pugliese, L. Zolin, C. Gerbaldi, *Electrochim. Acta* **2017**, *237*, 87.
[397] A. Poskela, K. Miettunen, M. Borghei, J. Vapaavuori, L. G. Greca, J. Lehtonen, K. Solin, M. Ago, P. D. Lund, O. J. Rojas, *ACS Sustainable Chem. Eng.* **2019**, *7*, 10257.
[398] E. Doelker, in *Biopolymers I* (Eds: R.S. Langer, N.A. Peppas), Springer, Berlin **1993**, pp. 199–265.
[399] S. Rudhziah, A. Ahmad, I. Ahmad, N. S. Mohamed, *Electrochim. Acta* **2015**, *175*, 162.
[400] C. Naceur Abouloula, M. Rizwan, V. Selvanathan, A. Hassan, R. Yahya, A. Oueriagli, *Cellulose* **2019**, *26*, 1605.
[401] V. Selvanathan, R. Yahya, M. H. Ruslan, K. Sopian, N. Amin, M. Nour, H. Sindi, M. Rawa, M. Akhtaruzzaman, *Polymers* **2020**, *12*, 516.
[402] K. C. Yogananda, E. Ramasamy, S. Kumar, S. Vasantha Kumar, M. Navya Rani, D. Rangappa, *Mater Today: Proc.* **2017**, *4*, 12238.
[403] YoganandaK.C , E. Ramasamy, Vasantha KumarS , D. Rangappa, *Ionics* **2019**, *25*, 6035.
[404] P. Nagaraj, A. Sasidharan, V. David, A. Sambandam, *Polymers* **2017**, *9*, 667.
[405] I. Sagaidak, G. Huertas, A. Nguyen Van Nhien, F. Sauvage, *Energies* **2016**, *9*, 241.
[406] C. L. Boldrini, N. Manfredi, F. M. Perna, V. Capriati, A. Abbotto, *ChemElectroChem* **2020**, *7*, 1707.
[407] V. Selvanathan, A. D. Azzahari, A. A. Adyani, R. Yahya, *Carbohydr. Polym.* **2017**, *167*, 210.
[408] S. Sharma, M. Khannam, M. Boruah, B. C. Nath, S. K. Dolui, *IEEE J. Photovoltaics* **2015**, *5*, 1665.
[409] B. C. Nath, B. Gogoi, M. Boruah, S. Sharma, M. Khannam, G. A. Ahmed, S. K. Dolui, *Electrochim. Acta* **2014**, *146*, 106.
[410] M. Shaheer Akhtar, J. M. Chun, O. B. Yang, *Electrochem. Commun.* **2007**, *9*, 2833.
[411] M. Khannam, R. Boruah, S. K. Dolui, *J. Photochem. Photobiol., A* **2017**, *335*, 248.
[412] H. Iftikhar, G. G. Sonai, S. G. Hashmi, A. F. Nogueira, P. D. Lund, *Materials* **2019**, *12*, 1998.
[413] M. Taki, B. Rezaei, N. Fani, S. Borandeh, A. Abdolmaleki, A. A. Ensafi, *Appl. Surf. Sci.* **2017**, *403*, 218.
[414] V. Sudhakar, C. Das, K. Krishnamoorthy, *ChemistrySelect* **2018**, *3*, 7195.
[415] C. P. Lee, K. Y. Lai, C. A. Lin, C. T. Li, K. C. Ho, C. I. Wu, S. P. Lau, J. H. He, *Nano Energy* **2017**, *36*, 260.
[416] Y. Di, Z. Xiao, X. Yan, G. Ru, B. Chen, J. Feng, *Appl. Surf. Sci.* **2018**, *441*, 807.
[417] A. Shrestha, M. Batmunkh, C. J. Shearer, Y. Yin, G. G. Andersson, J. G. Shapter, S. Qiao, S. Dai, *Adv. Energy Mater.* **2017**, *7*, 1602276.
[418] K. Karthick, U. Nithiyanantham, S. R. Ede, S. Kundu, *ACS Sustainable Chem. Eng.* **2016**, *4*, 3174.
[419] V. Periasamy, G. P. M. K. Ciniciato, K. Yunus, A. C. Fisher, *Appl. Phys. Express* **2015**, *8*, 027002.
[420] F. Hu, W. Liu, W. Li, Z. Xu, Y. Y. Diao, N. B. Lin, W. Guo, L. Shi, J. H. van Esch, X. Y. Liu, *Small* **2019**, *15*, 1804171.
[421] S. A. Akalin, E. Celik, *J. Electron. Mater.* **2019**, *48*, 6786.
[422] G. Dennler, C. Lungenschmied, H. Neugebauer, N. S. Sariciftci, A. Labouret, *J. Mater. Res.* **2005**, *20*, 3224.
[423] K. Yuwawech, J. Wootthikanokkhan, S. Wanwong, S. Tanpichai, *J. Appl. Polym. Sci.* **2017**, *134*, 45646.
[424] M. Bonomo, B. Taheri, L. Bonandini, S. Castro-Hermosa, T. M. Brown, M. Zanetti, A. Menozzi, C. Barolo, F. Brunetti, *ACS Appl. Mater. Interfaces* **2020**, *12*, 54862.
[425] V. Selvanathan, R. Yahya, H. F. Alharbi, N. H. Alharthi, Y. S. Alharthi, M. H. Ruslan, N. Amin, M. Akhtaruzzaman, *Sol. Energy* **2020**, *197*, 144.
[426] M. Torculas, J. Medina, W. Xue, X. Hu, *ACS Biomater. Sci. Eng.* **2016**, *2*, 1211.
[427] H. Hug, M. Bader, P. Mair, T. Glatzel, *Appl. Energy* **2014**, *115*, 216.
[428] A. M. J. S. Weerasinghe, M. A. K. L. Dissanayake, G. K. R. Senadeera, V. A. Senaviratne, C. A. Thotawatthage, J. M. K. W. Kumari, *Ceylon J. Sci.* **2017**, *46*, 93.
[429] J. J. Kaschuk, K. Miettunen, M. Borghei, E. Frollini, O. J. Rojas, *Cellulose* **2019**, *26*, 6151.

© 2021 The Authors. Advanced Energy Materials published by Wiley-VCH GmbH

16146840, 2021, 43, Downloaded from https://onlinelibrary.wiley.com/doi/10.1002/aenm.202100520 by Universita Di Torino, Wiley Online Library on [21/02/2025]. See the Terms and Conditions (https://onlinelibrary.wiley.com/terms-and-conditions) on Wiley Online Library for rules of use; OA articles are governed by the applicable Creative Commons License

Luca M. Cavinato received his B.Sc. in Chemistry and his M.Sc. in Industrial Chemistry at the University of Turin, Italy in 2017 and 2019, respectively. After one year of work experience as a research assistant at IMDEA Materials Institute, Getafe, Spain he moved to Germany where he is currently a Ph.D. candidate at the chair of Biogenic functional Materials at the Technical University of Munich under the supervision of Prof. Costa. His research activity focuses on the study and development of innovative organic and organometallic materials with photovoltaic and electroluminescent properties, with special emphasis on sustainability.

Elisa Fresta received both her B.Sc. (2014) and M.Sc. (2016) in Chemistry from the University of Turin, Italy, and her Ph.D. in Advanced Materials and Nanotechnologies from the University Autónoma of Madrid/IMDEA Materials Institute (2020), Spain. Since October 2020, she is working as a postdoc in the chair of Prof. Rubén D. Costa, at the Technical University of Munich. Her research focuses on the selection, characterization, and implementation of new, sustainable emitters in optoelectronic devices.

Sara Ferrara got both her B.Sc. in Chemistry and Chemical Technologies (2017) and her M.Sc. in Industrial Chemistry (2019) from the University of Turin (Italy). After working as a research assistant in IMDEA Materials (Getafe, Spain), she is now attending her Ph.D. studies at the Technical University of Munich in the Chair of Biogenic Functional Materials (Prof. Rubén D. Costa). Her research focuses on the application of artificial fluorescent proteins as emitters in down converting materials for bio-hybrid white LEDs. The main aim is the production of highly stable and efficient bio-inspired and fully biogenic phosphors.

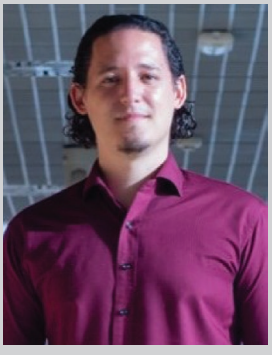

Rubén D. Costa received his Ph.D. from the U. Valencia (Spain) in 2010 and was Humboldt postdoc at the U. Nürnberg-Erlangen (Germany) from 2011 to 2013. In 2014 he started the Hybrid Optoelectronic Materials and Devices Lab as Liebig group leader (2014–2017). In 2017, he moved his group to IMDEA Materials (Spain) and expanded to U. Waseda (Tokyo) as an associate professor in 2018. Since 2020 he leads the chair for Biogenic Functional Materials at the Technical University of Munich. He has reported >150 scientific publications/books/patents and has been recipient of >35 awards/mentions/fellowships.

© 2021 The Authors. Advanced Energy Materials published by Wiley-VCH GmbH

16146840, 2021, 43, Downloaded from https://onlinelibrary.wiley.com/doi/10.1002/aenm.202100520 by Universita Di Torino, Wiley Online Library on [21/02/2025]. See the Terms and Conditions (https://onlinelibrary.wiley.com/terms-and-conditions) on Wiley Online Library for rules of use; OA articles are governed by the applicable Creative Commons License